Report of Investigations No. 142

ENHANCED GAS RECOVERY FROM WATERED-OUT RESERVOIRS

Port Arthur Field, Jefferson County, Texas

A. R. Gregory
Z. S. Lin
R. S. Reed
R. A. Morton
T. E. Ewing

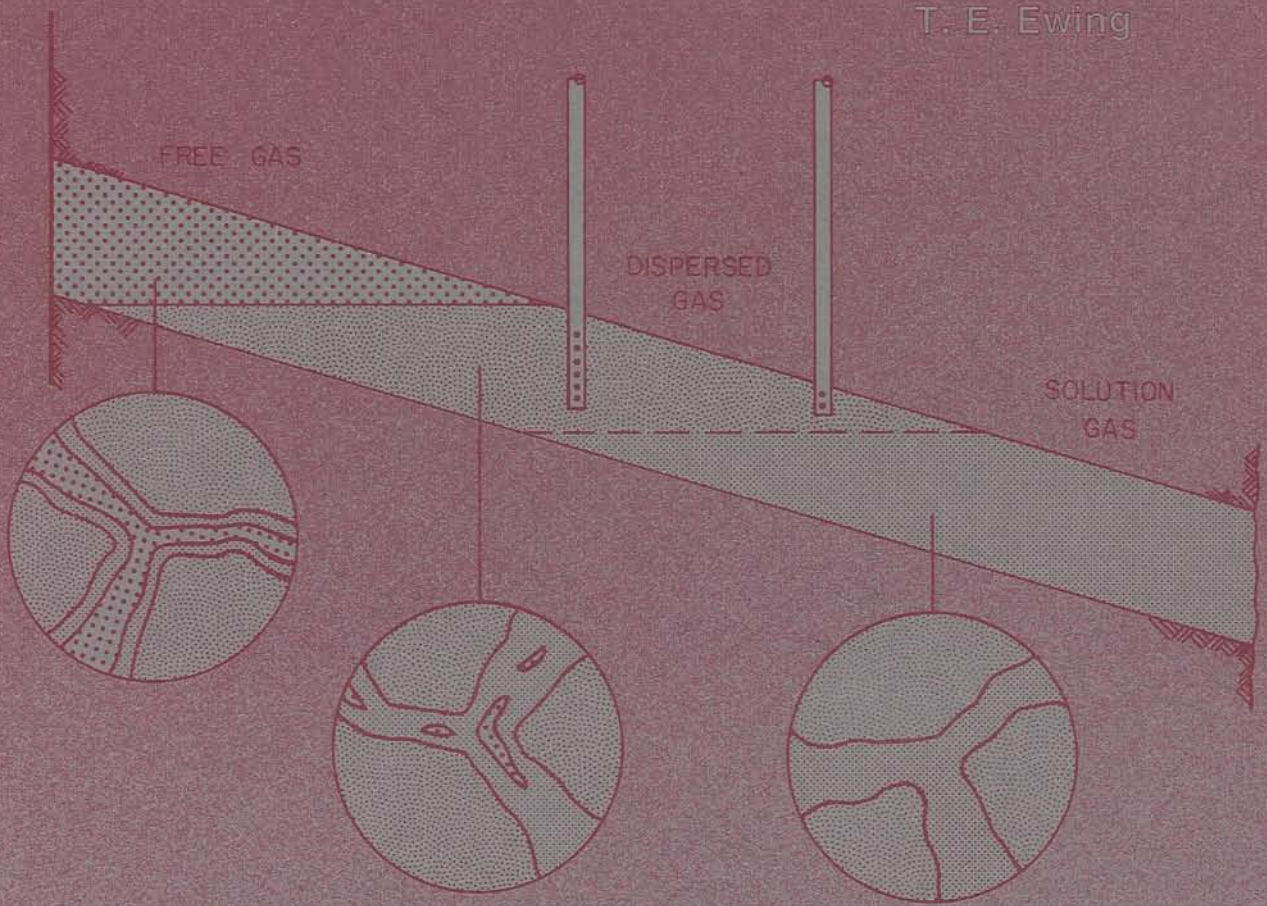

1984

BUREAU OF ECONOMIC GEOLOGY
W. L. Fisher, Director
The University of Texas at Austin
Austin, Texas 78712

Report of Investigations No. 142

ENHANCED GAS RECOVERY FROM WATERED-OUT RESERVOIRS—
Port Arthur Field, Jefferson County, Texas

A. R. Gregory,
Z. S. Lin,
R. S. Reed,
R. A. Morton, and
T. E. Ewing

assisted by

Y. Chen, S. J. Cho, D. W. Downey, M. B. Edwards, S. L. Hallam,
H. S. Hamlin, E. U. Jegbefume, L. A. Jirik, V. H. Lombeida,
W. Mirza, S. Mishra, R. A. Schatzinger, N. Tyler,
B. R. Weise, and J. S. Yoong

Funded by the Gas Research Institute under
Contract No. 5080-321-0398

1984

BUREAU OF ECONOMIC GEOLOGY
W. L. Fisher, Director

The University of Texas at Austin
Austin, Texas 78712

CONTENTS

FIGURES

TABLES

ABSTRACT

Gas reservoirs that water out under moderate to strong water drives are normally abandoned when the expenses associated with salt-water disposal make continued operations uneconomical. Under favorable conditions, however, watered-out reservoirs can continue to produce substantial quantities of gas at competitive prices if operators are prepared to dispose of large volumes of water. Enhanced gas recovery (EGR) techniques can extend production from many reservoirs that are now watering out and will soon be abandoned if conventional practices are followed.

The EGR method involves co-production of gas and water. If large volumes of water are produced, the reduced reservoir pressure causes expansion of free gas formerly trapped in the water-invaded zone during the primary production stage. Some of this free gas becomes mobilized and producible. Also, pressure reduction at the surface releases additional but minor amounts of gas dissolved in the formation water.

The Port Arthur field, Jefferson County, Texas, contains several watered-out gas reservoirs, thick sandstone aquifers, and gas stringers that collectively make the field ideal for testing the co-production technology. The objective sandstones occur in the lower Hackberry (Oligocene) interval at depths of 10,850 to 11,700 ft. The field covers about 1,900 acres (3 mi^2) and originally produced gas condensate from an anticlinal closure on the downthrown side of a major fault that separates the Port Arthur field from the Port Acres field. Some of the lower Hackberry sandstones, interpreted as submarine channel and fan deposits, are laterally extensive and have excellent physical characteristics for producing gas and water. Net-sandstone thickness averages 350 ft. Core data and well log analyses show that porosities average 30 percent, permeabilities average 60 md, salinities average 67,900 ppm sodium chloride, and methane solubility averages 25.7 scf/bbl. Abundant shallow Miocene sands in the area could be used for salt-water disposal. Available well logs were analyzed to determine porosity and other formation characteristics of reservoirs being studied. Water saturations were also calculated from logs to help locate gas-water contacts.

Seismic data were acquired and reprocessed to (1) provide structural information to supplement geological interpretations, (2) locate boundaries of aquifers and gas reservoirs, and (3) evaluate seismic response to low saturations of free gas dispersed in water-invaded zones of watered-out gas reservoirs. Attaining these objectives was severely limited by the poor signal-to-noise ratio in the seismic data. The quality of data was adequate for structural interpretation but was not suitable for reservoir delineation or detection of gas zones. Modeling studies showed what kind of seismic response should be expected from known subsurface geology and suggested that better reservoir delineation could be achieved with increased bandwidth, improved signal-to-noise ratio, and a better knowledge of reservoir acoustic impedances; but it remains unclear whether dispersed free gas in a watered-out reservoir can be detected with seismic data.

The Hackberry C reservoir was selected for numerical modeling because of its high productivity, high average abandonment pressure gradient (0.67 psi/ft), and excellent physical properties. The original gas in place (OGIP) was estimated to be 56.2 Bcf, 35 percent of which was recovered during primary production. A three-dimensional, two-phase model was used to perform history matches and to predict the amount of fluid that might be produced under natural flow conditions if a new well were drilled. During a projected 8-year production period, the predicted reservoir bottom-hole flowing pressure would decline from 6,600 to 4,200 psi. Predicted production was 5.1 Bcf of gas, 51,000 bbl of condensate, and about 9 million bbl of water. An additional 10 percent of the OGIP was predicted as recoverable if the EGR co-production method were used. These results of the simulation study predicted the reservoir performance if a new well were drilled to a depth of 11,650 ft and located on a site near the Meredith No. 2 Doornbos (well 14). Because the reservoir is still geopressured, artificial lift methods would not be required to produce from this test well.

Cash-flow calculations show that the break-even gas price is $2.40/Mcf for a 15-percent rate of return after payment of Federal income tax. The net present worth of the investment is about $968,000 for a gas price of $3.00/Mcf, and it increases substantially at higher gas prices. The economic outlook for the prospect would be even better if production from the C reservoir were commingled with production from other reservoirs in the field.

KEYWORDS: gas production, gas reservoirs, reservoir performance, well logging, computerized simulation, economic analysis, Jefferson County, Texas

INTRODUCTION

A watered-out reservoir comprises essentially three fluid zones, each with different gas saturations (fig. 1). Gas is dissolved in the aquifer pore water, free but immobile gas is dispersed throughout the water-invaded zone, and free mobile gas is in the residual gas cap. These three zones also represent the continuum from conventional free gas to unconventional solution gas. Free mobile gas in this study may also refer to producible gas present in thin stringer sandstones that have not been previously produced (fig. 2). Production of solution gas was the primary focus of the U.S. Department of Energy's geopressured geothermal program, whereas our study emphasized the retrieval of dispersed gas left in the reservoir by conventional production practices.

Gas reservoirs that water out under moderate to strong water drives are normally abandoned when the expenses associated with salt-water disposal make continued operations uneconomical. Under favorable conditions, however, watered-out reservoirs can continue to produce substantial quantities of gas at competitive prices. Enhanced gas recovery (EGR) techniques can be used to extend the production from many reservoirs that are now watering out and will soon be abandoned unless unconventional practices are adopted. Further gas production from these reservoirs would be a welcome addition to our nation's reserves. Now may be the time for the gas-producing industry to reconsider when to abandon reservoirs.

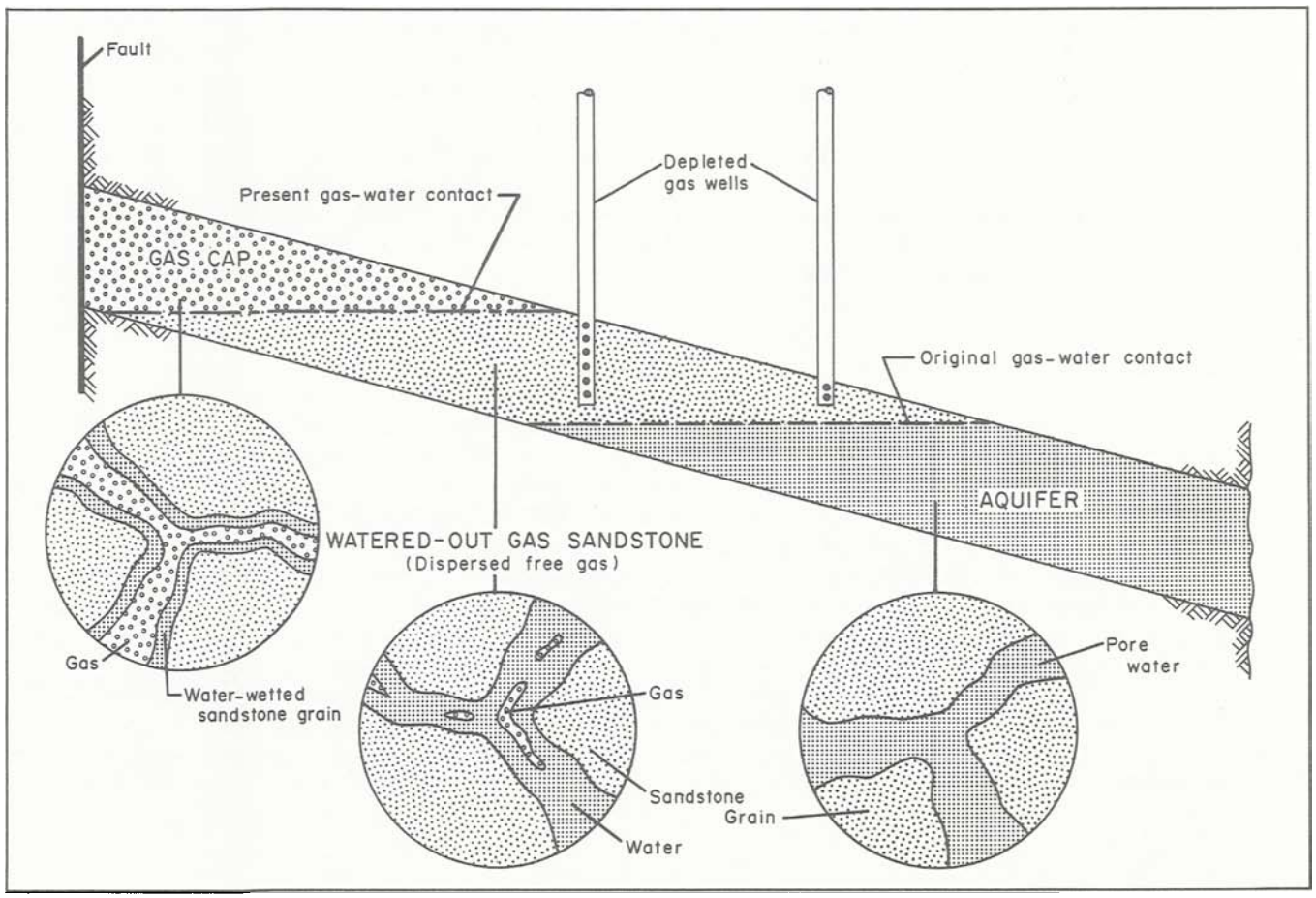

FIGURE 1. Fluid saturation zones within a hypothetical watered-out reservoir.

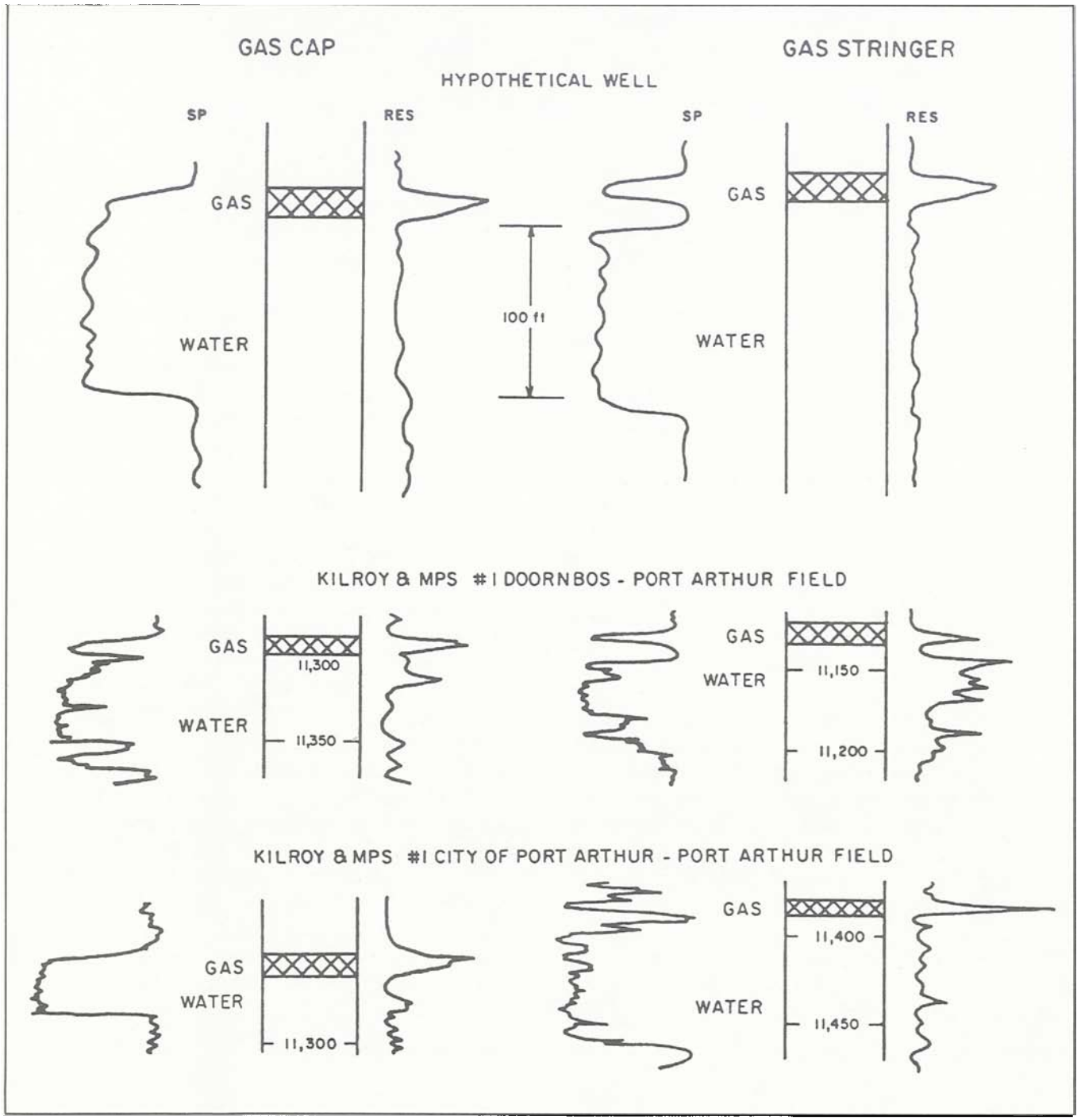

FIGURE 2. Typical well log response for thick aquifers with gas caps and thin gas stringers.

The EGR method, which could prolong operations, involves the co-production of gas and water. Large volumes of water are deliberately produced to reduce reservoir pressures; the lower pressure allows expansion of the free gas that was trapped in the water-invaded zone during the primary production stage. Some of this free gas becomes mobilized and producible. Also, pressure reduction at the surface releases additional but minor amounts of gas dissolved in the formation water.

Formation fluid properties of pressure, temperature, and salinity significantly influence the amount of methane gas that can be

held in solution. Solution gas, however, is minor in enhanced gas recovery because it represents a relatively small part of the total gas resource. Therefore, the influence of high salinity on the resource is minor. High-salinity waters, however, may cause scaling and corrosion of production equipment.

A computer model describing the performance of a geopressured watered-out reservoir (Geer and Cook, 1978) was used to predict that over 20 percent of the otherwise unrecovered gas could be produced by the co-production method. Field experience with EGR techniques has been favorable in hydropressured Wilcox and Frio reservoirs of the Texas Gulf Coast. Results from the Katy V-C reservoir (Lutes and others, 1977) and from the Lovells Lake Frio 1 reservoir (Brinkman, 1981) show that recovery factors exceed 20 percent of the original gas in place (OGIP) for additional gas produced during the blowdown period. A field test currently being conducted in the Double Bayou Frio 13 reservoir indicates that secondary gas recovery will be about 10 percent of the OGIP (Boyd and others, 1982). In another EGR project in the North Alazan H-21 reservoir, Chesney and others (1982) concluded that the recovery process is dominated by gravity forces and is sensitive to vertical permeability and formation dip.

These four field cases involved pumping large volumes of water from water-drive hydropressured reservoirs located at depths between 7,200 and 8,750 ft.* Although significant amounts of additional gas and some oil are recovered by EGR methods, discussion of the economic factors involved is omitted in the published results. Generally, the economic outlook for EGR methods improves if (1) gas prices are high, (2) artificial lift methods are not required, and (3) waste brine can be injected into shallow aquifers or discharged at the surface.

An integrated geological and engineering approach was used in this study to select a prospective geopressured watered-out gas reservoir having characteristics favoring co-production of gas and water. During the screening phase of the project, several fields having reservoirs potentially suitable for enhanced gas recovery were identified, and one, the Port Arthur field, Jefferson County, Texas, was selected for more detailed evaluation (Gregory and others, 1981). All available data for the field were collected and analyzed by various methods, which are broadly classified as reservoir engineering analysis, geophysical interpretation, well log analysis, and economic analysis. Seismic data obtained for more than 31 mi of lines located in or near the Port Arthur field were reprocessed to improve interpretation. Well logs were analyzed to determine porosity and gas-water contacts in the field.

A reservoir simulation study was made on the geopressured Hackberry C sandstone located at an average depth of 11,130 ft. After history matches were made to reproduce the pressure behavior and water production rates during primary production, prediction of reservoir performance showed that gas recovery would increase from 35 percent (primary) to 44 percent of OGIP by using the co-production method. Furthermore, economic analyses of the simulated field test are encouraging (Gregory and others, 1983a, 1983b).

*Metric conversion factors are given in appendix A; nomenclature and abbreviations are given in appendix B.

SELECTION OF TEST AREA

Guidelines and test criteria were established to select a prospective watered-out gas field where free gas and water containing gas in solution could be co-produced in economically significant quantities. The criteria included depth, pressure, temperature, salinity, methane solubility, gas sand and aquifer volumes, porosity, permeability, and production history. More than 150 gas fields in the Frio/Vicksburg and Wilcox trends were screened; potential prospects were finally reduced to 3 fields that satisfied most of the test criteria. The best prospects were the Port Arthur and Port Acres fields in Jefferson County, Texas, and the

Algoa field in Brazoria and Galveston Counties, Texas. Many fields were eliminated in the screening process because their wells were actively producing hydrocarbons from reservoirs of potential interest to co-production studies. The Port Arthur field was the best prospect because it contained multiple gas reservoirs having excellent physical properties for co-production of gas and water. In addition, all of the lower Hackberry reservoirs had watered out and were abandoned by previous operators.

STUDIES OF THE PORT ARTHUR AREA

REGIONAL GEOLOGICAL SETTING

The Frio Formation is one of the major clastic progradational units of the Texas Gulf Coast (Galloway and others, 1982). Two large delta systems, the Norias in South Texas and the Houston in East Texas, prograded more than 60 mi basinward of the previous continental margin, causing the development of large regional growth-fault systems and stimulating salt movement. Barrier-bar and strandplain systems extended both between the principal deltas (the Greta-Carancahua system) and east of the Houston delta system into Louisiana (the Buna system).

Shale and sandstone of the Hackberry Member of the Frio Formation form a seaward-thickening wedge within the normal Frio marine succession in southeast Texas and southwestern Louisiana (fig. 3). The wedge pinches out to the north along a zone that Bornhauser (1960) termed the Hartburg flexure. The term "Hackberry" was first used by Garrett (1938) for the bathyal (deep-water) foraminiferal assemblage at Hackberry salt dome in Louisiana but was later generalized by Bornhauser (1960) and Paine (1968) to refer to a member or a facies, or both, of the Frio Formation.

In most areas, the lower Hackberry is a sand-rich unit that fills channels eroded more than 800 ft into the pre-Hackberry sediments. Previous studies have indicated that these sands were deposited in a submarine canyon-fan environment (Paine, 1968; Berg and Powers, 1980). A more uniformly distributed, seaward-thickening wedge of shale overlies the lower Hackberry sands; it grades upward into upper Frio sediments of shallow-water origin. The lower Hackberry sands are significant oil and gas reservoirs in the area; exploration for deeper geopressured gas fields is currently active.

No adequate regional structural and stratigraphic study of the Hackberry in southeast Texas has been published. Thus, the location of the major submarine channels, the geometries of the sandstone bodies, and the evolution of the Hackberry depositional system are incompletely known. Reedy (1949) studied the Frio Formation in the area. Berg and Powers (1980) examined cores from two wells in Jefferson County. The geology and early production history of Hackberry sandstones in the Port Arthur and Port Acres fields were discussed by Halbouty and Barber (1961).

The Port Arthur field and surrounding area were studied in our project to achieve a better understanding of the regional geology. This area extends from the updip limit of the Hackberry wedge to the downdip limit of well control in Jefferson and Orange Counties, Texas, and adjacent parts of Louisiana. More than 220 electric logs of deep wells were obtained and correlated. Paleontological data were extensively used in picking the basal Hackberry unconformity and in defining the lower Frio and Vicksburg units. Six seismic sections were interpreted to assist in determining structure and channel distribution downdip of the Port Arthur field. Information from seismic sections and well logs was merged to produce structural and net-sandstone maps of the study area. In addition,

well logs in the Port Arthur field were studied to evaluate sand-body geometry, depositional setting, and continuity.

FRIO STRATIGRAPHY

The Frio Formation in the Port Arthur area ranges from approximately 2,000 to 6,000 ft thick; thickness increases basinward. In the updip part of the area, the Frio consists of stacked barrier-bar and strandplain sandstones of the Buna barrier system. Downdip the sandstone content decreases, except within the deep-water sandstone-shale wedge of the Hackberry Member.

The Frio can be divided into three units (fig. 3). The lower unit (between the top of the Vicksburg at *Textularia warreni* and *Nodosaria blanpiedi*) is very thin and sandstone-poor and is nearly indistinguishable from the underlying Vicksburg. The middle unit (from *Nodosaria*

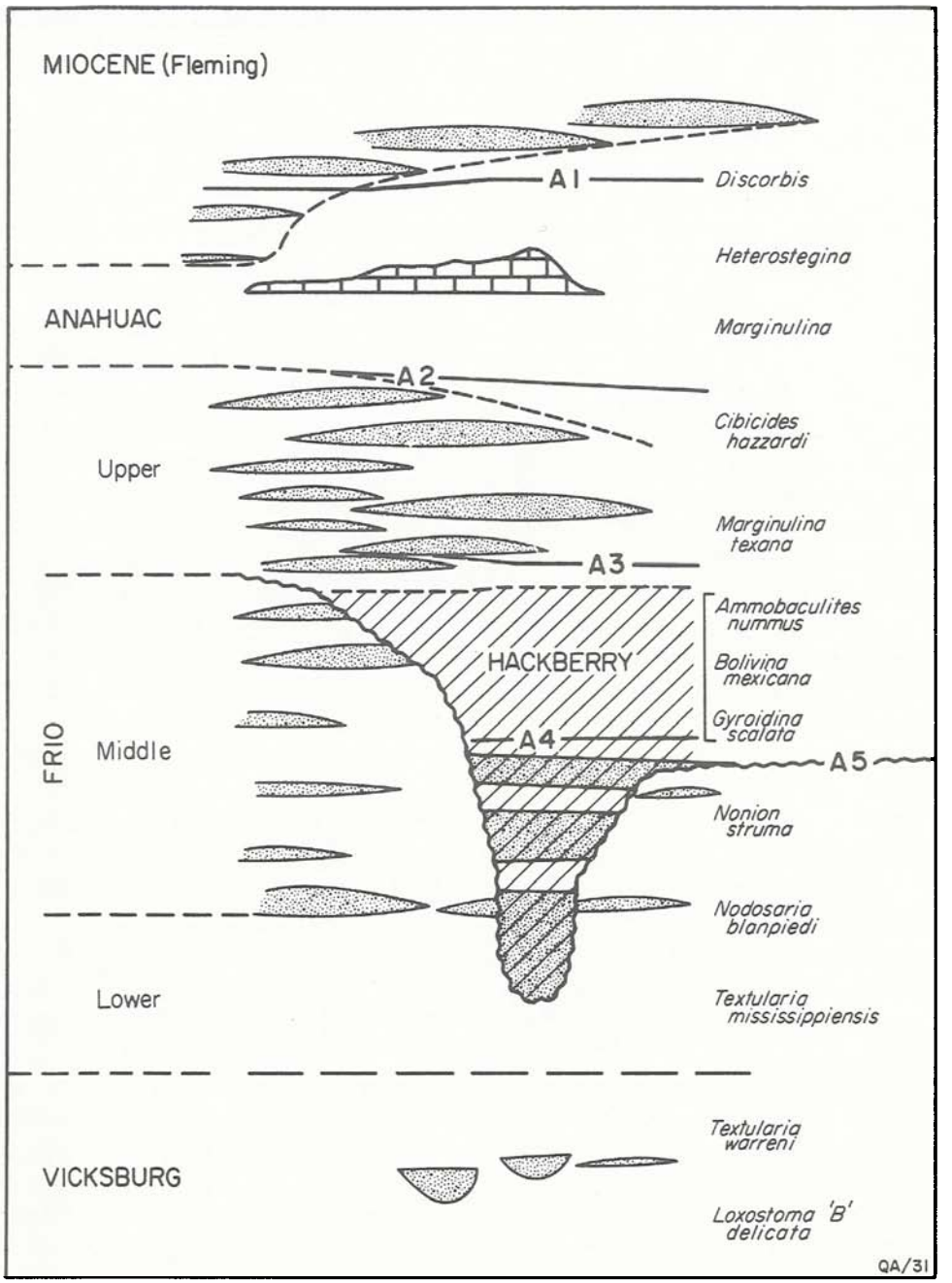

FIGURE 3. Stratigraphic diagram of Tertiary strata, paleomarkers, sand-body distribution (shaded), and marker horizons, Jefferson County area (from Ewing and Reed, in press).

blanpiedi to about *Marginulina texana*) contains abundant sandstone updip but only a few discontinuous sandstones of undetermined origin downdip. At the pre-Hackberry unconformity, the middle unit is extensively eroded, so original thickness and geometry are difficult to determine. The Hackberry wedge lies between *Nonion struma* and *Marginulina texana*; that is, it is late-middle Frio in age. The upper Frio consists of nearly continuous sand updip and alternating sand and shale downdip. These sands contain upward-coarsening cycles, are continuous along strike, shale out fairly rapidly downdip, and are inferred to represent barrier-bar or strandplain sand bodies or both. The upper Frio barrier system prograded, capping the deep-water Hackberry Member.

Correlation markers A1 thru A5 range from the top of the Anahuac to the pre-Hackberry unconformity (fig. 3). Markers A1 through A3 subdivide shallow-water deposits, whereas A4 to A5 subdivide deep-water strata of the Hackberry Member. Within the downdip parts of the study area, no units below the pre-Hackberry unconformity can be correlated in enough wells to determine their structural configuration reliably. Furthermore, the seismic data are of insufficient quality to determine the nature of the deep structures.

PORT ARTHUR FIELD

GEOLOGY

The Port Arthur field is located in east-central Jefferson County immediately northwest of the city of Port Arthur (fig. 4). The field is adjacent to the Port Acres field on the west; the two fields are separated by a major fault (fig. 5). The major sandstone deposits and the productive area of the Port Arthur field cover about 1,900 acres (3 mi^2). Before abandonment, the field produced gas and condensate from lower Hackberry (Frio) sandstones that are interpreted as being submarine-fan deposits (Bornhauser, 1960; Paine, 1968; Berg and Powers, 1980). The *Nodosaria* sandstone and the Vicksburg Formation also produced gas in this field.

The structure of the field is dominated by a northeast-trending anticline caused by the rollover into the major fault separating the Port Arthur and Port Acres fields (Weise and others, 1981) (figs. 6 and 7). Closure on the structure is about 100 ft in all directions, but structure to the east is unclear because of sparse well control. A structure map contoured on the pre-Hackberry unconformity shows the effect of the canyon-cutting episode that preceded Hackberry deposition (fig. 8). Wells 23 and 31 are located near the axis of a canyon on the west side of the field. Wells 5, 6, 14, 29, and 30 are on the flanks of this canyon. A major canyon occurs north of and at well 37 along the northern fault. There is a minor channel on the east side of the field, with an axis near wells 34 and 36.

The lower Hackberry sands are lenticular and range in thickness from a few feet to more than 150 ft. The sandstones are thickest in relatively narrow, dip-aligned bands or channels (figs. 6 and 9); these geometries are consistent with a submarine-fan system. The channels contain massive sandstones with blocky spontaneous potential (SP) log patterns.

The field operators divided the lower Hackberry interval into 14 individual reservoirs (fig. 10). Log patterns of the six major reservoirs were studied to help determine the component depositional facies in the units. These patterns can be interpreted by using the submarine-fan facies model by Walker (1979) (fig. 11) as described by Ewing and Reed (in press).

The Hackberry H sandstone is present in only six wells and does not produce hydrocarbons. It rests directly on the pre-Hackberry unconformity, filling a channel as wide as 6,000 ft. The H sandstone displays an SP log pattern characteristic of confined channel-fill or

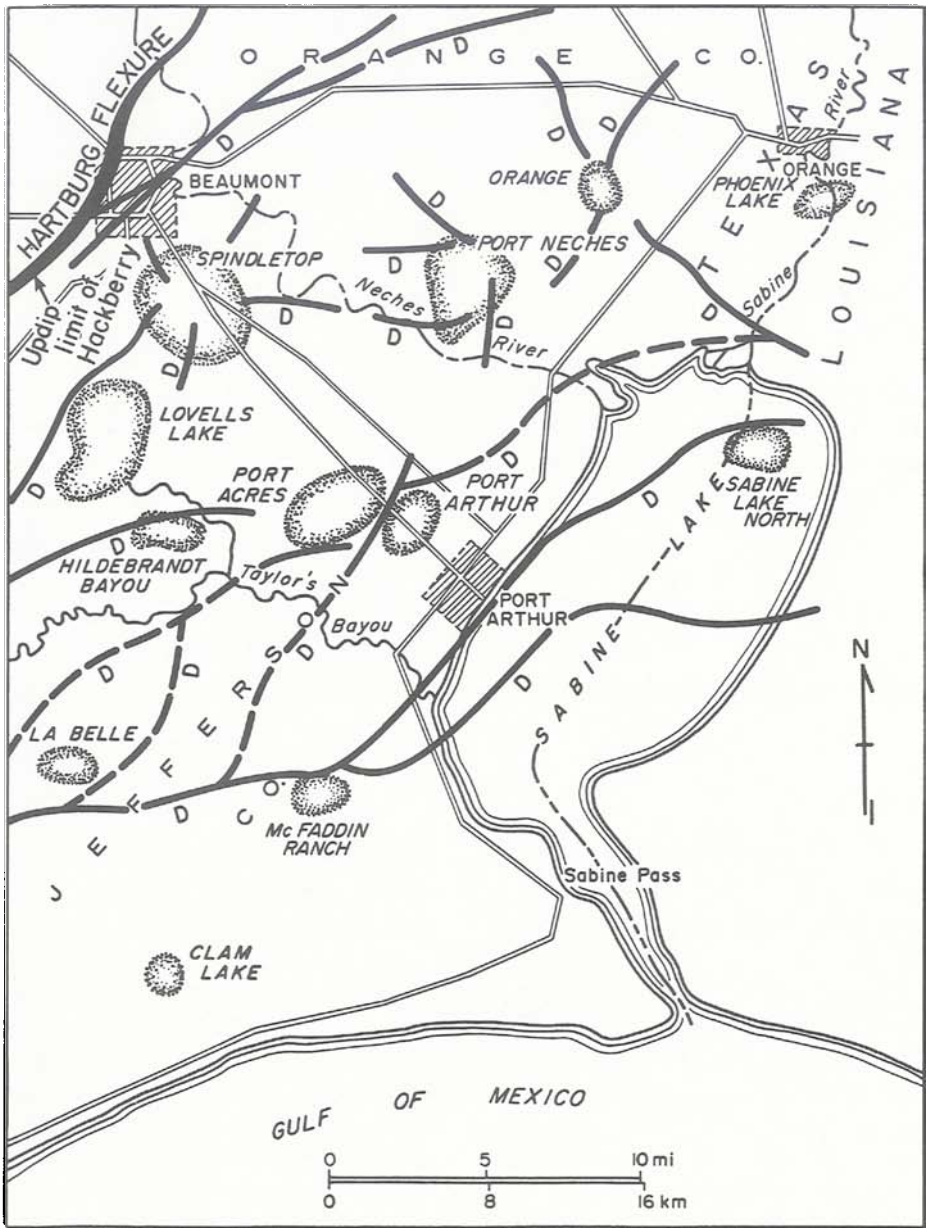

FIGURE 4. Map showing location of Port Arthur field with respect to major faults, other nearby fields, and points of interest (modified from Halbouty and Barber, 1961).

feeder-channel deposits. These deposits are massive, blocky sandstones with few shale partings. Along the axis of the channel is the thickest sand, which has no shale partings and has an abrupt change in SP response from the overlying and underlying shale sections.

The Hackberry G sandstone produced gas and condensate from depths of 11,458 to 11,463 ft in well 31. Log patterns of this sandstone indicate braided channel-fill deposits with some fan-plain overbank deposits (fig. 12). Wells 12, 28, and 36 exhibit generally blocky SP patterns, indicating broad channel-fill deposits, but show more frequent shale partings than does the confined-channel H sand. SP curves for wells 11, 23, and 29 are inferred to be overbank deposits, containing 2- to 10-ft-thick turbidite sandstones with interbedded shales. Well 31, which produces from this sandstone, is located on the flanks of the canyon and on the crest of the anticlinal structure.

Well 14 produced gas and condensate from the Hackberry F sandstone in the depth interval from 11,350 to 11,359 ft. The SP curve for the F sandstone in most of the wells has a serrated blocky pattern but in some wells has an

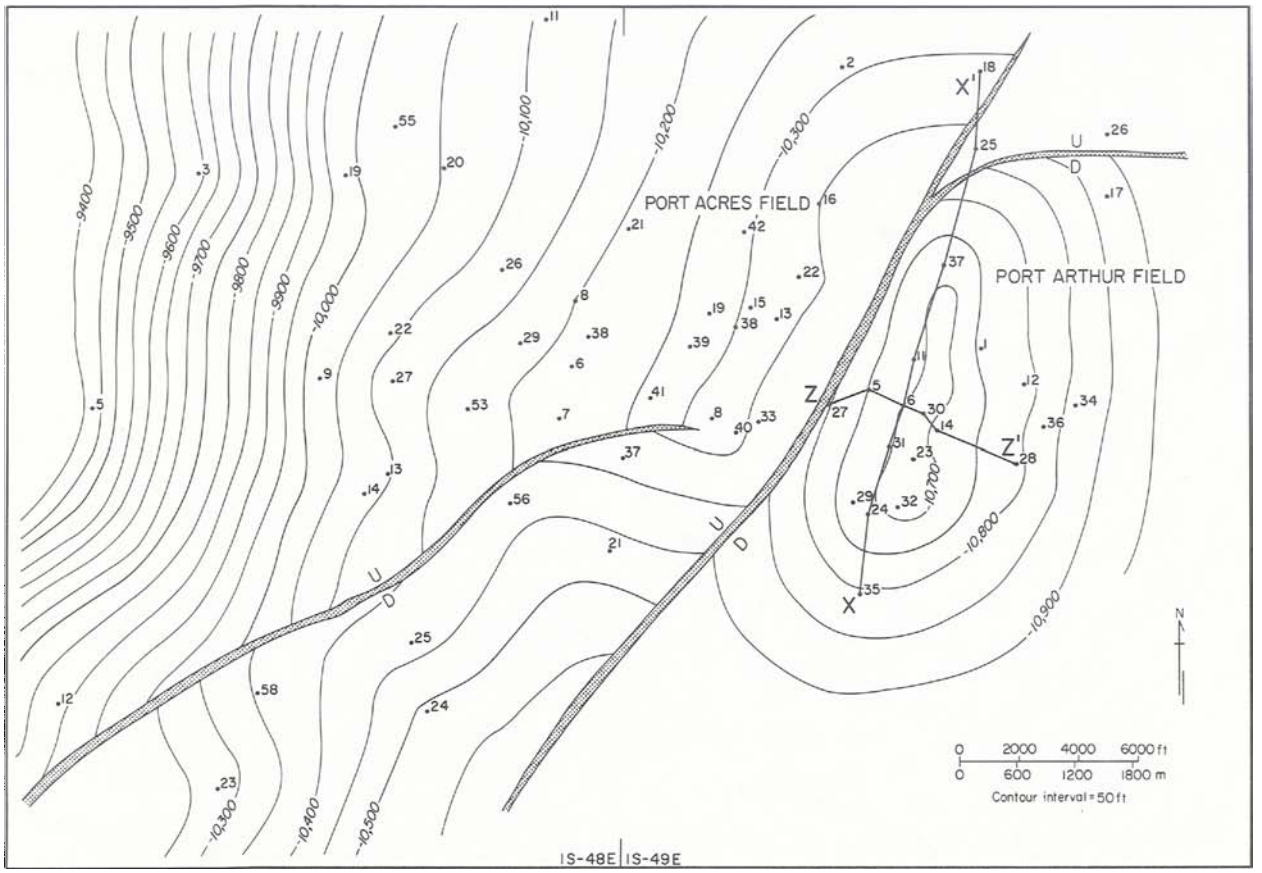

FIGURE 5. Well locations, lines of cross sections, and structural configuration on top of the lower Hackberry sequence, Port Arthur - Port Acres area.

upward-fining pattern (fig. 13). This pattern is common to the proximal suprafan and is best developed in wells 1, 12, 34, and 36. Wells 24, 29, and 32 have a blocky SP pattern indicative of braided-fan-channel-fill deposits. The SP curve for well 35 is very blocky and shows that a new confined channel developed at the southern end of the field.

Wells 6, 14, and 23 produced gas and condensate from the Hackberry E sandstone at depths of 11,276 to 11,301 ft. The E sandstone also displays serrate blocky patterns characteristic of braided-fan-channel-fill deposits. On the northeast side of the field, however, SP curves for wells 1, 12, and 36 show that a younger confined fan channel cut through the field.

The Hackberry C and D sandstones have SP curves representing all the facies of the submarine-fan model, as demonstrated by the C sandstone in figure 14. This reservoir is a broad, braided-fan-channel-fill deposit characterized by erratic blocky to serrate SP patterns passing laterally and downdip into intermediate suprafan deposits having upward-coarsening cycles. Well 1 displays a blocky pattern, suggesting the presence of a deeper incised channel. Overbank deposition is inferred to have occurred at the southwest end of the field (well 35). The C sandstone produced gas and condensate from wells 6, 11, 14, and 23 in the depth range from 11,128 to 11,257 ft. These wells penetrate the sand at the crest of the anticline (fig. 15).

The overlying Hackberry A-1, A-2, B, B-1, and B-2 reservoirs all appear to be thin turbidite sandstones and a few thin, scattered channel deposits. Several wells produce from these sands; well 31 is a good producer from a completion in the B-2 sand. The lower C, upper D, and lower E sandstone stringers are similar to A and B sandstones.

The geometry of the submarine channel sandstones and the succession of facies in the Port Arthur field suggest that the lower Hackberry unit is an aggrading submarine-fan-channel sequence (fig. 16). The initial canyons

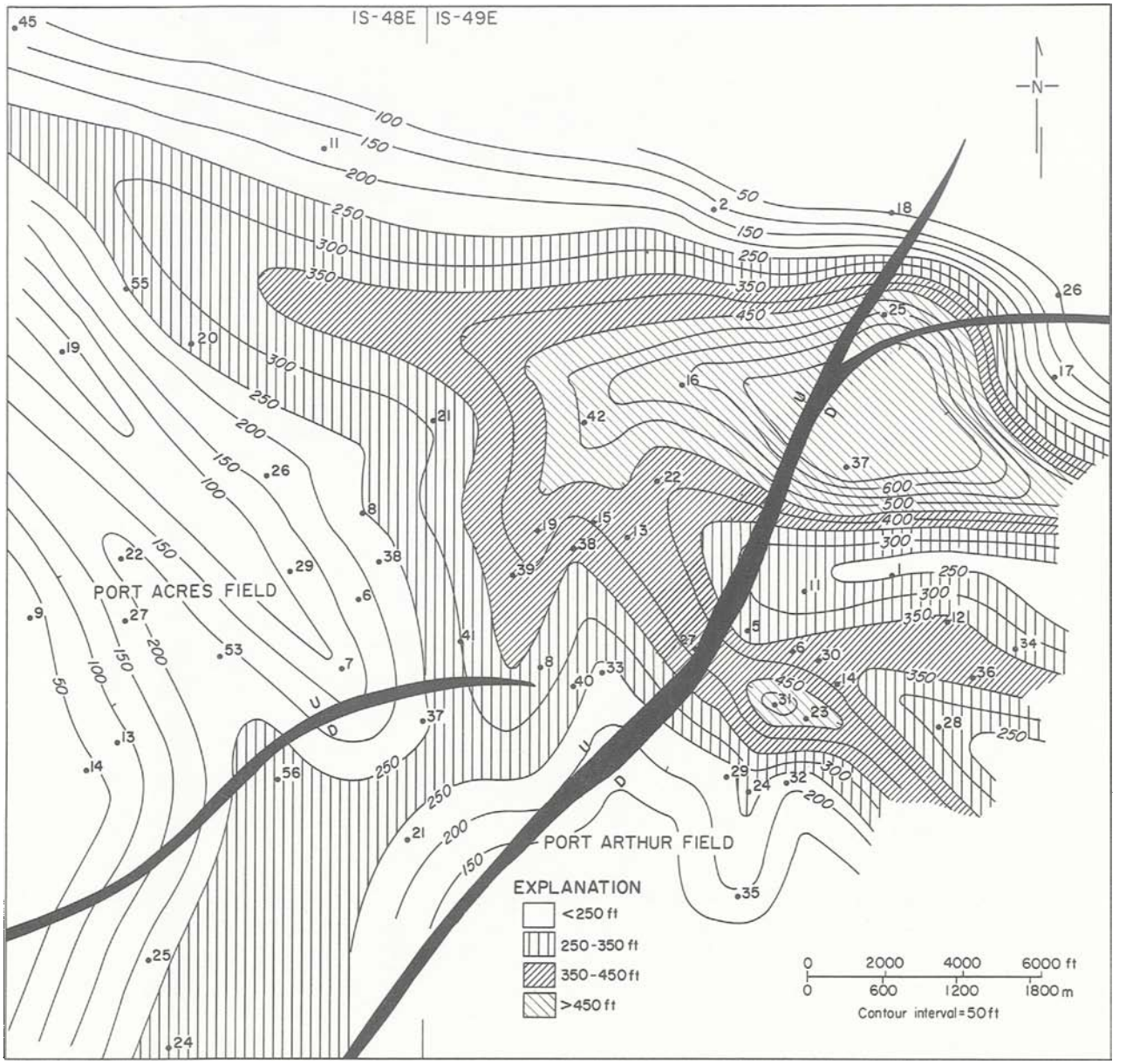

FIGURE 6. Net-sandstone distribution in the lower Hackberry sequence, Port Arthur - Port Acres area.

were cut during headward erosion of the channels into the flank of the Buna strandplain/barrier-bar sand system and underlying muds. The channel at Port Arthur field was first filled by a thick, coarse, confined-channel sand (H sandstone) representing the head of the fan complex; deposition of the sandstone may have been by grain flows and laminar flows as well as by proximal turbidity currents. As the fan aggraded, these deposits were overlain by proximal channel-fan deposits (D, E, and F sandstones). These sands occupied a broader valley in which broad-channel, proximal-fan, and overbank deposits were preserved. At about this stage, the secondary, or crossover, channels formed and were filled by confined-fan-channel sands. Further aggradation of the fan led to the deposition of thinner, complex sand bodies (B and C sandstones), which include thin channels and suprafan deposits. Final deposition, which formed the upper Hackberry shale sequence, was either from turbidity currents on the distal fan or from suspension.

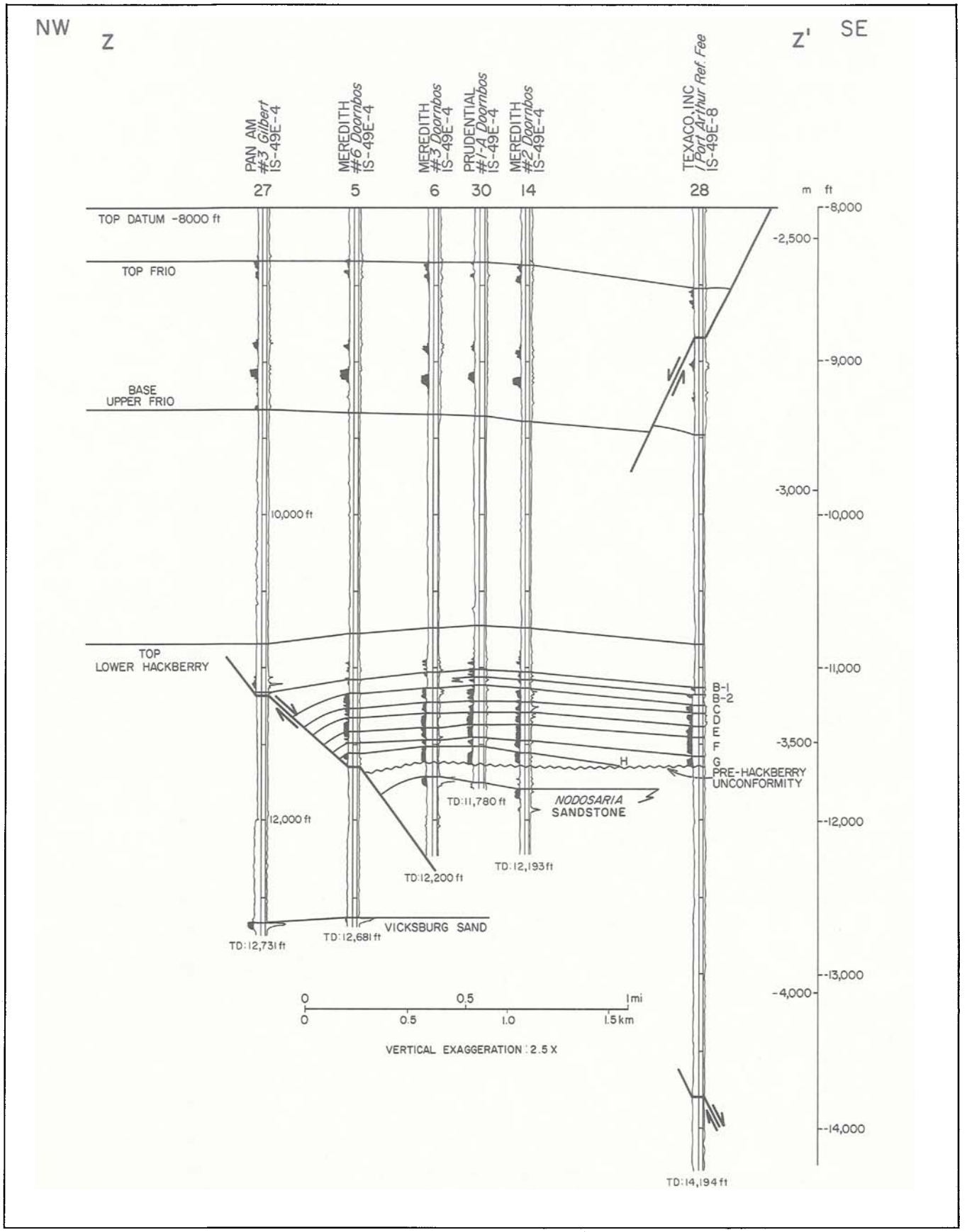

FIGURE 7. Structural dip cross section Z-Z', Port Arthur field.

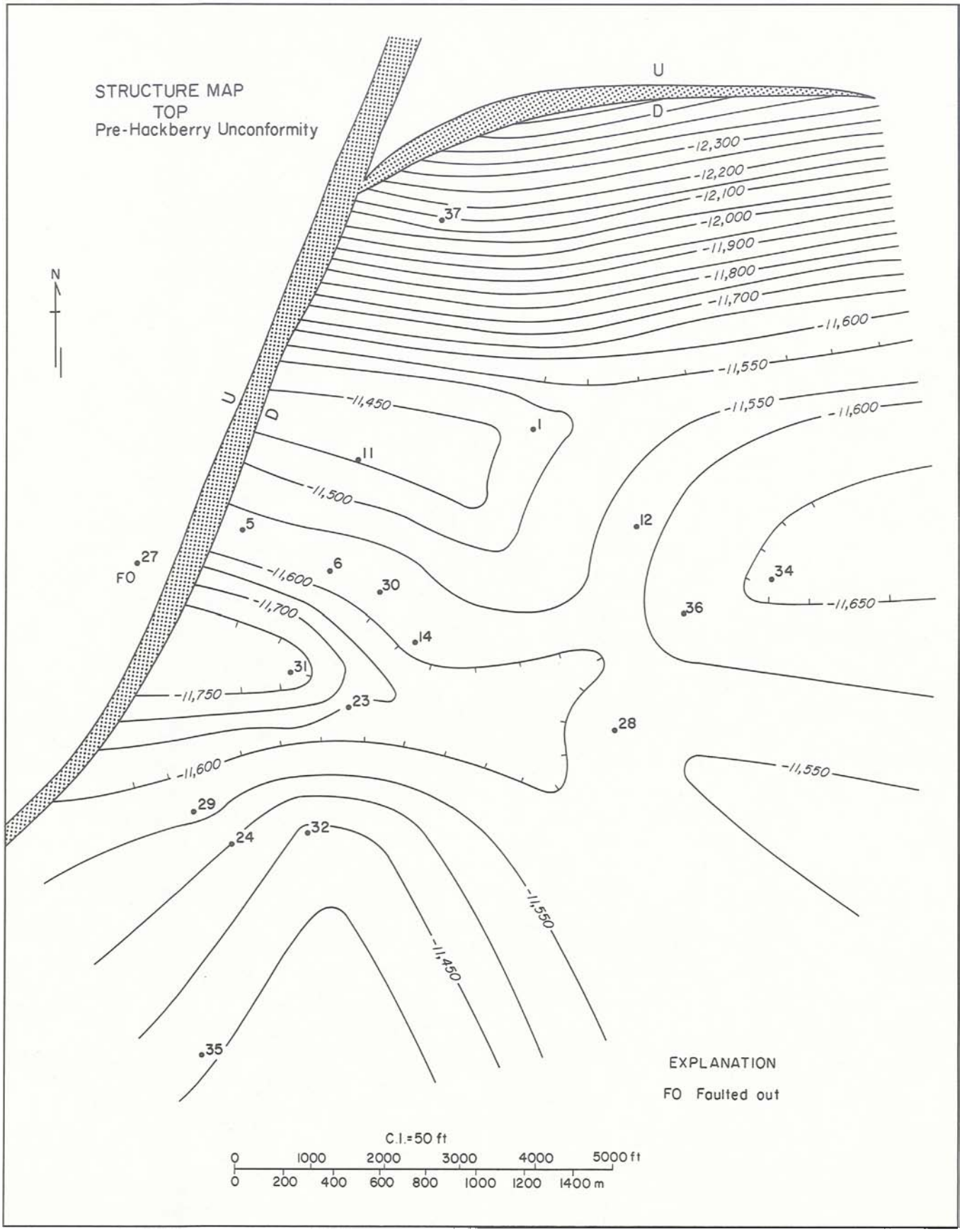

FIGURE 8. Structure map contoured on the pre-Hackberry unconformity, Port Arthur field.

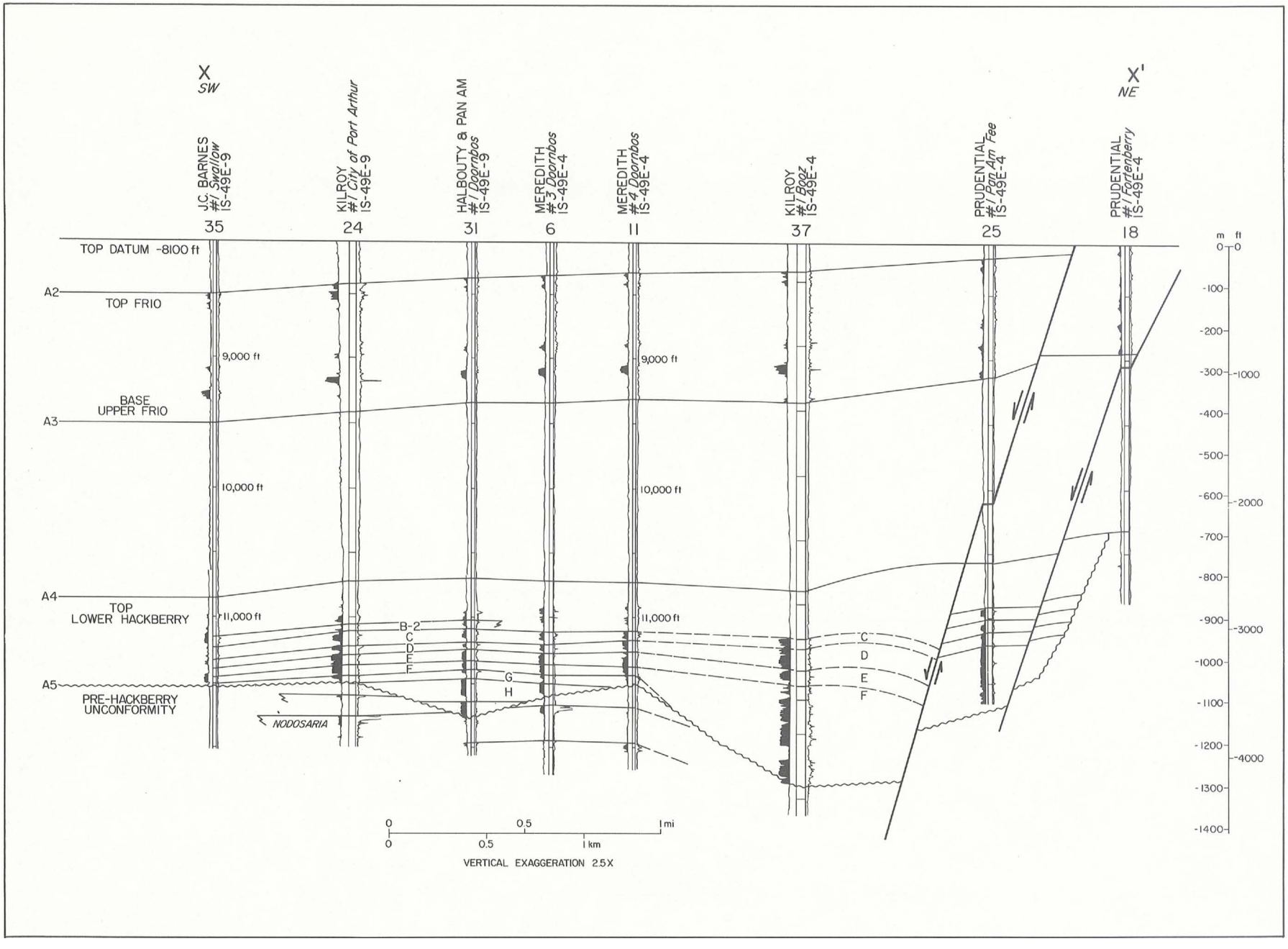

FIGURE 9. Stratigraphic strike cross section X-X', Port Arthur field.

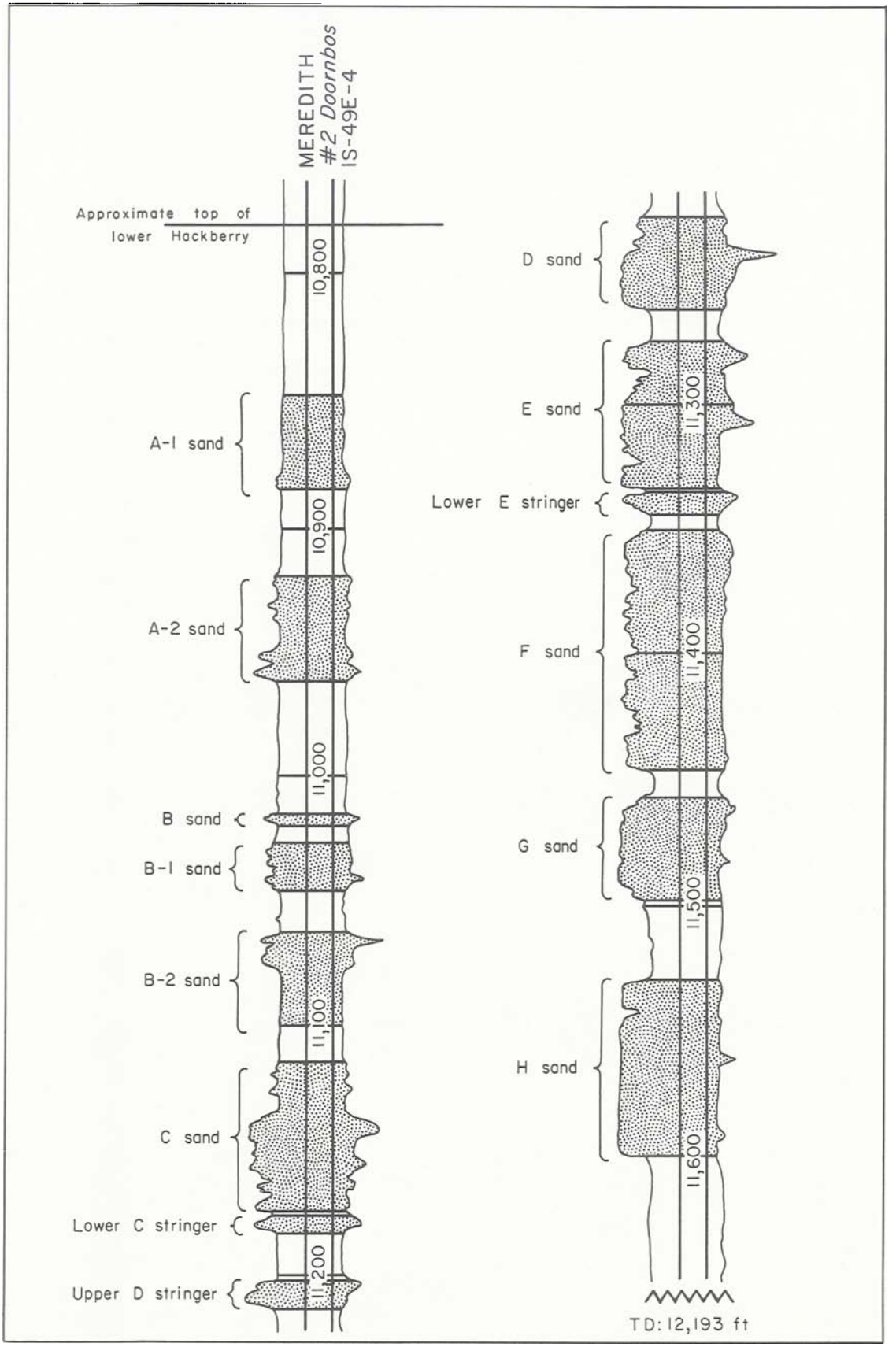

FIGURE 10. Type log showing reservoir intervals, Port Arthur field. The well is number 14 on cross sections Z-Z', figures 5 and 7 (from Weise and others, 1981).

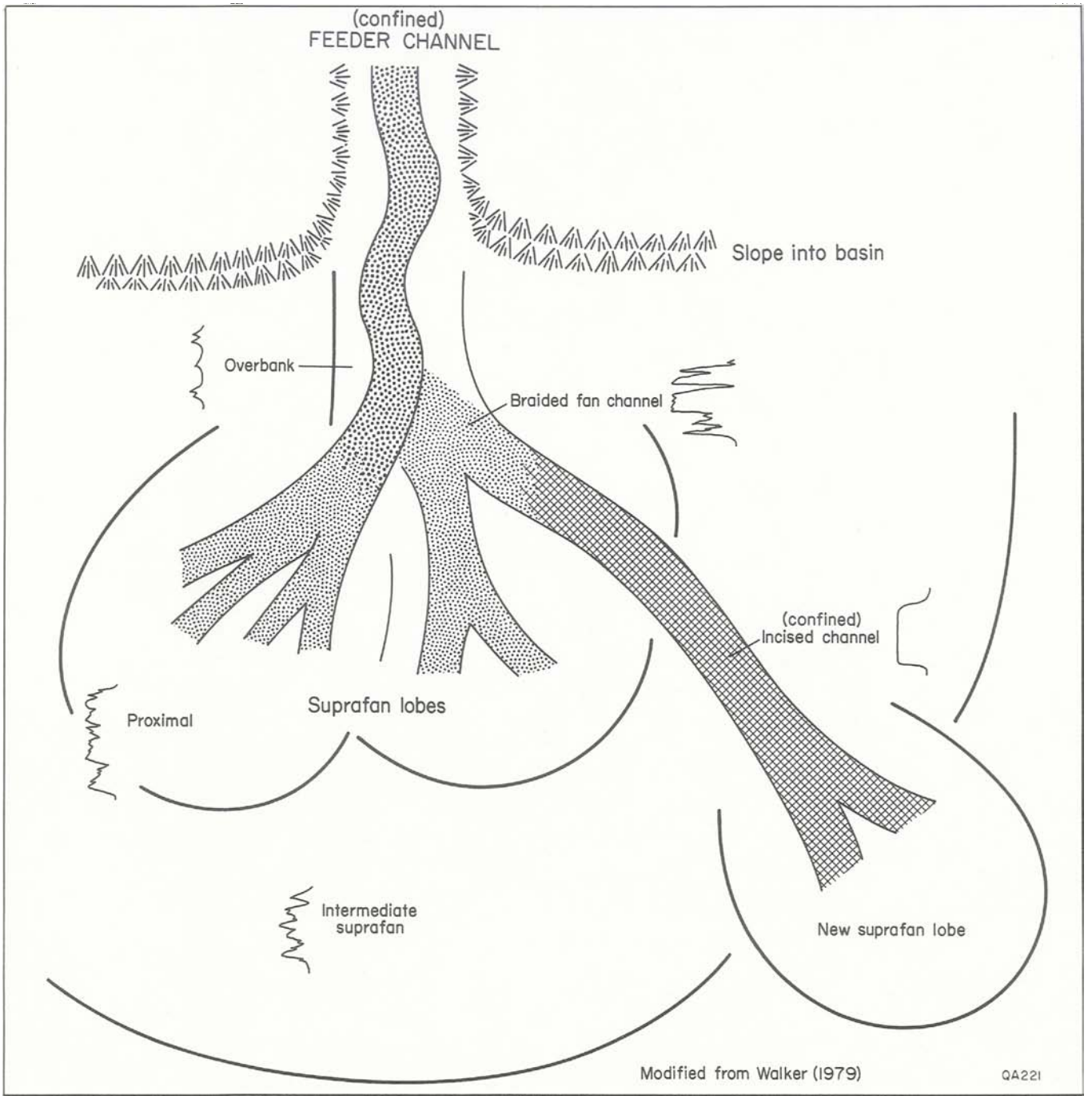

FIGURE 11. Submarine-fan facies model (Walker, 1979) showing SP curves from the Hackberry C sandstone, Port Arthur field.

POTENTIAL SALT-WATER DISPOSAL SANDS

The predicted production of 8.94 million bbl of salt water from natural flow during an 8-year period, discussed later, requires that suitable disposal sands be located near the test well site. More than 2,000 ft of net sandstone are available for potential salt-water injection at depths between 2,000 and 7,500 ft in the Port Arthur field. Cross section T-T′ (fig. 17) shows the sandstones available for salt-water injection at depths between 3,850 and 6,200 ft. These thick Miocene aquifers are below the base of fresh water (−500 ft) and above the depth of shallowest hydrocarbon production; they offer numerous zones for brine disposal. During primary

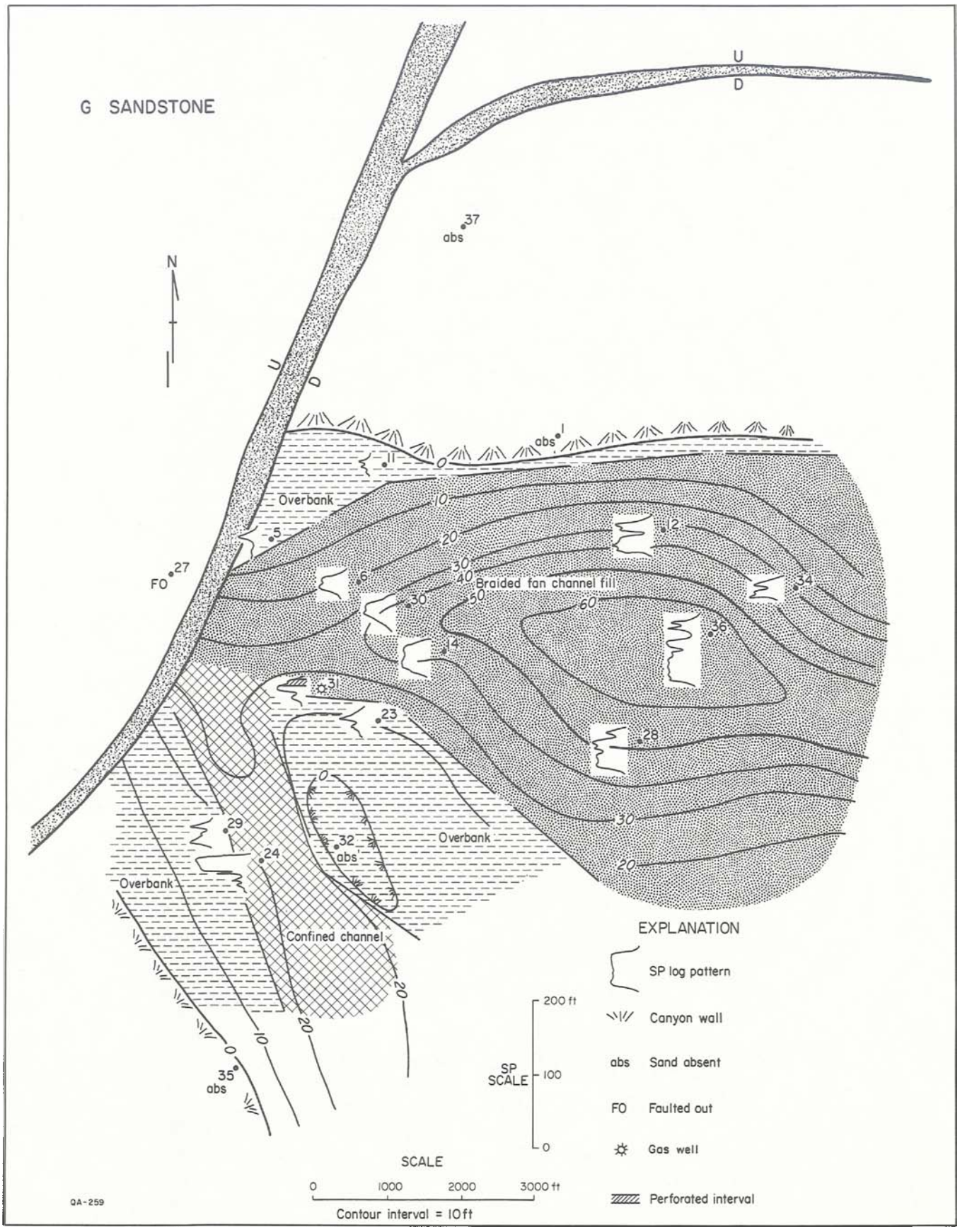

FIGURE 12. Isopach map showing distribution and log character of the Hackberry G sandstone, Port Arthur field.

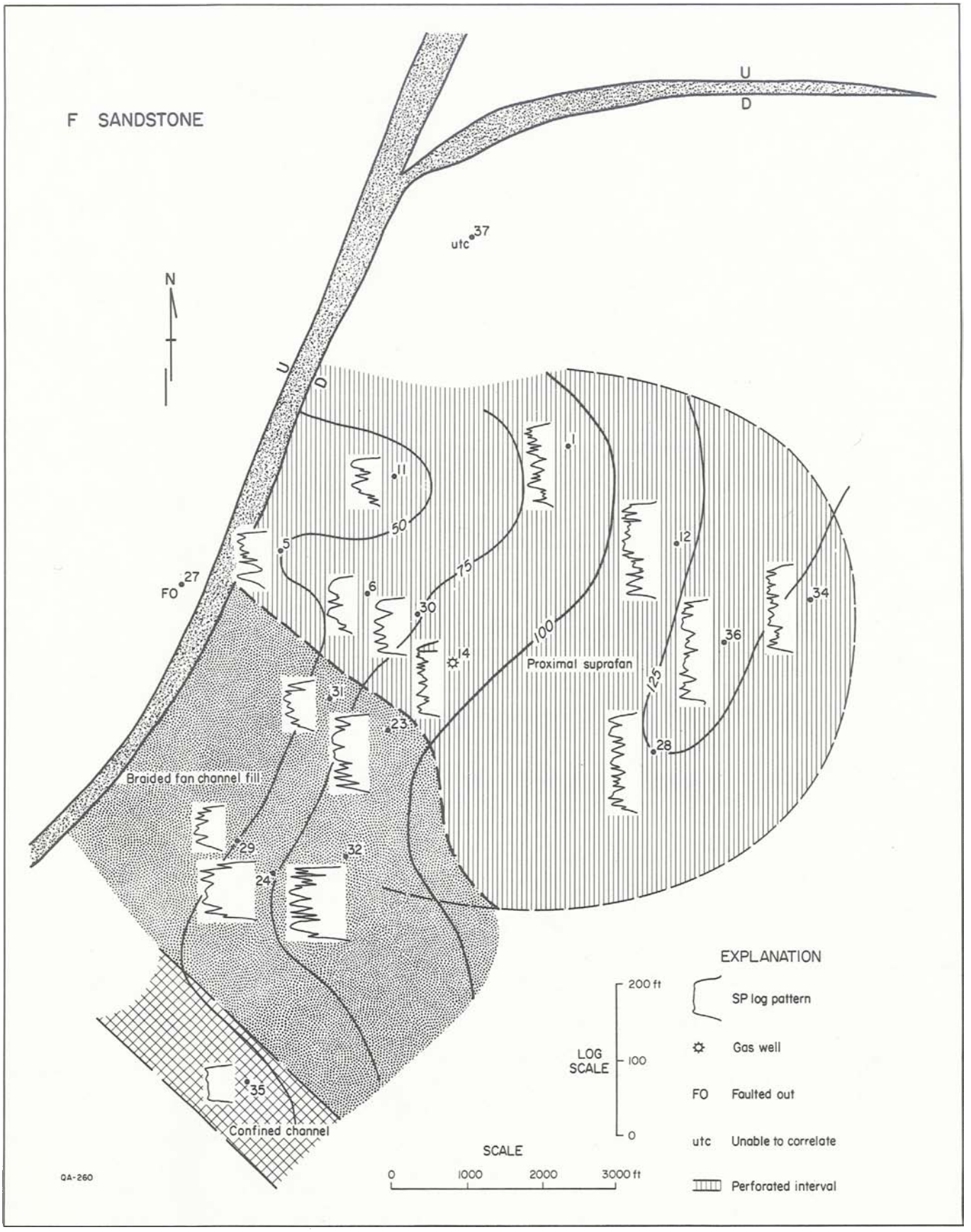

FIGURE 13. Isopach map showing distribution and log character of the Hackberry F sandstone, Port Arthur field.

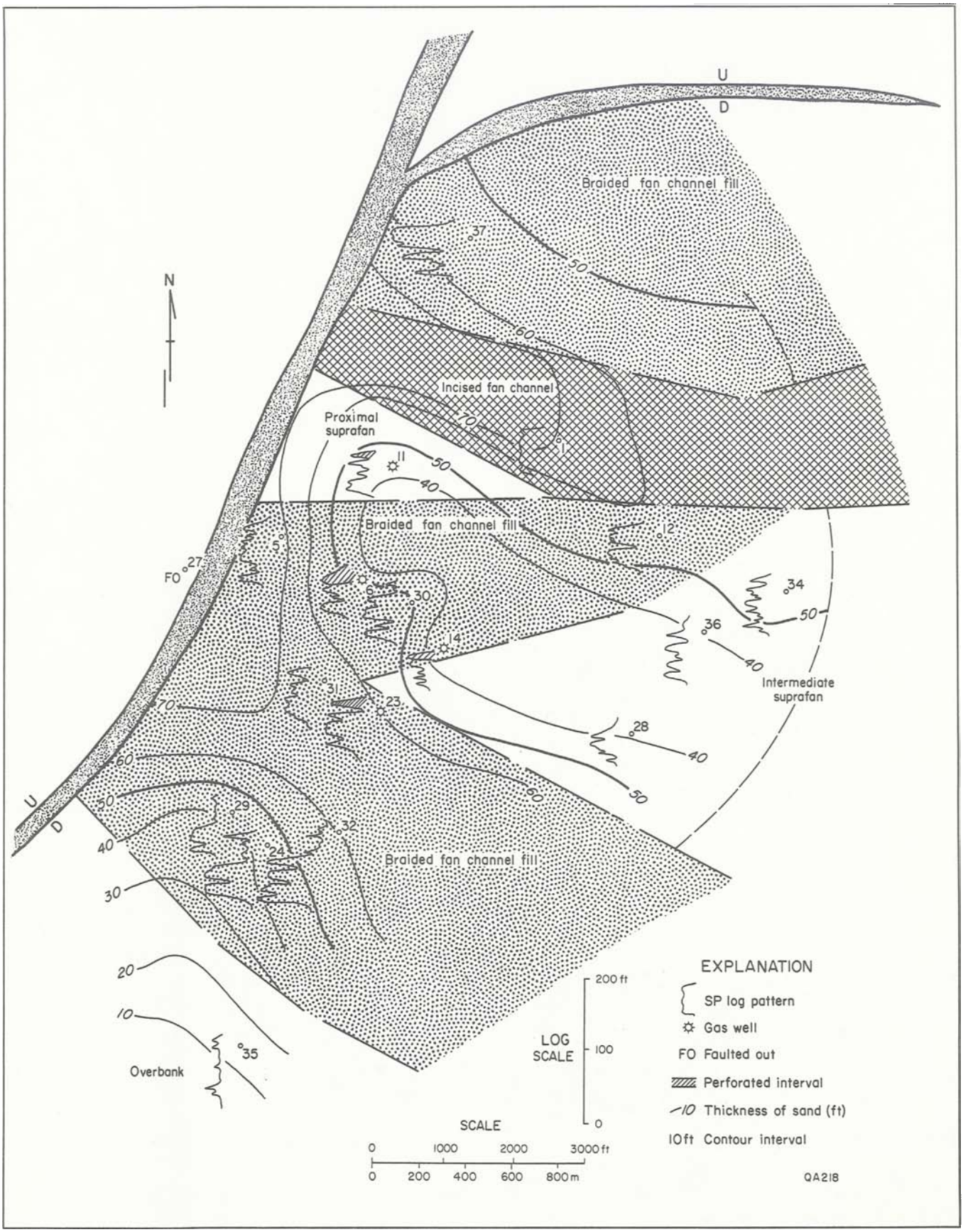

FIGURE 14. Isopach map showing distribution and log character of the Hackberry C sandstone, Port Arthur field.

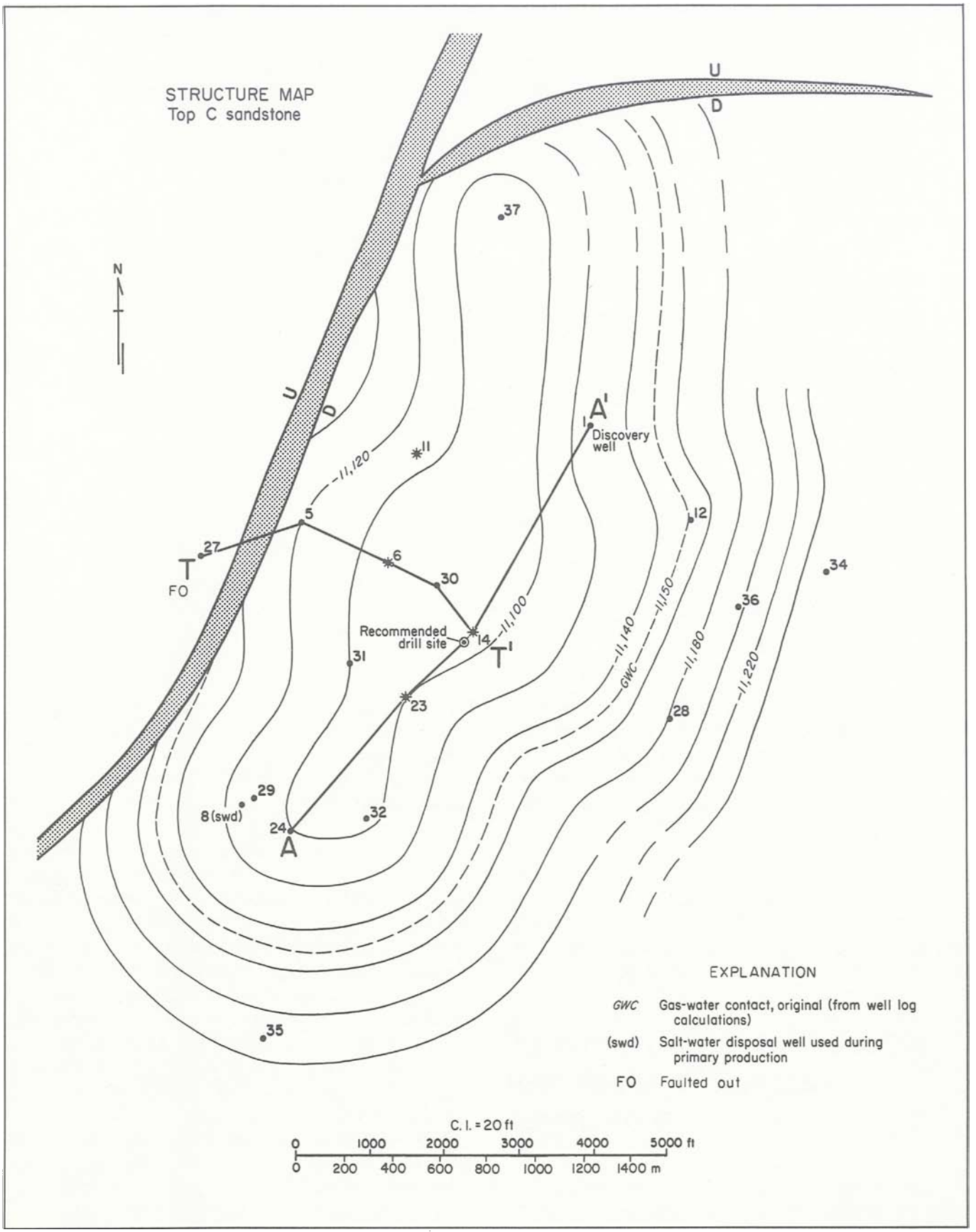

FIGURE 15. Structure map contoured on top of the C sandstone, Port Arthur field.

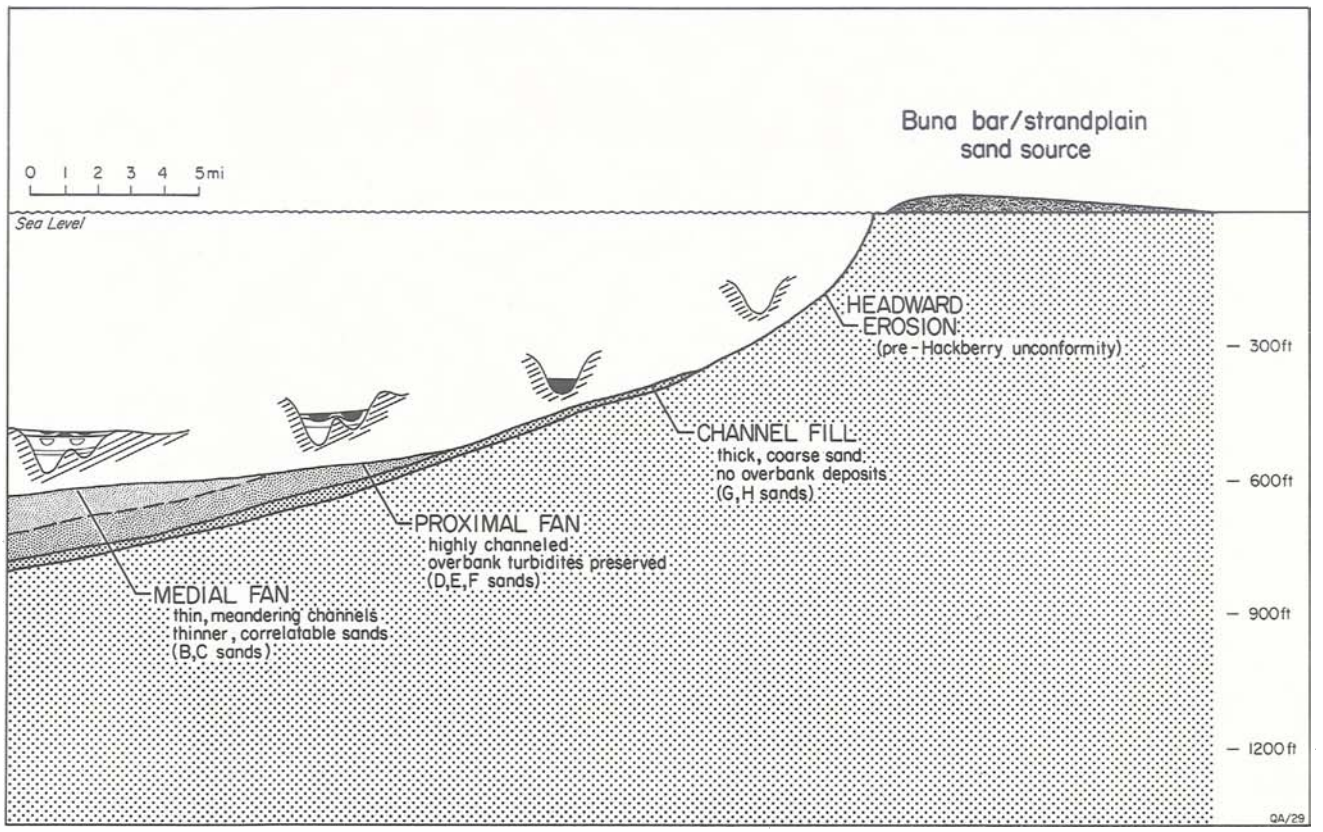

FIGURE 16. Onlapping submarine-fan depositional model of lower Hackberry sandstones, Port Arthur field.

production, brine was injected in two wells at depths of 1,400 to 3,500 ft. Since the proposed test site is near several plugged wells, it may be possible to use one of the abandoned wells for disposal rather than to drill a new injection well. Log calculations for well 14 indicate that the Miocene sands contain waters with salinities of about 180,000 ppm sodium chloride compared with 68,000 ppm sodium chloride for the lower Hackberry sandstones. The effect of mixing moderately saline and highly saline waters on the stability of clays will need to be evaluated.

WELL LOCATIONS, STATUS OF WELLS, AND RESERVOIR PROPERTIES

The Port Arthur field has 18 wells (table 1 and fig. 15). Eleven of these wells produced gas and condensate from one or more lower Hackberry reservoirs (table 2); four wells (1, 6, 24, and 32) produced from the *Nodosaria* sandstone; three wells (5, 27, and 36) produced from the Vicksburg interval; two wells (28 and 34) were dry holes; and production from well 37 was reported as being suspended (table 1).

Gas was produced from the lower Hackberry (Frio) sandstones in the depth interval from 10,850 to 11,700 ft. Reservoirs designated as C, D, and E are laterally continuous and have the best characteristics for producing gas and water. The last producing well watered out and was plugged and abandoned in March 1981.

The lower Hackberry sandstones have high porosity, fairly high permeability, moderate temperature, and moderate to high salinity. Sidewall-core studies of seven wells in the field show that permeabilities range from 0.0 to 314 md and that porosities vary from 12.9 to 36.5 percent in the C reservoir. Two cores from the perforated interval of well 14 had an average permeability of 156.5 md and an average porosity of 33.4 percent. Average water saturation and oil saturation in the perforated interval were 65.2 percent and 1.55 percent, respectively.

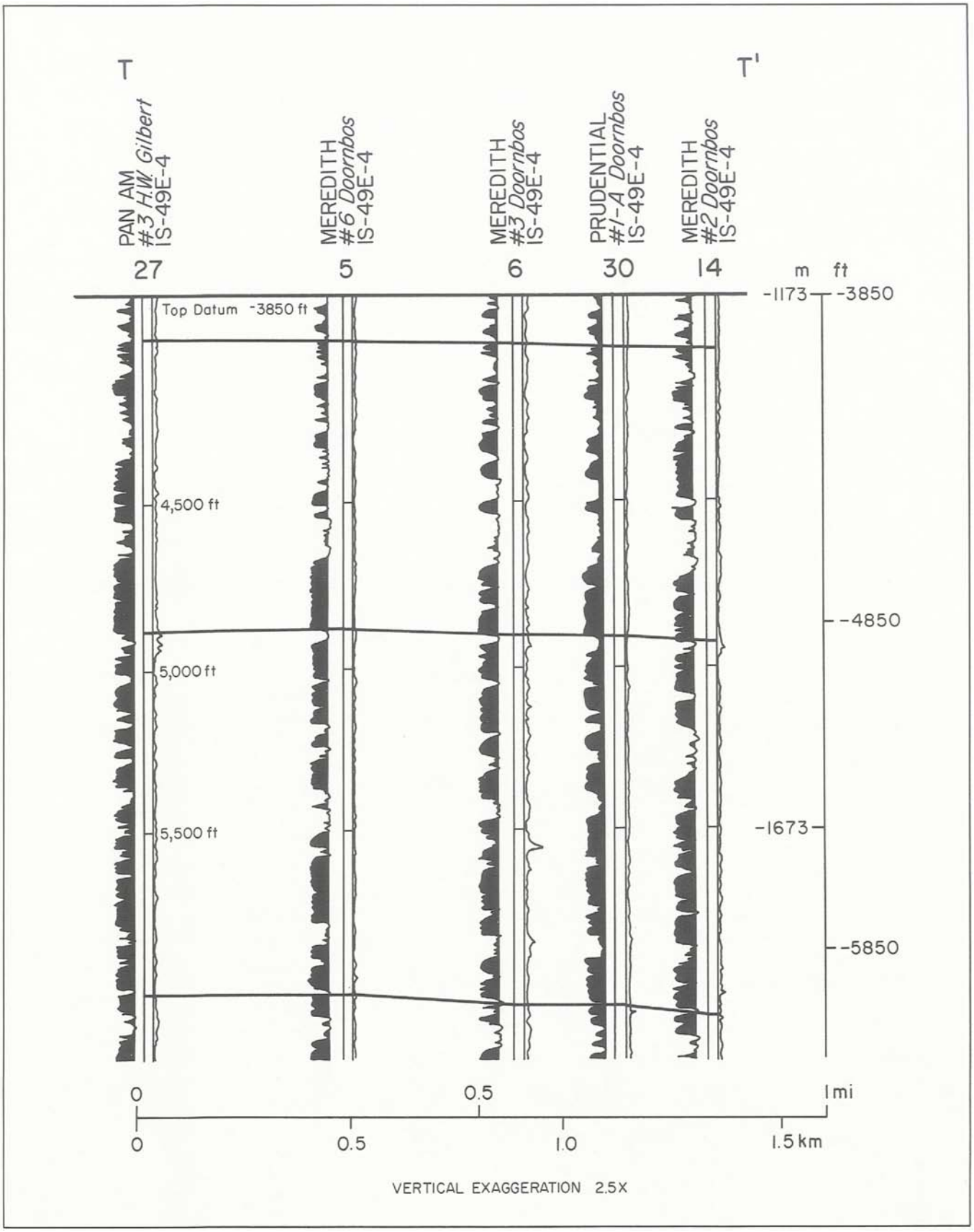

FIGURE 17. Cross section T-T' showing thickness of shallow Miocene sands suitable for disposal of waste salt water (see figure 15 for location of cross section).

TABLE 1. Identification, location, and status of wells, Port Arthur field, Jefferson County, Texas.

Well no.	Original operator and well name	Tobin grid	Well status*	Total depth (ft)
1	Meredith No. 1 Doornbos	1S-49E-4	P & A	12,290
5	Meredith No. 6 Doornbos	1S-49E-4	P & A	12,681
6	Meredith No. 3 Doornbos	1S-49E-4	P & A	12,200
11	Meredith No. 4 Doornbos	1S-49E-4	P & A	12,175
12	Meredith No. 5 Doornbos	1S-49E-5	P & A	12,352
14	Meredith No. 2 Doornbos	1S-49E-4	P & A	12,200
23	Kilroy & M.P.S. No. 1 Doornbos	1S-49E-9	P & A	12,160
24	Kilroy & M.P.S. No. 1 City of Port Arthur	1S-49E-9	P & A	12,001
27	Pan Am. No. 3 H.W. Gilbert	1S-49E-4	P & A	12,751
28	Texaco, Inc., No. 1 Port Arthur Refinery Fee	1S-49E-8	Dry	14,200
29	Halbouty & Pan Am. No. 2 Doornbos	1S-49E-9	P & A	12,202
30	Prudential No. 1-A Doornbos	1S-49E-4	P & A	11,809
31	Halbouty & Pan Am. No. 1 Doornbos	1S-49E-9	P & A	12,103
32	Kilroy & M.P.S. No. 2 Doornbos	1S-49E-9	P & A	12,208
34	Meredith No. 1 Doornbos - Port Arthur Vicksburg Gas Unit 1	1S-49E-5	Dry	14,125
35	J. C. Barnes No. 1 Swallow	1S-49E-9	P & A	12,000
36	Texaco, Inc., No. 1 Park Place Gas Unit	1S-49E-8	P & A	14,050
37	Kilroy No. 1 Booz	1S-49E-4	Sus.	12,641

*P & A - plugged and abandoned; Sus. - suspended (as defined in Weise and others, 1981, table 3, p. 52).

TABLE 2. Pressure gradients and production history by reservoir and well, Port Arthur field, Jefferson County, Texas.

Lower Hackberry reservoirs	Well no.*	Perforated interval (ft)	BHSIP gradient (psi/ft) Initial	Last	Production period	Cumulative production Gas (Bscf)	Cond. (bbl)
A-1	12	10,946-10,956	0.84	0.57	12/59-7/68	0.989	93,934
	35	10,966-10,978	0.80	0.74	8/60-5/61	0.138	-----
A-2	29	10,925-10,955	0.82	0.59	9/59-2/62	0.054	228
	6	10,936-10,946	0.83	0.54	3/66-8/71	0.784	31,492
	11	10,934-10,950	0.69	-----	12/59-9/61	0.121	-----
Upper B stringer	31	10,986-10,994	0.83	0.64	3/66-1/72	0.200	8,115
B	6	10,995-11,000	0.81	0.77	5/67-5/79	0.088	4,952
	30	10,994-11,002	0.73	-----	8/78-2/80	0.002	387
B-1	24	11,052-11,058	0.58	0.44	9/68-3/70	0.003	148
	23	11,021-11,029	0.82	0.78	6/62-9/65	3.323	172,158
B-2	31	11,077-11,101	0.84	0.69	9/59-1/66	13.343	720,286
C	23	11,128-11,131	0.75	0.64	7/65-8/71	1.249	38,404
	14	11,136-11,144	0.83	0.70	7/61-7/72	10.535	455,783
	6	11,130-11,135	0.70	0.45	8/71-12/72	0.099	2,301
	11	11,130-11,138	0.75	0.60	9/61-10/69	7.754	366,494
Upper D stringer	30	11,204-11,208	0.73	0.68	5/75-5/79	0.616	27,963
D	14	11,225-11,243	0.53	0.50	6/68-10/72	0.517	19,719
	6	11,218-11,228	0.82	0.63	3/60-4/66	4.310	174,229
	23	11,251-11,256	0.67	0.63	7/65-8/71	1.881	66,583
	24	11,250-11,257	0.65	0.62	1/68-8/68	0.126	6,430
E	14	11,276-11,286	0.83	0.66	5/59-12/60	1.620	87,638
	23	11,290-11,299	0.81	0.73	11/59-6/62	2.072	109,115
	6	11,296-11,301	0.80	0.73	3/66-8/71	0.552	24,357
Lower E stringer	24	11,387-11,391	0.70	-----	11/67-12/67	0.034	1,225
F	14	11,350-11,359	0.81	0.80	7/61-6/68	6.212	224,288
G	31	11,458-11,463	0.77	0.76	3/66-1/67	0.449	17,606
					Total	57.071	2,653,835

*Well locations are shown in figure 15; Tobin grids are shown in table 1.

RESERVOIR FLUID PROPERTIES

Methane Solubility

The solubility of methane in water and in sodium chloride solutions has been determined from laboratory measurements for salinities of 0 to 300 g/L, a temperature range of 160° to 464°F, and a pressure range of 3,500 to 22,500 psi (Price and others, 1981). Equations (1) and (2) below give the "best fit" to the average experimental data; either equation can be used.

$$\log_e CH_4^* = -1.4053 - 0.002332t + 6.30 \times 10^{-6}t^2 - 0.004038S - 7.579 \times 10^{-6}p + 0.5013 \log_e p + 3.235 \times 10^{-4}t \log_e p \quad (1)$$

Standard deviation of residuals = 0.0706
Multiple R = 0.9944

$$\log_e CH_4^* = -3.3544 - 0.002277t + 6.278 \times 10^{-6}t^2 - 0.004042S + 0.9904 \log_e p - 0.0311 (\log_e p)^2 + 3.204 \times 10^{-4}t \log_e p \quad (2)$$

Standard deviation of residuals = 0.0709
Multiple R = 0.9943

where t = temperature (°F)
S = salinity (g/L)
p = pressure (psi)

*CH_4 is in standard cubic feet (scf) per petroleum barrel (42 gallons) at 25° C (77° F) and 1 atmosphere pressure.

Both equations show that an increase in formation fluid pressure or temperature causes an increase in methane solubility, whereas an increase in salinity reduces methane solubility. In general, pressure and temperature are more predictable than is salinity, which varies greatly throughout the Gulf Coast area. Because salinity data from chemical analyses of water samples are seldom available, SP well logs are often used to calculate salinity. The reliability of the SP method depends primarily on the chemical properties of the mud and the mud weight used in the borehole when the well is logged. Other factors, such as the relation between the temperature variations and the resistivities of mud (R_m) and mud filtrate (R_{mf}), are also involved. The Schlumberger Limited (1978) chart, Gen 7, gives satisfactory salinity values for some mud systems. However, major errors can occur when high-density lignosulfonate muds are used because R_{mf} values listed on well log headings are commonly too large and the resulting calculated salinity is too low (Dunlap and Dorfman, 1981).

Most salinities in this study were determined from the SP log by the Schlumberger Gen 7 method because most muds were either lime-base or gypsum-base oil emulsion mixtures. These calculated salinities are thought to be reasonably reliable, according to comparisons with chemical analyses of water samples from the E and F sandstones in well 14 (table 3). Salinities calculated for these two sandstones are only 2 to 5 percent less than the total dissolved solids content of the water samples.

The curve method (Dunlap and Dorfman, 1981) was used for determining salinity in wells 30 and 37, which were logged with lignosulfonate mud. These two wells were the only ones in which calculated salinities exceeded 100,000 ppm sodium chloride in the lower Hackberry sandstones (table 3).

As stated earlier, formation fluid temperature influences methane solubility. In this report, wellbore temperatures taken from well logs have been corrected to equilibrium values that represent formation fluid temperatures by the following equation by Kehle (1971):

$$T_E = T_L - 8.819 \times 10^{-12}D^3 - 2.143 \times 10^{-8}D^2 + 4.375 \times 10^{-3}D - 1.018 \quad (3)$$

where T_E = equilibrium temperature (°F)
T_L = temperature recorded on well log header (°F)
D = depth (ft)

In dry holes where drill-stem-test pressure data are not available, formation fluid pressures were derived from shale resistivity or acoustic travel time data by using the method of Hottmann and Johnson (1965). Shale resistivity values (R_{sh}) from amplified short normal resistivity curves of induction logs were plotted as a function of depth for both hydropressured and geopressured zones. The normal compaction curve is drawn by a least-squares regression method. All R_{sh} data fall near this curve when shales are normally pressured or slightly geopressured; R_{sh} data to the left of the curve

TABLE 3. Salinity, temperature, pressure, and methane solubility at initial reservoir conditions, lower Hackberry reservoirs, Port Arthur field, Jefferson County, Texas.

Lower Hackberry reservoirs	Well no.[a]	Perforated interval (ft)	Salinity (ppm[b] or mg/L[c] NaCl)	Equilibrium temperature (°F)	Initial BHSIP (psi)[d]	Methane solubility (scf/bbl)[e]
A-1	12	10,946-10,956	33,500	214	9,192	29.41
	35	10,966-10,978	44,200	224	8,778	28.41
A-2	29	10,925-10,955	27,100	208	8,917	29.18
	6	10,936-10,946	68,100	212	9,059	24.96
	11	10,934-10,950	44,900	217	7,542	25.64
Upper B stringer	31	10,986-10,994	68,000	219	9,171	25.72
B	6	10,995-11,000	66,700	214	8,955	25.14
	30	10,994-11,002	101,000[f]	232	8,029	21.67
B-1	24	11,052-11,058	72,000	237	6,412	22.35
	23	11,021-11,029	59,500	230	9,041	27.54
B-2	31	11,077-11,101	86,300	223	9,302	24.18
C	23	11,128-11,131	73,300	232	8,398	25.15
	14	11,136-11,144	72,600	243	9,284	27.61
	6	11,130-11,135	68,600	218	7,775	23.55
	11	11,130-11,138	55,300	224	8,350	26.41
Upper D stringer	30	11,204-11,208	132,000[f]	245	8,180	19.79
D	14	11,225-11,243	69,900	247	5,954	22.56
	6	11,218-11,228	56,700	222	9,203	27.36
	23	11,251-11,256	63,800	234	7,540	25.02
	24	11,250-11,257	77,100	246	7,315	24.24
E	14	11,276-11,286	65,200 68,790[c]	249	9,400	29.36
	23	11,290-11,299	64,200	235	9,148	27.63
	6	11,296-11,301	74,700	224	9,023	25.19
Lower E stringer	24	11,387-11,391	77,700	250	8,012	25.71
F	14	11,350-11,359	63,500 64,970[c]	252	9,197	29.59
G	31	11,458-11,463	78,000	237	8,820	25.69

[a]Well locations shown in figures 5 and 15; Tobin grid given in table 1.
[b]From SP log using the Schlumberger Gen 7 method.
[c]Total dissolved solids from water sample analyses, mg/L.
[d]From completion cards or calculated from WHSIP.
[e]Calculated from equation of Price and others (1981) at initial conditions of pressure, temperature, and salinity.
[f]From the SP log using method of Dunlap and Dorfman (1981).

are lower than normal, indicating that pressure gradients are significantly higher than normal and may approach 1 psi/ft in highly geopressured zones. Deviations of R_{sh} data points from the normal compaction curve were calibrated from shut-in pressures or pressure gradients measured by drill-stem tests (DST) in wells (Gregory and others, 1980).

Aquifers in the lower Hackberry sandstones in the Port Arthur field initially contained waters characterized by high geopressures, moderate to high salinities, and moderate temperatures and methane solubilities (table 3). Distribution maps (figs. 18 to 21) demonstrate the interrelationships between these parameters in the C sandstone. There are two high-pressure areas in the field (fig. 18); one is a large area aligned along strike that includes well 12, and the other is a smaller area updip that includes wells 5 and 6. The highest temperatures occur near the center of the structure (fig. 19) and exceed 240° F only in wells 14 and 24. Salinities increase rapidly from 72,000 ppm sodium chloride in well 14 to 157,000 ppm sodium chloride in well 30, located less than 1,000 ft northwest of well 14 (fig. 20). The high salinities at wells 30 and 37, however, may be caused by the intrinsic unreliability of the curve calculation method discussed earlier. Salinities in the C sandstone (excluding wells 30 and 37) vary from 55,300 ppm sodium chloride (well 11) to 99,800 ppm sodium chloride (well 31) and average 70,050 ppm sodium chloride. The distribution of salinities in the Port Arthur field is more strike aligned (fig. 20) than are the geologic structural features (fig. 15); as would be expected, a similar strike-aligned trend is evident for methane solubility (fig. 21).

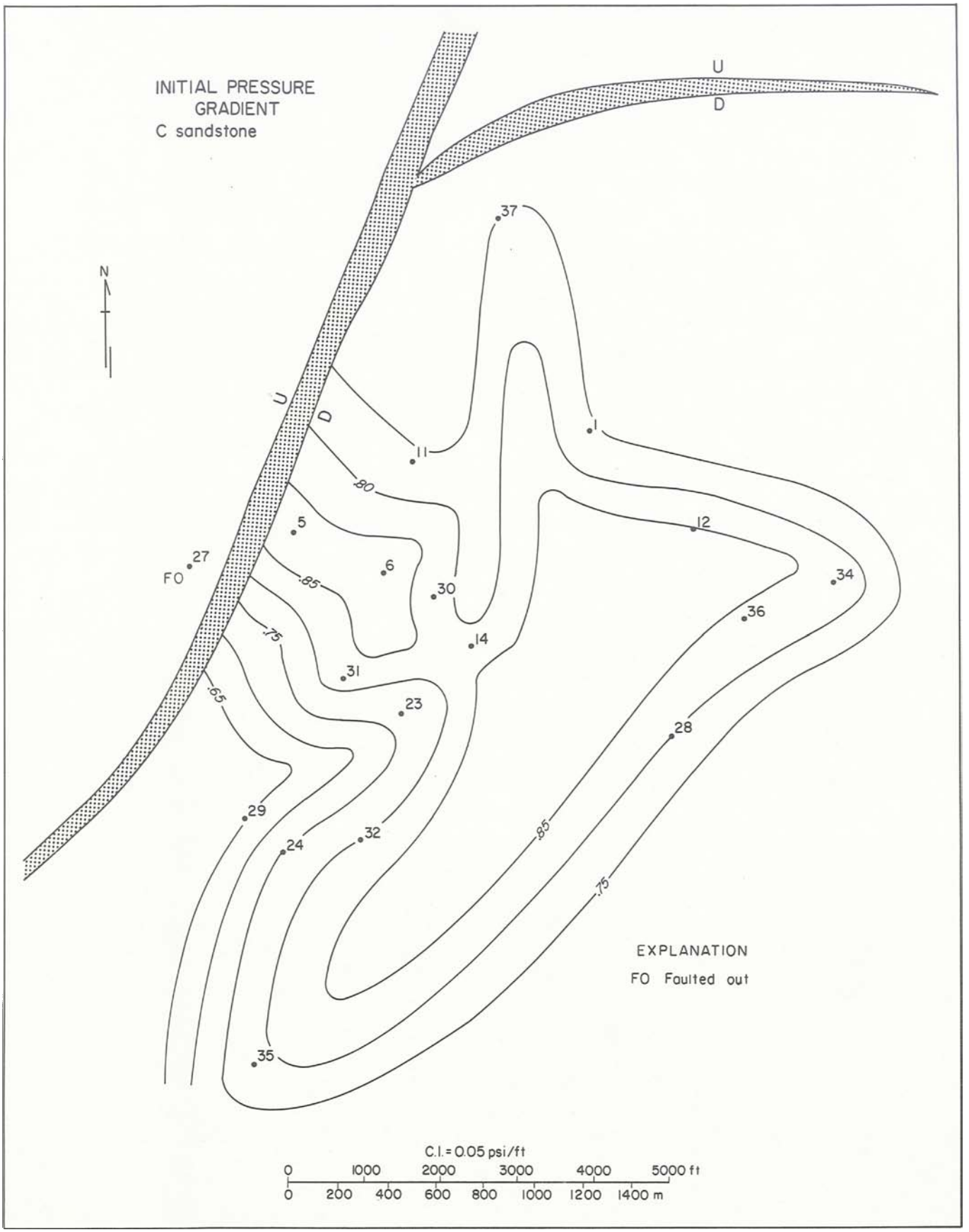

FIGURE 18. Distribution of initial pressure gradients (psi/ft), Hackberry C sandstone, Port Arthur field.

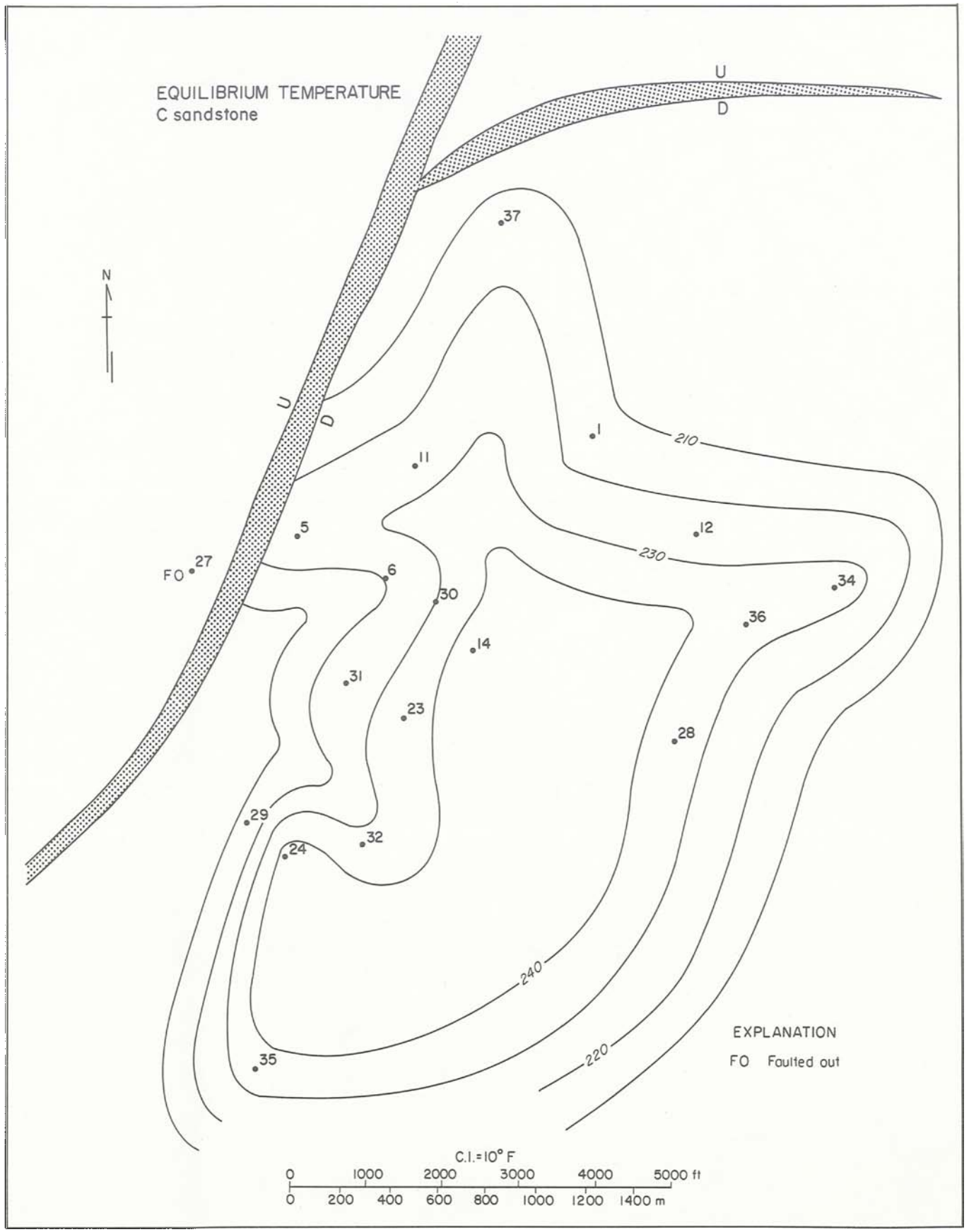

FIGURE 19. Distribution of temperature (°F), Hackberry C sandstone, Port Arthur field.

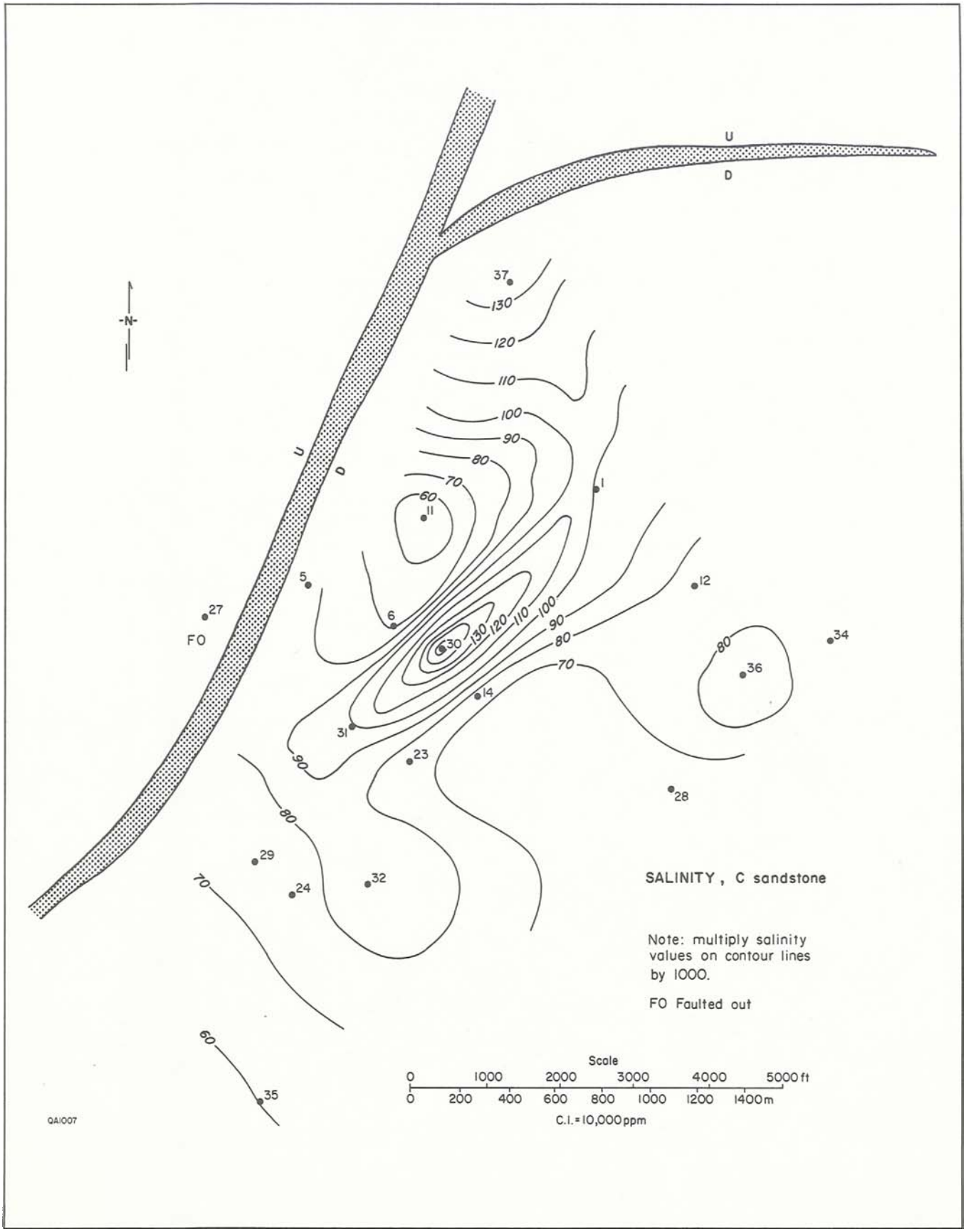

FIGURE 20. Distribution of salinity, Hackberry C sandstone, Port Arthur field.

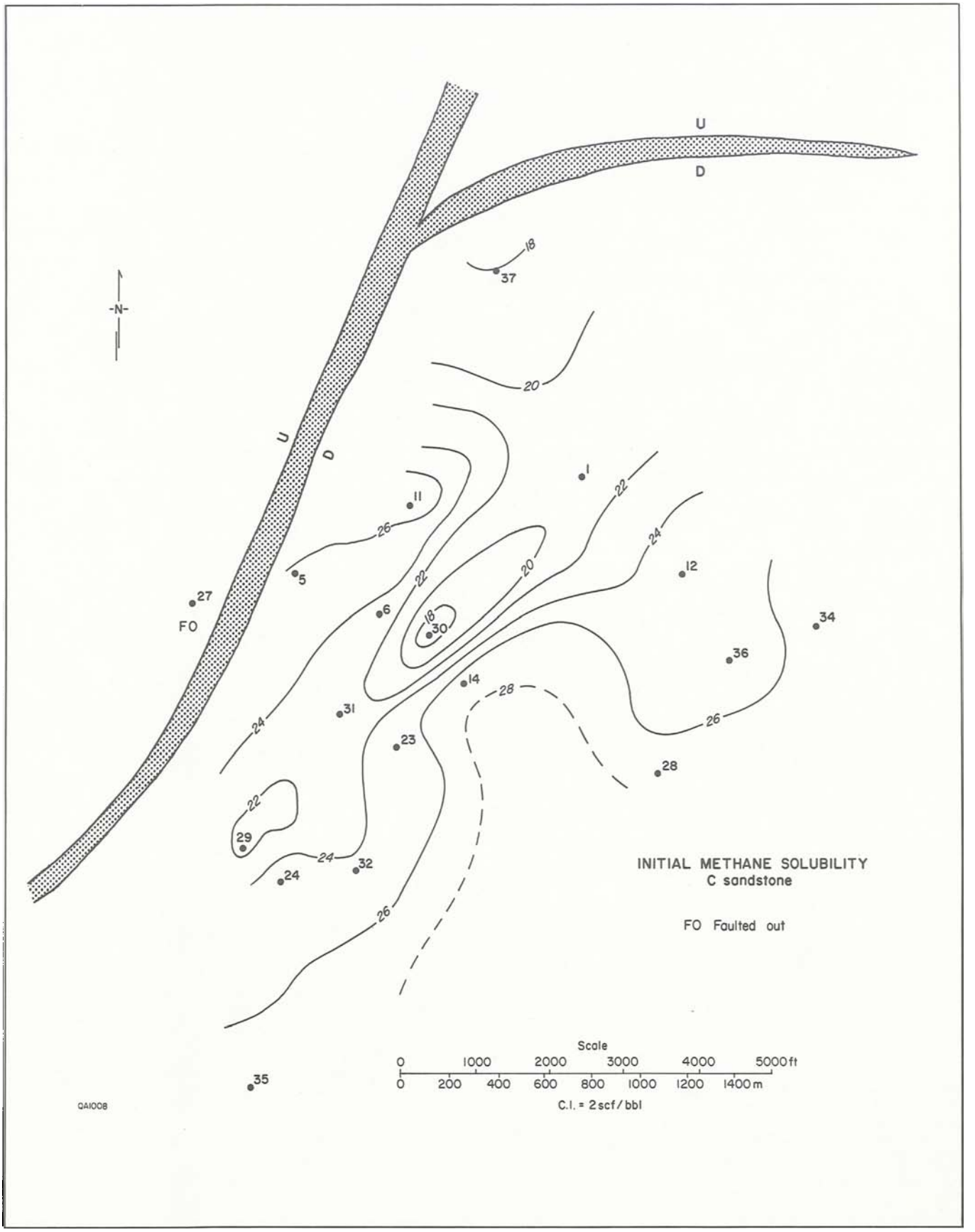

FIGURE 21. Distribution of initial methane solubility, Hackberry C sandstone, Port Arthur field.

Values of pressure, salinity, temperature, and methane solubility for the best thick Hackberry aquifers were plotted versus depth at original reservoir conditions for well 14 (fig. 22). Solubility values increase with depth; typical data vary from 4 to 5 scf/bbl at a depth of 2,000 ft and from 24 to 30 scf/bbl at 11,000 to 12,000 ft. In the lower Hackberry sandstone units, the average initial methane solubility is 25.7 scf/bbl, on the basis of a pressure gradient of 0.76 psi/ft, a salinity of 67,900 ppm, a temperature of 231° F, and an average depth of 11,150 ft. This means that on the average, only 514 Mscf/d of solution gas could be obtained from a well producing methane-saturated formation water at a rate of 20,000 bbl/d.

It is essential, therefore, to produce a substantial amount of free gas in addition to solution gas to make drilling a test well economically viable. The presence of many thick aquifers in the Hackberry sandstone units should simplify the task of finding reservoirs having suitable combinations of gas and water that will produce with a gas/brine ratio greatly exceeding the solution gas/brine ratio.

During primary production, the amount of methane dissolved in formation waters decreases as reservoir pressures decline. For

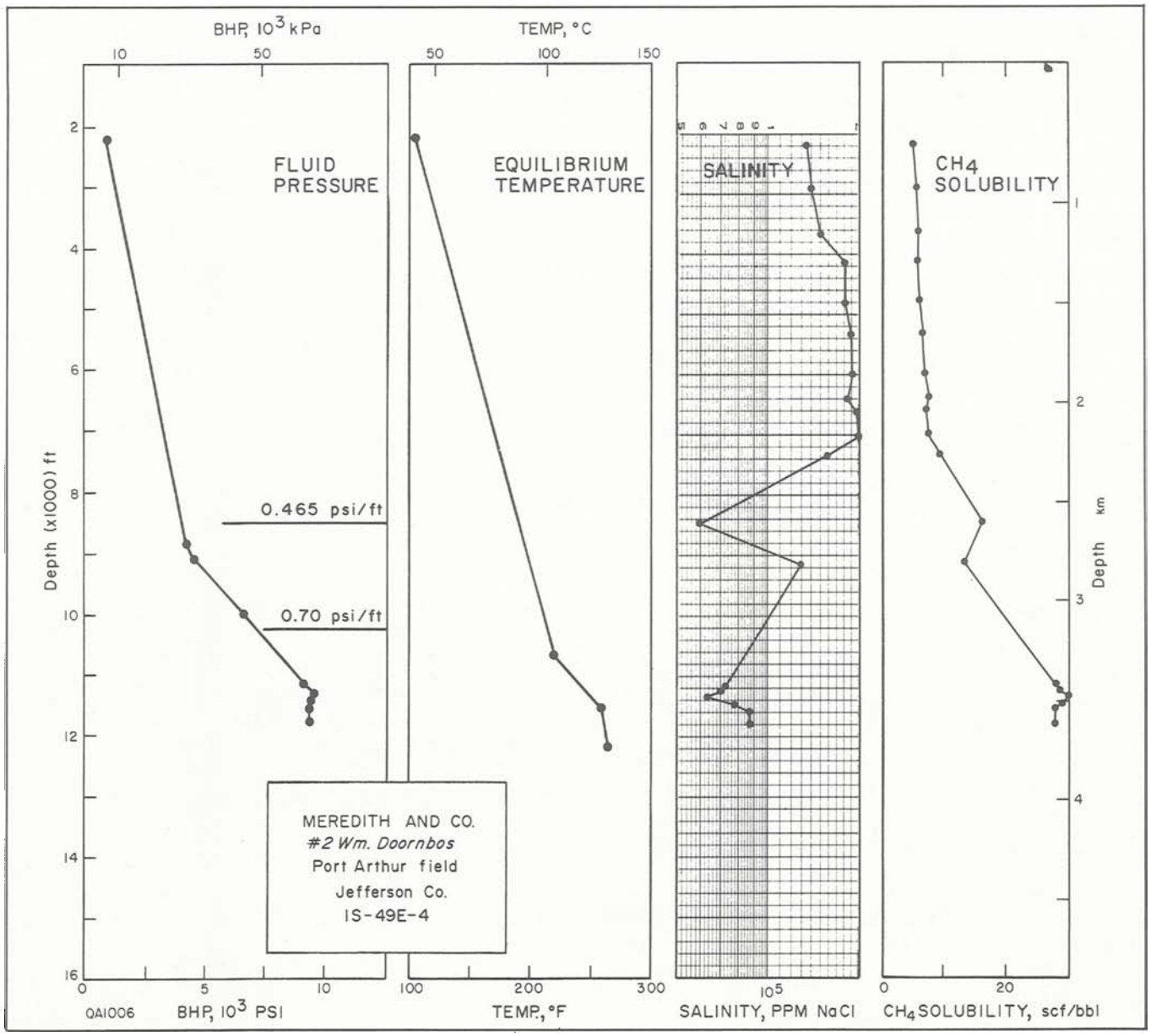

FIGURE 22. Pressure, temperature, salinity, and methane solubility versus depth, well 14, Port Arthur field.

example, the bottom-hole flowing pressure in the Meredith No. 2 Doornbos decreased 27 percent over a period of about 10 years in the C reservoir (11,136 to 11,144 ft). The corresponding decrease in methane solubility was 16 percent, changing from 27.7 scf/bbl in 1961 to 23.3 scf/bbl in 1971. It was assumed that reservoir temperature and formation-water salinity remained constant at 243° F and 72,600 ppm sodium chloride, respectively.

Temperature and Pressure Gradients

Temperatures from well log headers were corrected to equilibrium values and plotted versus depth (fig. 23). A geothermal gradient of 2.58° F/100 ft was determined by least-squares fit to the temperature data in sandstones below a depth of 10,500 ft in the geopressured zone. The top of the lower Hackberry sandstones near the structural high occurs at an average depth of about 10,850 ft.

Temperature data from well logs in the Port Arthur field were very limited for sands at depths of less than 10,500 ft. Additional temperature data from other wells in Jefferson County were used to extrapolate the temperature trend in the depth interval above 10,500 ft to a mean surface temperature of 72° F. A geothermal gradient of 1.3°F/100 ft was established for the shallow section.

The original formation fluid pressures in the Port Arthur field were obtained from bottom-hole shut-in pressures (BHSIP) measured by drill-stem tests and from shale resistivity data using the method of Hottmann and Johnson (1965). The top of geopressure in the lower Hackberry sandstones was estimated to be 8,900 ft by plotting BHSIP from DST versus depth and using average pressure gradients from shale resistivity data to extrapolate the trend line until it crosses the pressure gradient line of 0.465 psi/ft (fig. 24). Top of geopressure (8,900 ft) in the Port Arthur field is deeper than the 8,000 ft estimated for Jefferson County.

WELL LOG ANALYSES

Log analyses of Frio sandstones in the Port Arthur field provided a basis for determining the porosity and the original gas-water contact (GWC). To do this, it was necessary to establish net-sandstone thickness, porosity, and water saturation at each penetration of the sandstone being investigated. Details of the computation methods and results for the B-2, D, E, F, G, and H sandstones were reported by Gregory and others (1983a); the methods used in this study of the C sandstone (Ausburn and others, 1982) are summarized as follows.

Only one porosity log was available from the field (sonic log for well 37). The interval transit times and the correlative induction log resistivities provided a basis for estimating formation factor relations. The apparent relation between formation factor (F) and porosity (Ø) was found to be

$$F = 1.75 \times \emptyset^{-1.81} \quad (4)$$

and water saturation (S_w) was related to the resistivity ratio (R_o/R_t) by the equation

$$S_w = (R_o/R_t)^{-1/n} \quad (5)$$

where R_t = true resistivity of rock obtained from the induction log in the zone being investigated (ohm-meters)

R_o = resistivity of rock obtained from the induction log in a zone that is interpreted to be 100-percent saturated with water (ohm-meters)

n = saturation exponent, assumed to be 1.8

Using the established formation factor relation (equation 4) and resistivity values in zones interpreted to be wet ($S_w = 100$), we were able to estimate porosity from resistivity values for zones near the intervals being studied in each wellbore. For example, the porosity $\emptyset_w$ of the wet zone was computed from the relation

$$\emptyset_w = (aR_w/R_o)^{1/m} \quad (6)$$

where $a = 1.75$

$m = 1.81$

R_w = resistivity of water computed from salinity data (ohm-meters)

These wet-zone porosities were usually assigned to nearby zones being studied, but

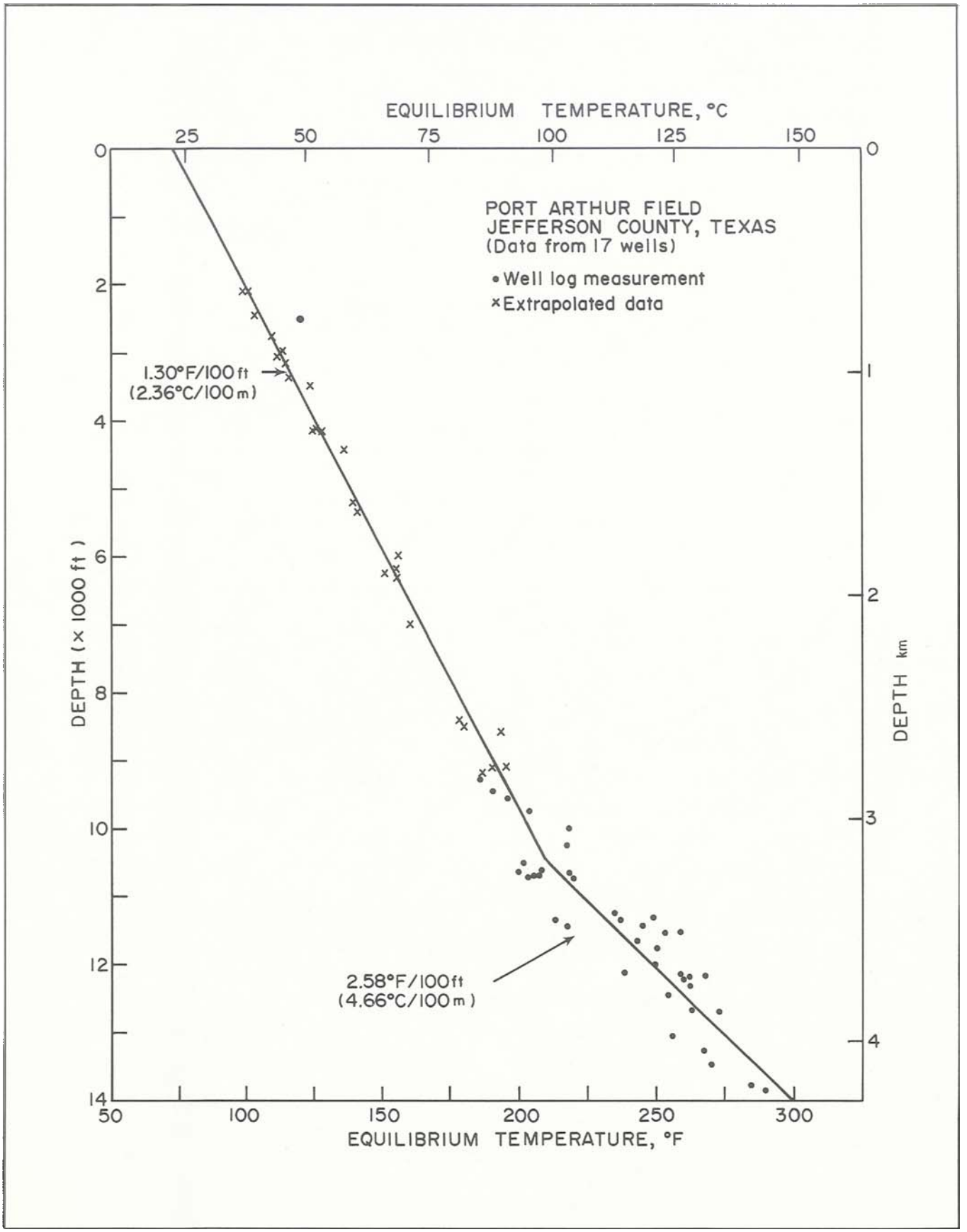

FIGURE 23. Geothermal gradients, Port Arthur field.

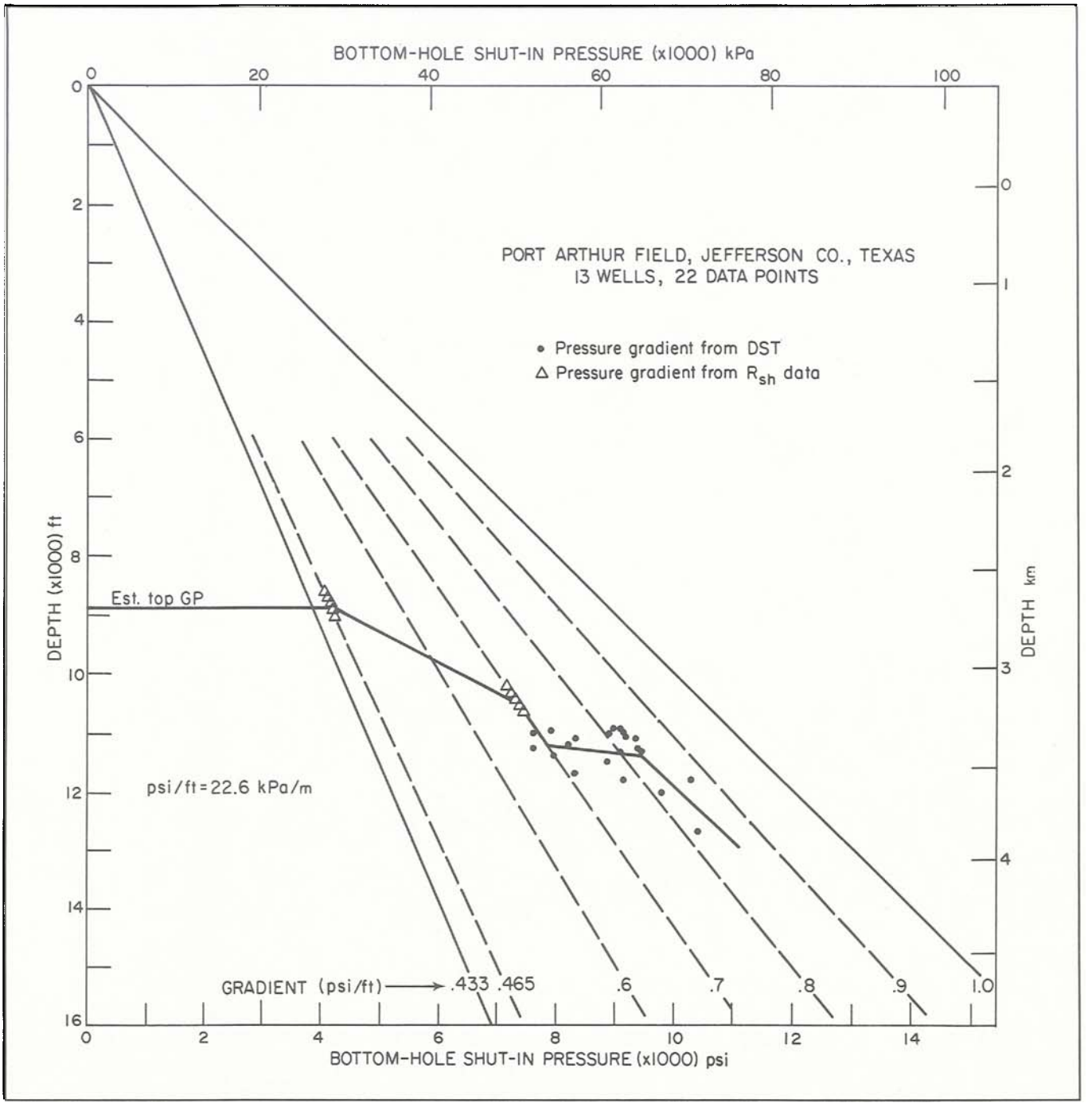

FIGURE 24. Bottom-hole shut-in pressure versus depth for 13 wells, Port Arthur field.

sidewall core data, where available, were used to guide the assignments. A comparison of porosity distribution plots (fig. 25) shows that porosity from sidewall core data peaks at higher values than do porosities from sonic log data or from resistivity data.

The original GWC was determined by inspection of the computed values of S_w. When values of S_w were consistently above 65 percent, a possible GWC was noted. These individual well values were compared, and the best estimate of GWC was determined by find-

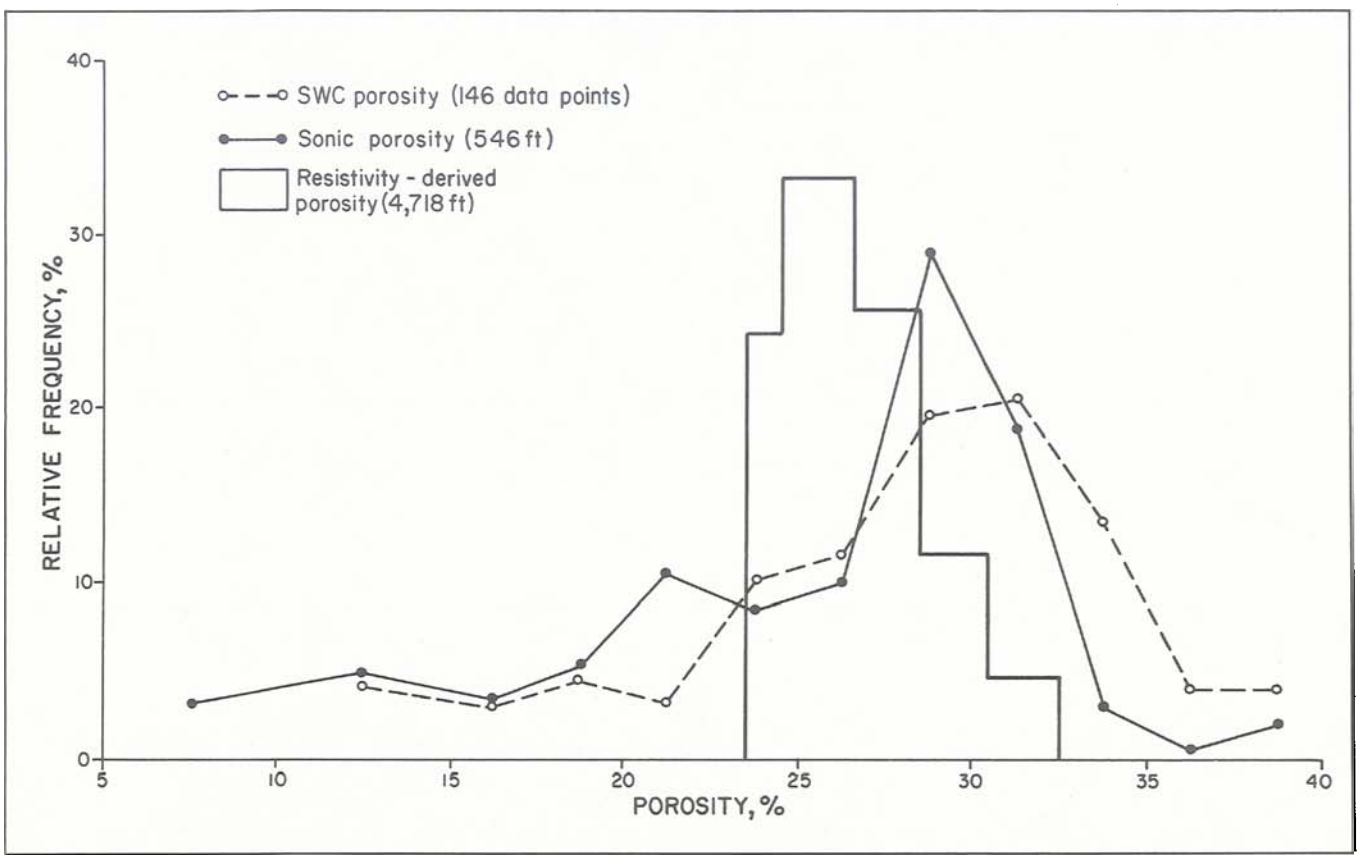

FIGURE 25. Porosity distribution, lower Hackberry sandstones, Port Arthur field.

ing the subsea depth compatible with the individual well determinations and existing structure and stratigraphic interpretations. The apparent GWC was determined to be −11,150 ft for the C sandstone, as indicated on the structure map (fig. 15).

SEISMIC DATA ACQUISITION AND PROCESSING

Seismic data (fig. 26) for this project were used to (1) provide structural information to supplement geological interpretations in areas with poor well control, (2) determine location and geometry of faults, (3) locate boundaries of gas reservoirs and aquifers, and (4) evaluate seismic reflection response to low saturations of free gas dispersed in the water-invaded zones of watered-out reservoirs. The detection of low saturations of free gas, approximately 5 percent or less, seems to be possible from general theoretical considerations (Geertsma, 1961) and from laboratory velocity measurements (Domenico, 1976). The aforementioned item 4 was intended to address the crucial question of whether dispersed gas in Tertiary sediments can be detected by seismic data. Several types of data were obtained as listed below.

1. Line A was recorded in 1980 using a thumper source. The data were recorded with a 200-ft group interval and a 24-fold stack from a 48-trace cable.
2. Lines 1, 2, and 3 were recorded in 1973 using a Vibroseis source (sweep 48 to 12 Hz). A 330-ft group interval, 24-trace cable developed a 12-fold stack.
3. Line B was recorded in 1979 using a dynamite source (10 pounds at 77 ft). A 330-ft group interval, 48-trace cable, and 12-fold stack were recorded.
4. Line 4 was recorded in 1969 using a dynamite source (15 pounds at 73 ft). A 300-ft group interval, 24-trace cable, and 6-fold stack were used.

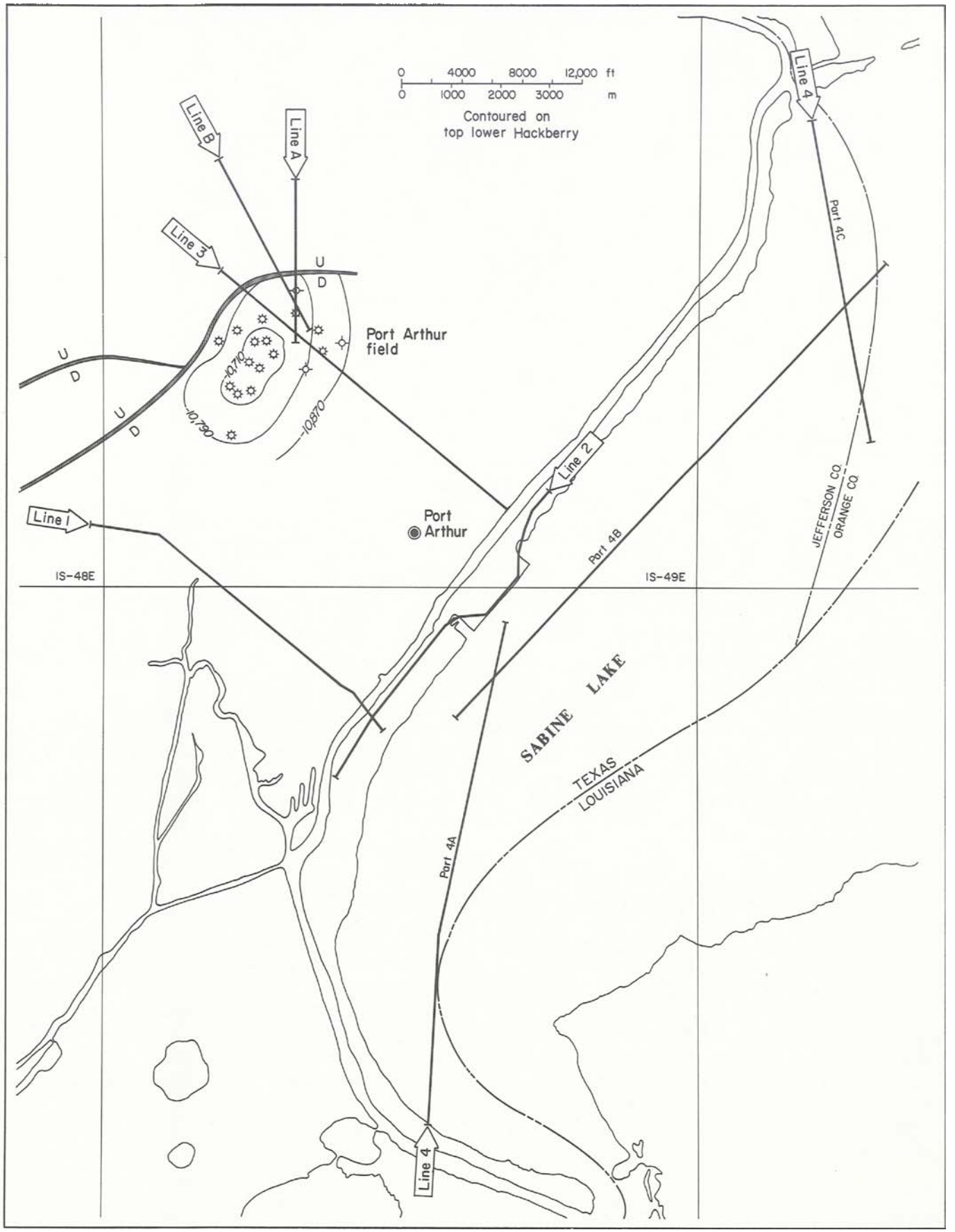

FIGURE 26. Location of seismic lines in the Port Arthur area.

This wide variation in energy source, group geometry, and stack fold results in appreciable differences in data quality, particularly when a broad-band spectral content is needed for detailed stratigraphic interpretation. Wavelet processing was used to compensate for source differences and the resulting character differences.

Data processing* focused on improving the interpretability of the seismic sections. The first approach was to shape the wavelet into a narrow symmetrical form and to migrate the data to enhance lateral resolution. The processing sequence, listed below, was intended to produce seismic sections with a near zero phase wavelet with the broadest spectral content supportable with the signal-to-noise ratio of the data:

1. Demultiplexing
2. Correlating if needed
3. Applying a gain-leveling function
4. Performing trace-to-trace normalization
5. Correcting field statics and geometry
6. Sorting to CDP gathers
7. Making velocity determination (one per km)
8. Correcting residual statics
9. Stacking
10. Deconvolution (predictive)
11. Enhancing time variant statistical wavelet
12. Performing migration
13. Converting to relative acoustic impedance sections

The objective of enhancing resolution by broadening the spectral bandwidth and by migration was severely hampered by the very poor signal-to-noise ratio of the data. Data quality was adequate for structural interpretation but was unsuitable for detailed reservoir delineation or detection of gas zones.

Seismic Modeling

Models using synthetic seismograms can show what kind of seismic response should be expected from known subsurface geology. Only limited well data were available for predicting acoustic properties. Thus the modeling effort focused on demonstrating the detectability of reservoir details in synthetic seismic data and on relating these data to the actual seismic data where possible. Modeling was applied to varying conditions of bandwidth, noise, and rock velocities.

Well data were used to develop the subsurface geologic model (fig. 27). Thick beds of lower Hackberry sandstones were correlated from well to well and projected onto the line of section that coincides with seismic line 3. Structure maps prepared on sand tops were useful in guiding the projection. Different gas sandstone velocities were assumed for the five models (fig. 27) because of the uncertainty of the values of this important parameter. Bed velocities were derived in part from the sonic log of the Kilroy No. 1 Booz (well 37), and density was computed from the relation developed by Gardner and others (1974).

The real seismic data (fig. 28) are very noisy and have poor reflection coherence. Interpretation of these data indicates that the top of the Hackberry C sandstone does not roll over into the major fault as much as the geologic model suggests. Comparisons can be made directly between the modeled synthetic sections discussed below and the corresponding part of seismic line 3 (fig. 28).

Effects of bandwidth are examined in the synthetic seismic sections of figures 29, 30, and 31. Each bed boundary of the geologic model (fig. 27) is represented by a spike that is two samples (2 ms) wide (fig. 29). These spikes are very broadband (0 to 500 Hz) and represent the ultimate resolution for the sample rate used. Amplitudes and polarities of the reflection coefficients at each bed boundary and each fluid contact are indicated by the size and sign of the spikes. Gas sandstones are shown by the shaded zones (fig. 29). Butterworth bandpass wavelets, used in each synthetic section, are shown at CDP 205 near the time of 2.97 seconds.

Synthetic sections, based on bed velocities in model 1, were made partly to show the effect of increasing the bandwidth (with no noise) from 15 to 45 Hz (fig. 30) to 15 to 65 Hz (fig. 31). Clearly, the broader bandwidth data having higher resolution without noise (fig. 31) enhance details that are essential to reservoir delineation. However, it is still not possible to

*The data processing and seismic modeling was by GeoQuest International. This discussion summarizes the more detailed report by Meanley (1982).

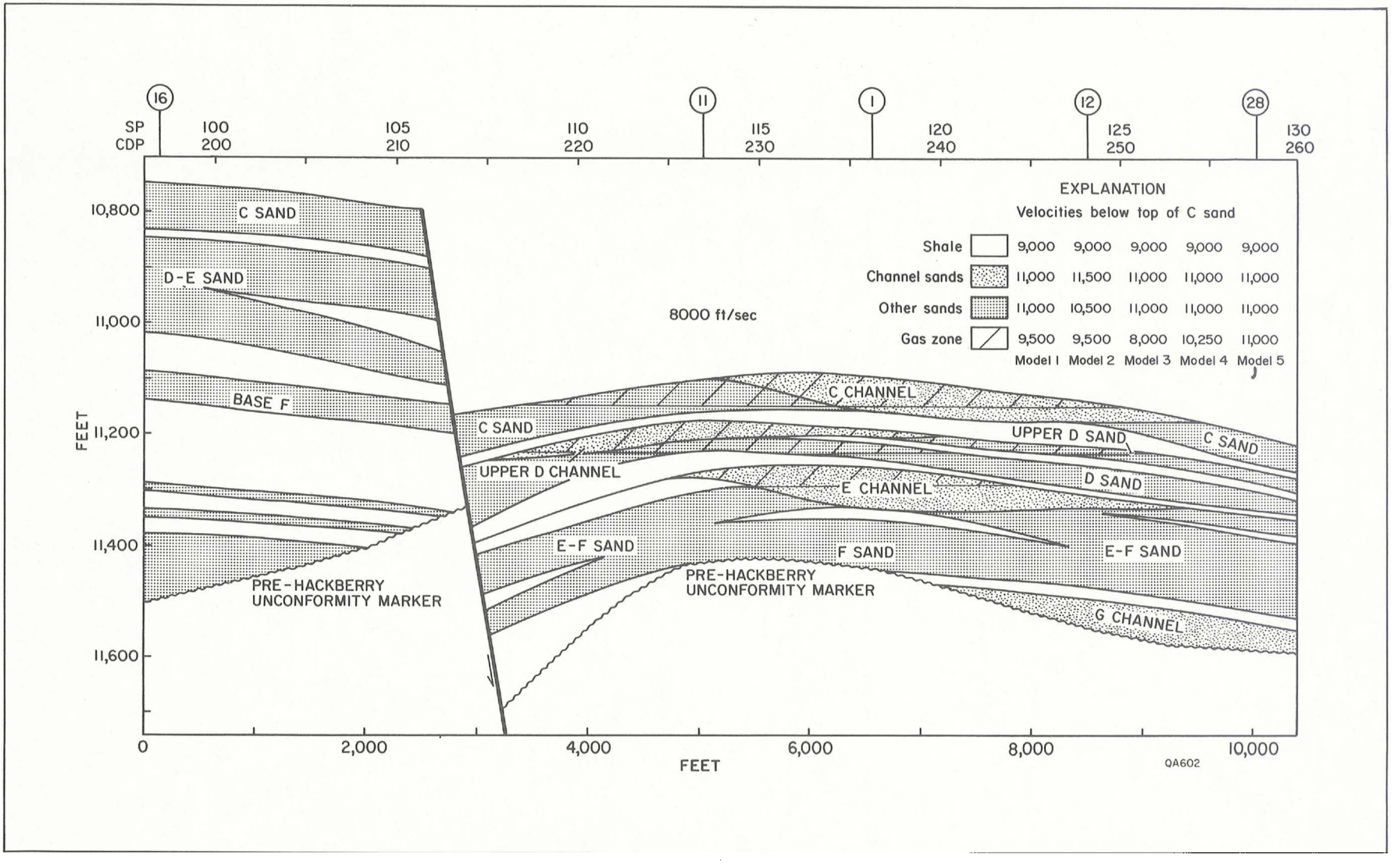

FIGURE 27. Model of the Hackberry sands along a cross section coincident with seismic line 3.

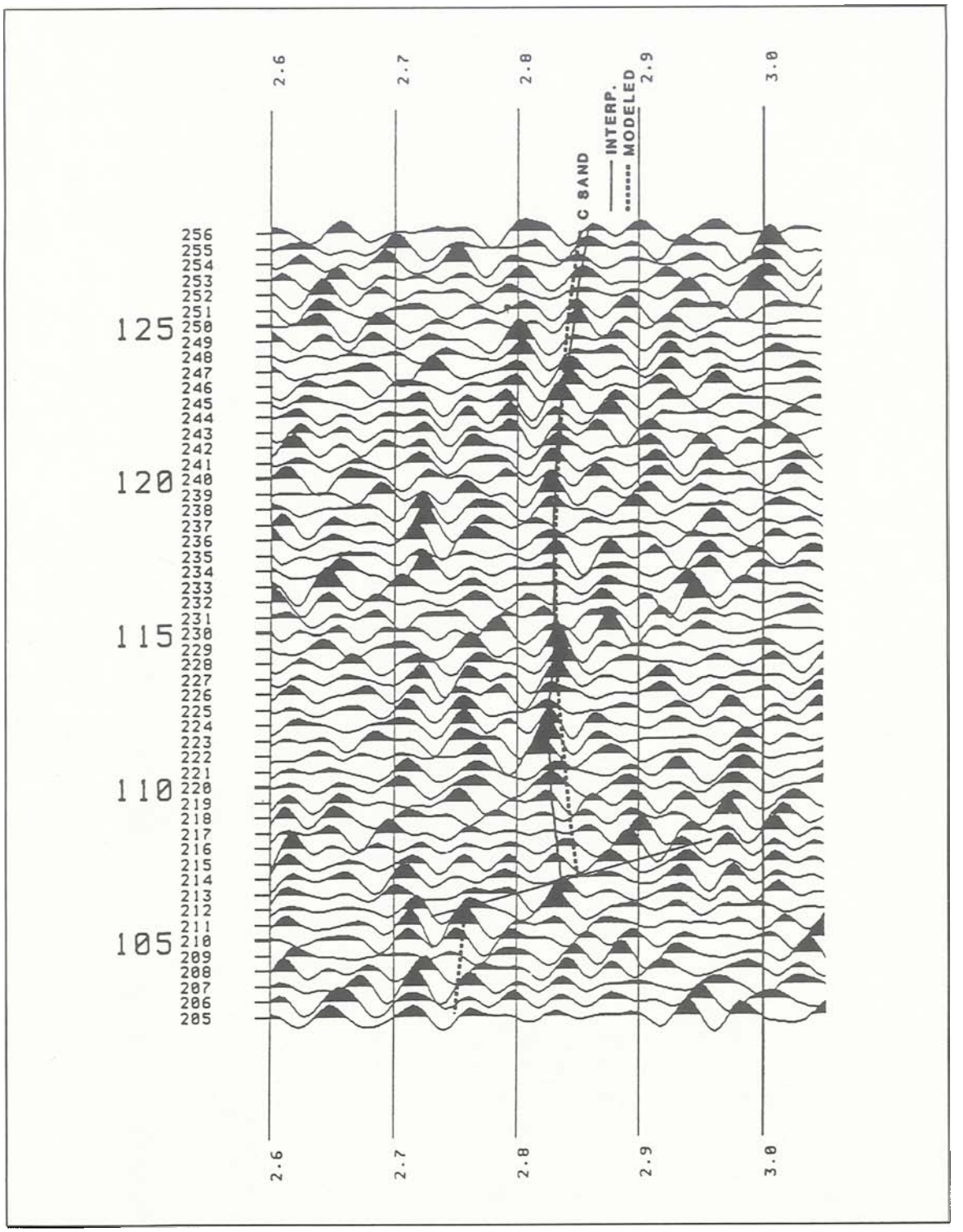

FIGURE 28. Line 3 showing interpreted and modeled top of Hackberry C sandstone.

map the reservoirs or to determine the lateral extent of hydrocarbon zones. The only clear indication of gas is the amplitude reduction (dimming) of the top reflection of the C sandstone over the crest of the structure. This is caused by the reduction of velocity contrast with respect to the overlying shales. As specified in model 1 (fig. 27), the gas sandstone velocity (9,500 ft/sec) is intermediate between the water sandstone velocity (11,000 ft/sec) and the shale velocity (9,000 ft/sec). In the real seismic data (fig. 28), there is no clear indica-

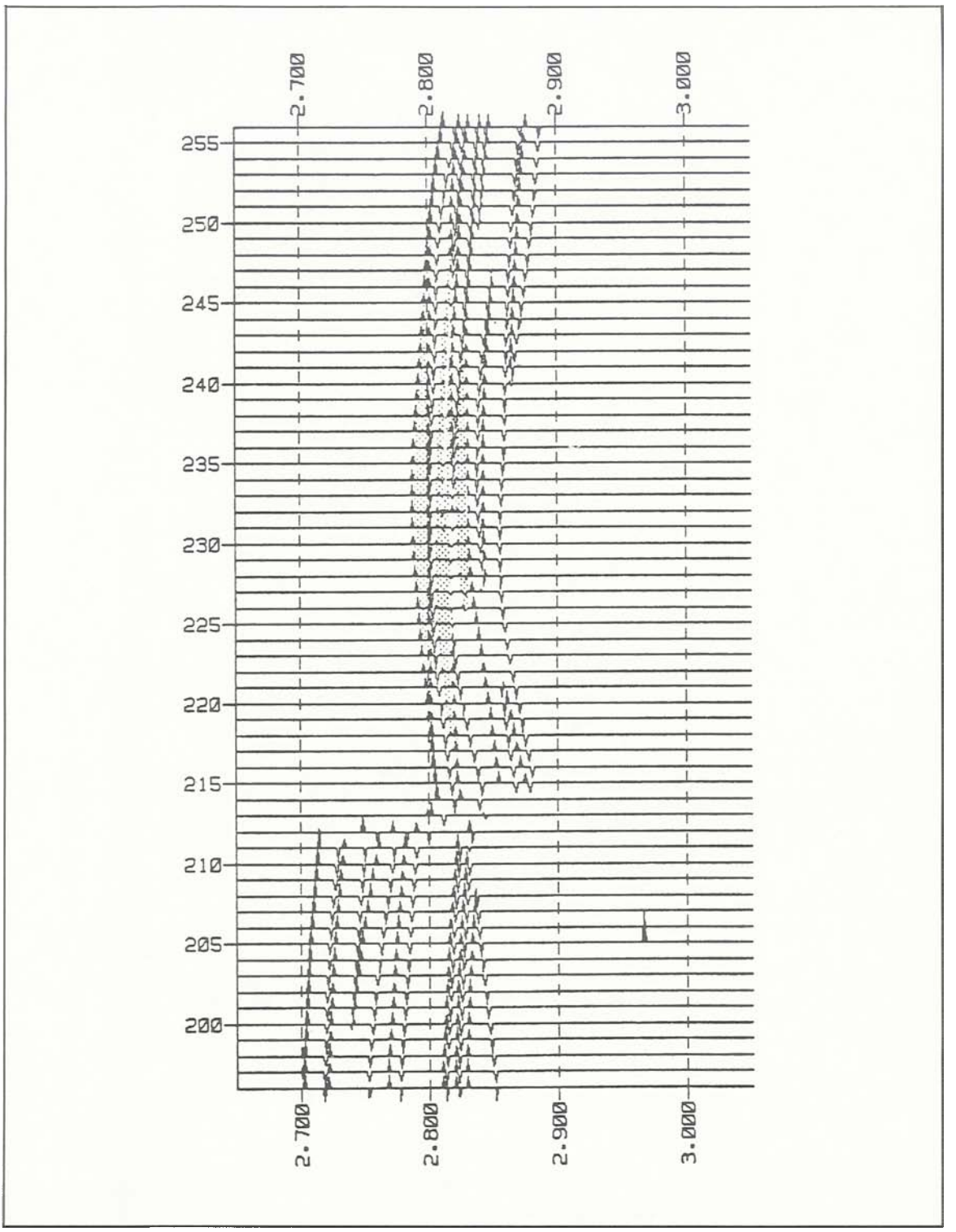

FIGURE 29. Spike synthetic seismic section with gas sands shaded (model 1), Port Arthur field.

tion of dimming; only noise fluctuations occur. A second dim zone in the synthetic sections occurs at the structural crest of the central part of the reservoir complex at a time of 2.82 seconds. This dimming feature simply indicates that here the acoustic contrasts approach zero. Dimming can also be caused by thinning of the reservoir bed or by contamination from nonreservoir rock. These other causes of dimming introduce ambiguity and complicate the interpretation. The only classic hydrocarbon indicator present in these syn-

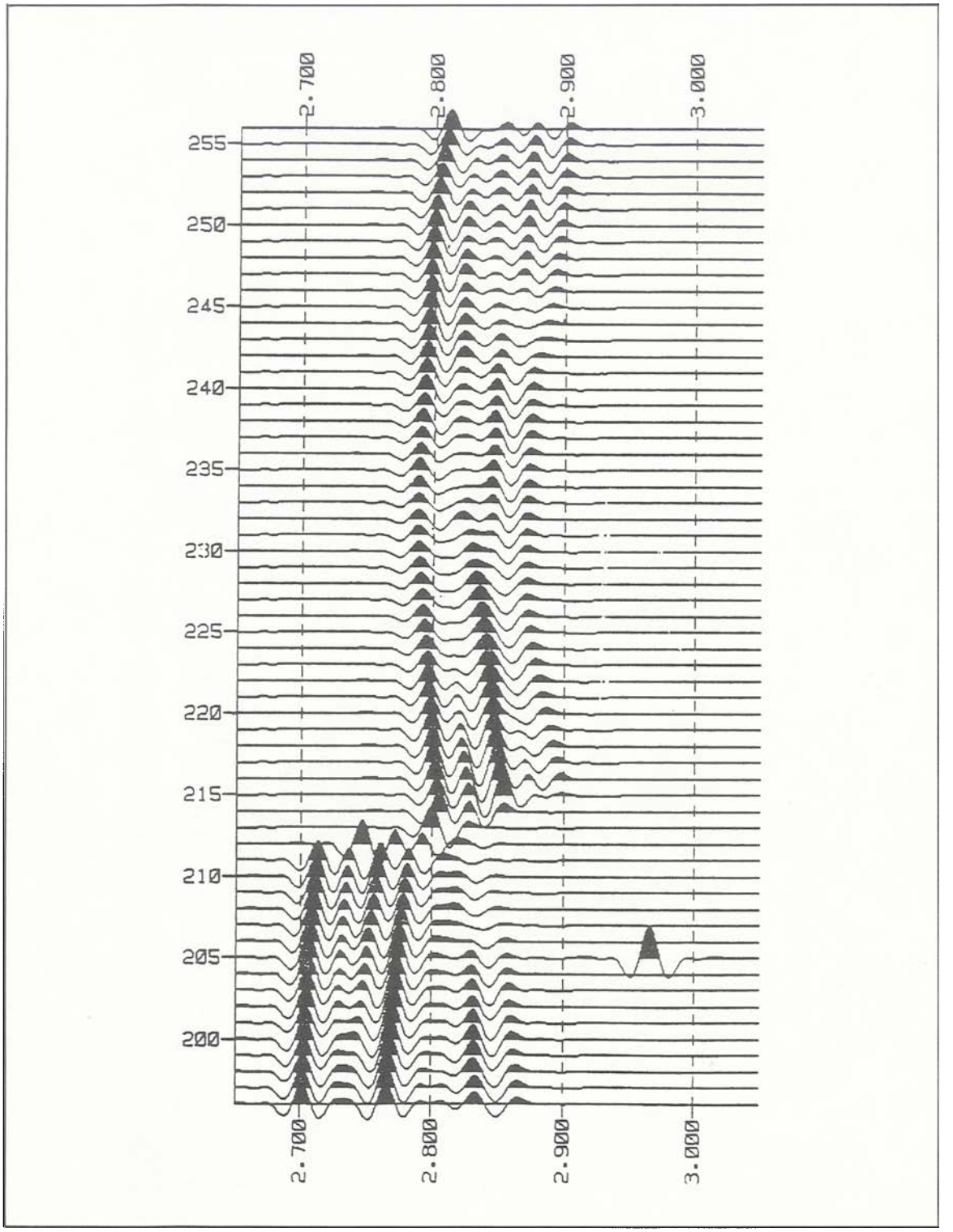

FIGURE 30. Synthetic seismic section with wavelet bandpass = 15 to 45 Hz (model 1), Port Arthur field.

thetic sections is the flat spot at the base of the E sandstone at 2.83 seconds (fig. 31). The flat spot just below the E sandstone is a shale stringer, not a fluid contact.

Addition of noise to the synthetic seismic sections reduces the detectability of reservoir details. Noise is measured here as the ratio of the largest signal amplitude (the amplitude of the wavelet) to the RMS value of the noise. For the signal-to-noise ratio of 25.1 (28 dB), a bandpass of 15 to 45 Hz and the velocity data of model 1 (fig. 32) illustrate that essential reser-

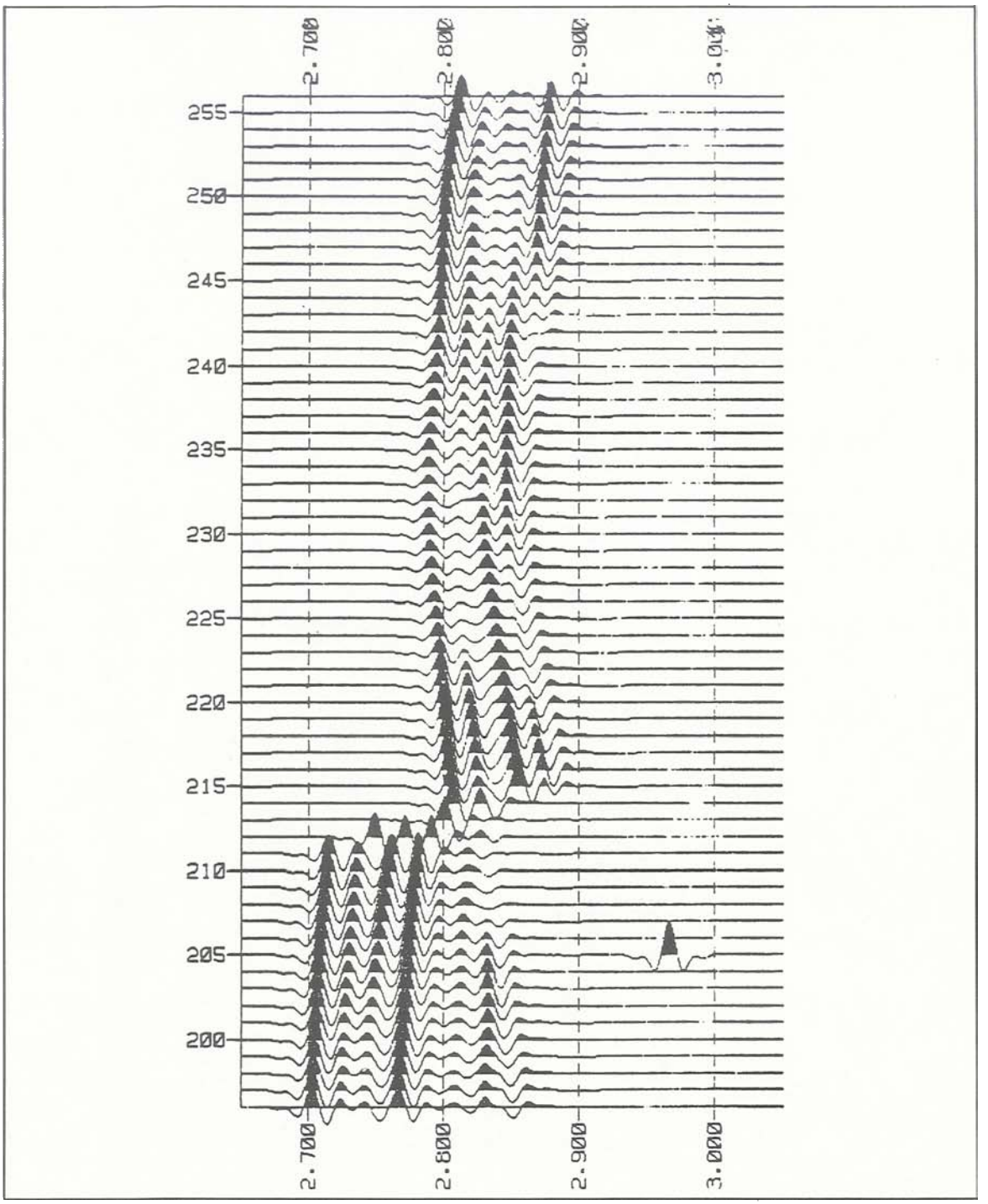

FIGURE 31. Synthetic seismic section with wavelet bandpass = 15 to 65 Hz (model 1), Port Arthur field.

voir elements in the noise-free section (fig. 30) are still discernible. As more noise is added, the usefulness of the section for modeling deteriorates drastically, and the synthetic section begins to look like the real seismic section in figure 28. This suggests that the noise level in the real data is four times the maximum tolerable level for modeling.

Detectability in synthetic sections that have a broader bandwidth (15 to 85 Hz) seems to be affected less by noise because of higher resolution and decline of destructive interference

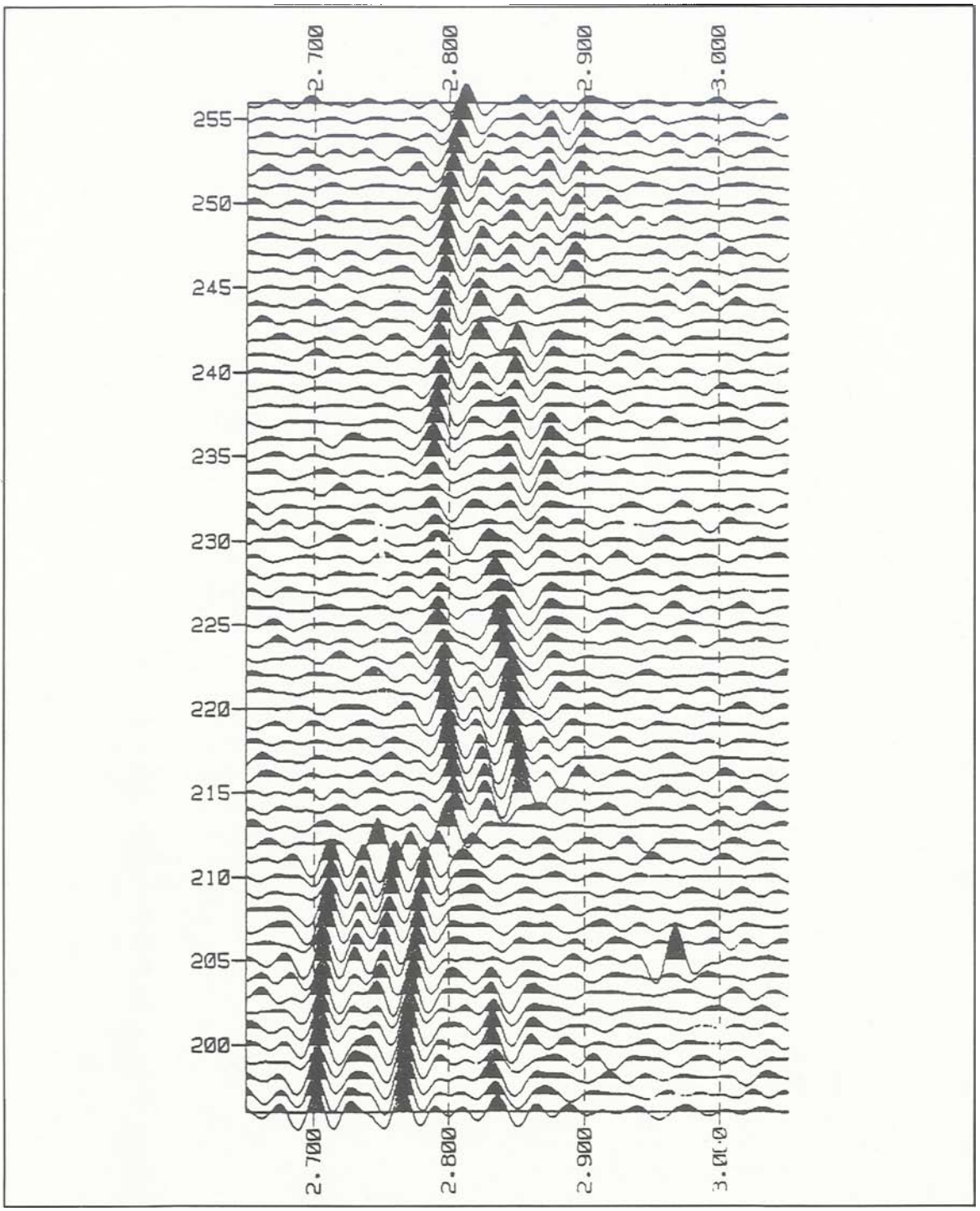

FIGURE 32. Synthetic seismic section with signal-to-noise ratio = 25.1 (bandpass = 15 to 45 Hz, model 1, Port Arthur field).

from adjacent beds. However, the improvement in detectability is not dramatic, and no classic indicators of gas sands, fluid contacts, or phase changes are obvious. The presence of gas creates more subtle features, which can be verified in this case only by comparing different velocity models with the seismic data.

Five velocity models (fig. 27) were considered by Meanley (1982). Different velocities were assumed and their effect on the synthetic sections was observed. This approach is useful for understanding how important the knowledge of acoustic impedances is to the detection of reservoir elements. Changing the velocities

of channel sandstones and other sandstones (model 2) had little effect on the synthetic sections; changing the gas sandstone velocity had a much greater effect.

In model 4, the gas sandstone velocity was increased from 9,500 to 10,250 ft/sec. The difference between the gas sandstone and the water sandstone (11,000 ft/sec) decreased, whereas the difference between gas sandstone and shale (9,000 ft/sec) increased. The resulting synthetic section (not shown) exhibits relatively small and subtle changes when compared with figure 31. Presence of gas causes less loss of amplitude at the tops of the C and D sandstones and reduces the amplitude of the flat spot (fluid contact) on the third black cycle. Other factors, such as the sidelobes from different reflectors and the gas-water contact in the E sandstone, also contribute to the observed changes in reflection amplitudes.

It is interesting to compare two extreme cases represented by model 3, which has a gas sandstone velocity of 8,000 ft/sec, and model 5, which has no gas in the reservoir (fig. 33). In model 3, the top of the C sandstone is lost because there is no contrast in acoustic impedance with the upper shale. The D and E sandstones are more visible because the largest amplitudes are associated with the gas. In model 5 (fig. 33) the reflectors are strong and continuous. Amplitude changes can be related to the presence or absence of shale stringers. Upon comparing this section (fig. 33) to model 1, which has a gas sandstone velocity of 9,500 ft/sec (fig. 31), the clues to the presence of hydrocarbons become more evident. These clues consist of the dimming of the top cycle, the central dim spot, and the fluid contact.

The modeling has been instructive in showing the possibilities of better reservoir delineation by using increased bandwidth, improved signal-to-noise ratio, and a better knowledge of reservoir acoustic impedances. In general, the noise level in the real seismic data precludes the detection of gas and reservoir details in the synthetic seismic data. The models also show that the thin reservoir beds and rapid lateral variations cause challenging problems for detailed seismic reservoir delineation in the Port Arthur field. The question posed at the beginning of this study about whether dispersed gas in a watered-out reservoir can be detected using seismic data remains unanswered.

Finally, the type of seismic data that would be needed to make visible the reservoir details desired in studies of this nature is given as follows: (1) A signal-to-noise level of four times that observed in seismic line 3 must be achieved; (2) a bandwidth of 10 to 85 Hz would be satisfactory but may not be possible; (3) dynamite would be the best source for both signal strength and static corrections but may be impractical in an urban environment; and (4) recording the shot signature with a special uphole geophone would improve the wavelet processing. In planning a new seismic survey, many different field parameters and geometries must be considered to provide maximum data quality and resolution in the zone of interest (Denham, 1981).

PRODUCTION HISTORY

The discovery well in the Port Arthur field, drilled by Meredith et al. No. 1 Doornbos (fig. 15), encountered gas condensate in several lower Hackberry sandstones and in a deeper *Nodosaria* (lower Frio) sandstone. Later developers of the field identified 24 separate reservoirs; 14 of these were productive in different wells during the life of the field. The productive reservoirs include thick sandstones with gas caps and thin stringer sandstones saturated with gas (fig. 34). Of the 18 wells drilled in the Port Arthur field, 10 wells produced a total of 57.1 Bcf of gas and 2.65 MMbbl of condensate from lower Hackberry sandstones during the primary production period (1959 to 1981).

The C Reservoir

The Hackberry C reservoir was chosen for detailed study because of its high abandonment pressure, excellent reservoir quality, high productivity, and good lateral continuity. Cumulative production from the C reservoir was 19.6 Bcf (table 4). Well 14 produced 54 percent of the gas and 53 percent of the condensate from the depth interval of from 11,136 to 11,144 ft during a period of about 11 years (July 1961 to July 1972). The well was plugged and abandoned in October 1972.

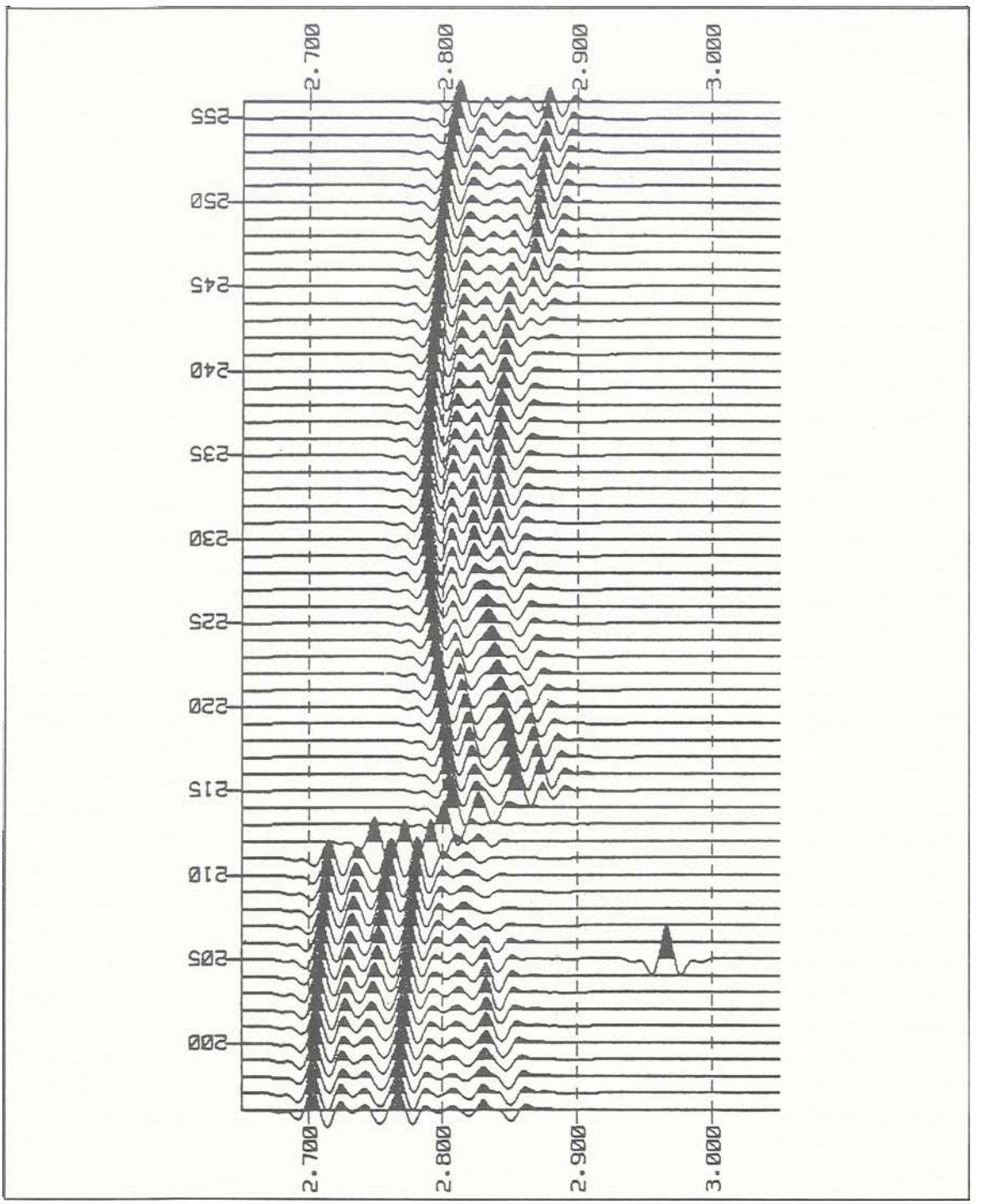

FIGURE 33. Synthetic seismic section with no gas, bandpass = 15 to 65 Hz (model 5), Port Arthur field.

Peak production of hydrocarbons from well 14 occurred between 1961 and 1965 when water production increased rapidly and peaked at 1,400 bbl/d (fig. 35). The bottom-hole flowing pressure (BHFP) decreased from 9,115 psi in 1961 to about 6,632 psi in 1971. A plot of P/Z versus cumulative gas production does not define a straight line and cannot be used to estimate the original gas in place (OGIP) because of substantial water production and encroachment of water into the gas reservoir. The OGIP was estimated to be 56.2 Bcf, according to reservoir simulation studies that are discussed later.

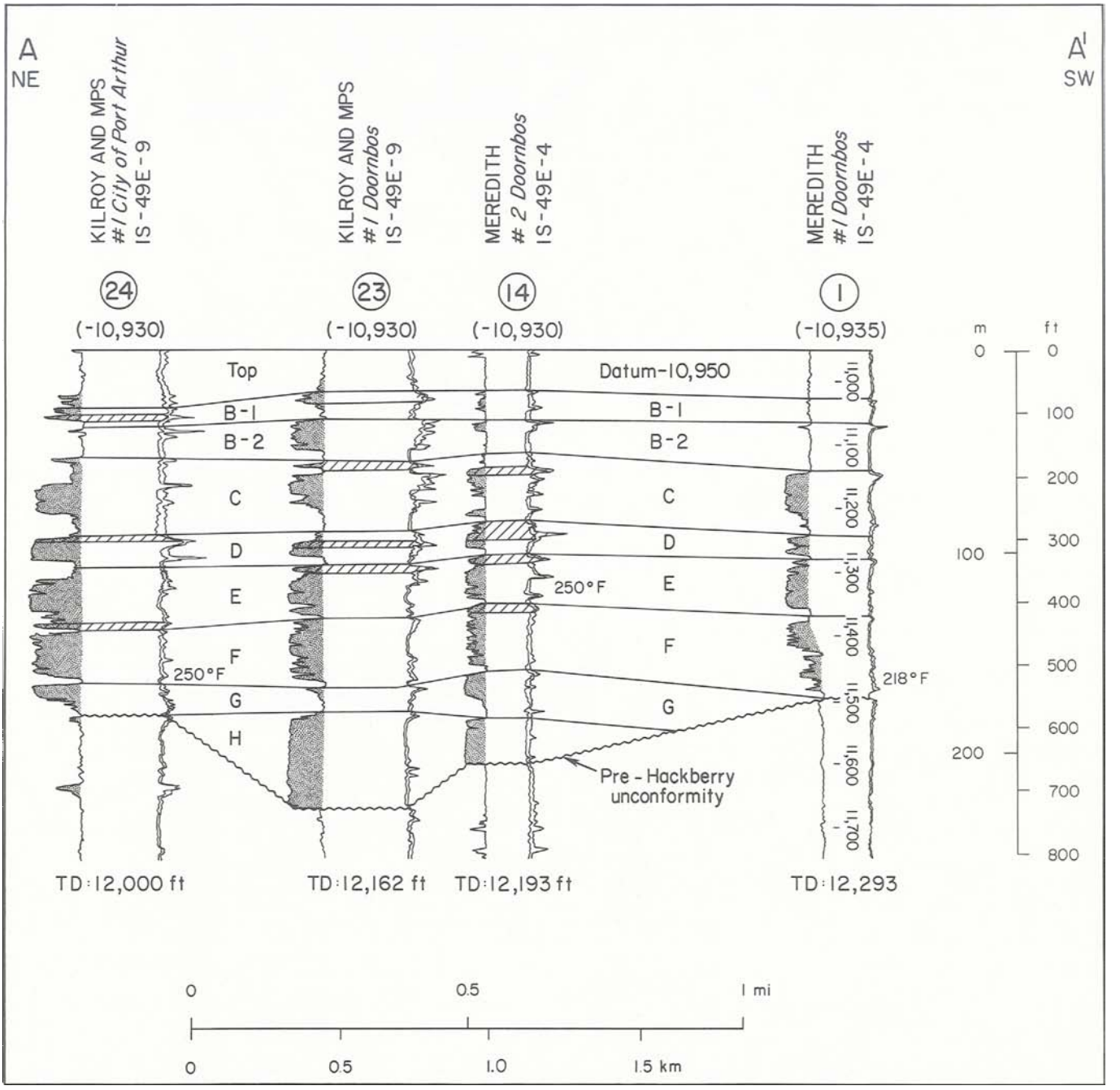

FIGURE 34. Stratigraphic strike cross section A-A' showing lower Hackberry sandstone intervals and perforated gas production zones (hachured intervals), Port Arthur field.

Well 23 produced for 6 years (July 1965 to August 1971) through perforations in the depth interval between 11,128 and 11,131 ft. Production rates, averaged over periods of 6 months, peaked at 1,186 Mcf/d of gas in 1966 and at 33.5 bbl/d of condensate in 1967 (fig. 36). Water production increased rapidly, beginning in 1965 and peaking at 722 bbl/d in January 1970. The BHFP dropped from 8,398 to 5,894 psi during the first year, then declined at a lesser rate to the last recorded test value of 5,054 psi in June 1971.

Well 11 produced gas and condensate for 8 years (September 1961 to October 1969) through the perforated depth interval between 11,130 and 11,138 ft. The BHSIP gradient decreased from 0.75 to 0.60 psi/ft during the production period.

TABLE 4. Cumulative production from Hackberry C reservoir, Port Arthur field.

Well no.*	Original operator and well name	Gas (Bcf)	Condensate oil (Mbbl)
14	Meredith No. 2 Doornbos	10.535	456
23	Kilroy & M.P.S. No. 1 Doornbos	1.250	38
11	Meredith No. 4 Doornbos	7.754	366
6	Meredith No. 3 Doornbos	0.099	2
	TOTAL	19.638	862

*Location of wells is shown in figure 15.

Well 6 produced small amounts of gas and condensate for about 16 months (August 1971 to December 1972) at the depth interval between 11,130 and 11,135 ft. The BHSIP gradient decreased from 0.70 to 0.45 psi/ft during the productive period.

Other Reservoirs

Several other lower Hackberry reservoirs (A-1 through F, table 2 and fig. 34) produced enough hydrocarbons to merit some attention in evaluating the Port Arthur field as an EGR prospect. Collectively these other reservoirs contributed 66 percent of the gas and 68 percent of the condensate that was produced from the field during primary production. Some of these reservoirs are lenticular and have limited lateral continuity; however, they may have sufficient production potential to influence the economic feasibility of an EGR test. The last recorded bottom-hole shut-in pressure gradients (table 2) indicate that some of these reservoirs were geopressured when abandoned. Salinity, pressure, temperature, and methane solubility data are listed in table 3. Structure maps, isopach maps, and sidewall core data for other reservoirs were given by Gregory and others (1983a).

A new well drilled near the top of the structure at the specified test site location near well 14 (fig. 15) in the Port Arthur field would offer numerous potentially productive lower Hackberry sandstones for testing and completion programs. An alternative drill site located about 200 ft from well 31 along a line connecting wells 31 and 14 would encounter better development of the B-2 sandstone. If a new well were drilled below the lower Hackberry sandstones, a *Nodosaria* sandstone and the Vicksburg interval would become potential producers.

PREDICTED RESERVOIR PERFORMANCE AND ECONOMIC ANALYSIS

Reservoir Simulation Studies

The objective of this investigation was to predict the amount of gas that could be produced from the Hackberry C reservoir by drilling a new well and co-producing the gas and gas-saturated reservoir brine. A numerical reservoir simulator model was used to approximate the physical characteristics of the reservoir by first matching the production history and then predicting the future reservoir behavior.

Model Description

A three-dimensional, two-phase (gas and water) reservoir simulator was used to match the production history of the Port Arthur field and to predict reservoir behavior if the field were reentered for co-production of gas and water. The model grid (fig. 37), representing the C sandstone, includes both the gas reservoir and its contiguous aquifer. A small grid size was used near the wells where pressure and water saturation are subject to rapid changes, whereas a larger grid was used to represent aquifers away from the gas cap. An overall grid dimension of 10×13 blocks is shown; however, certain blocks were deleted from the active system (fig. 37, hachured area) because some areas are not in communication with the primary area of interest. Elevations and net-sandstone thickness values (fig. 38) were assigned to individual blocks by overlaying the grid structure and isopach maps of the C sandstone (figs. 14 and 15). Permeability values varied from 200 to 300 md (fig. 39).

Although four wells are shown in the simulator grid, only wells 14 and 23 were modeled.

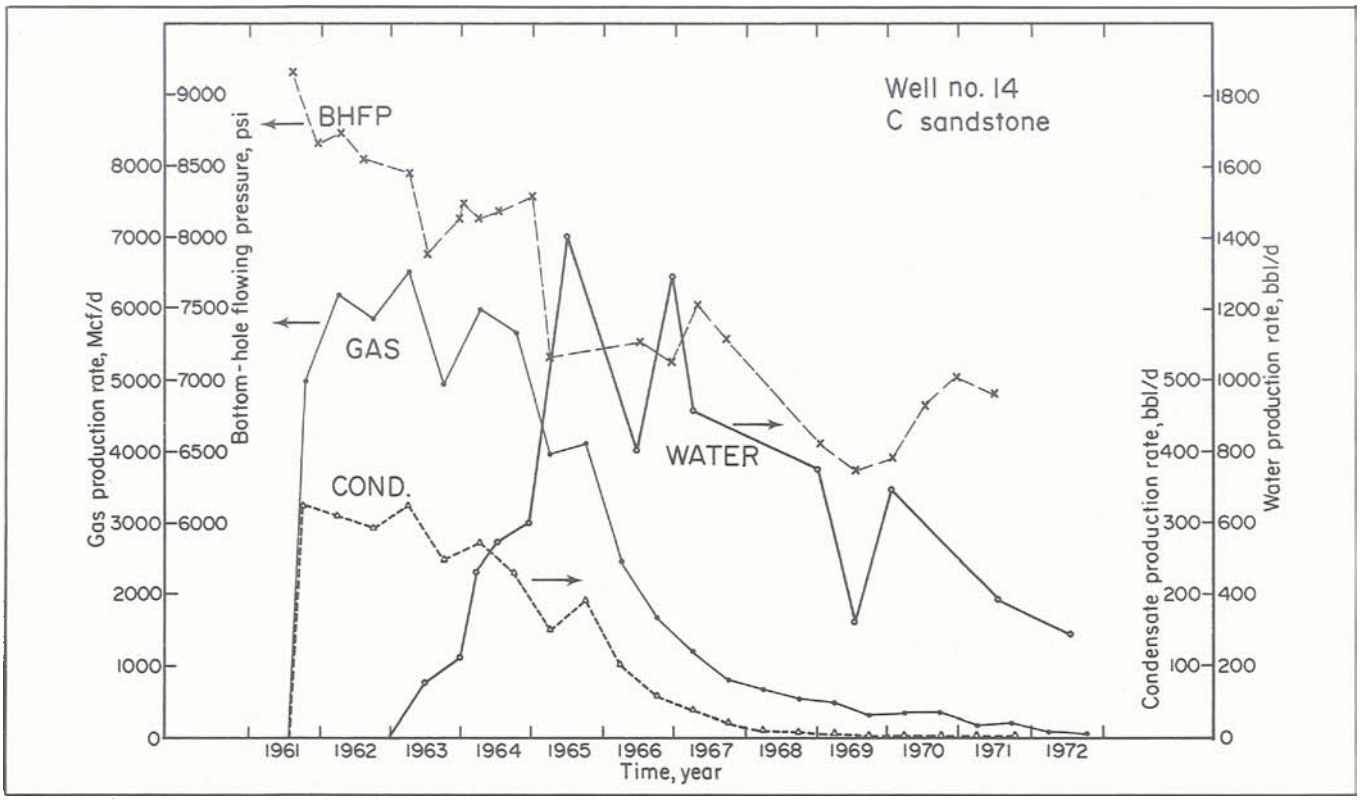

FIGURE 35. Reservoir production rates and bottom-hole flowing pressure versus time, Hackberry C sandstone, well 14, Port Arthur field.

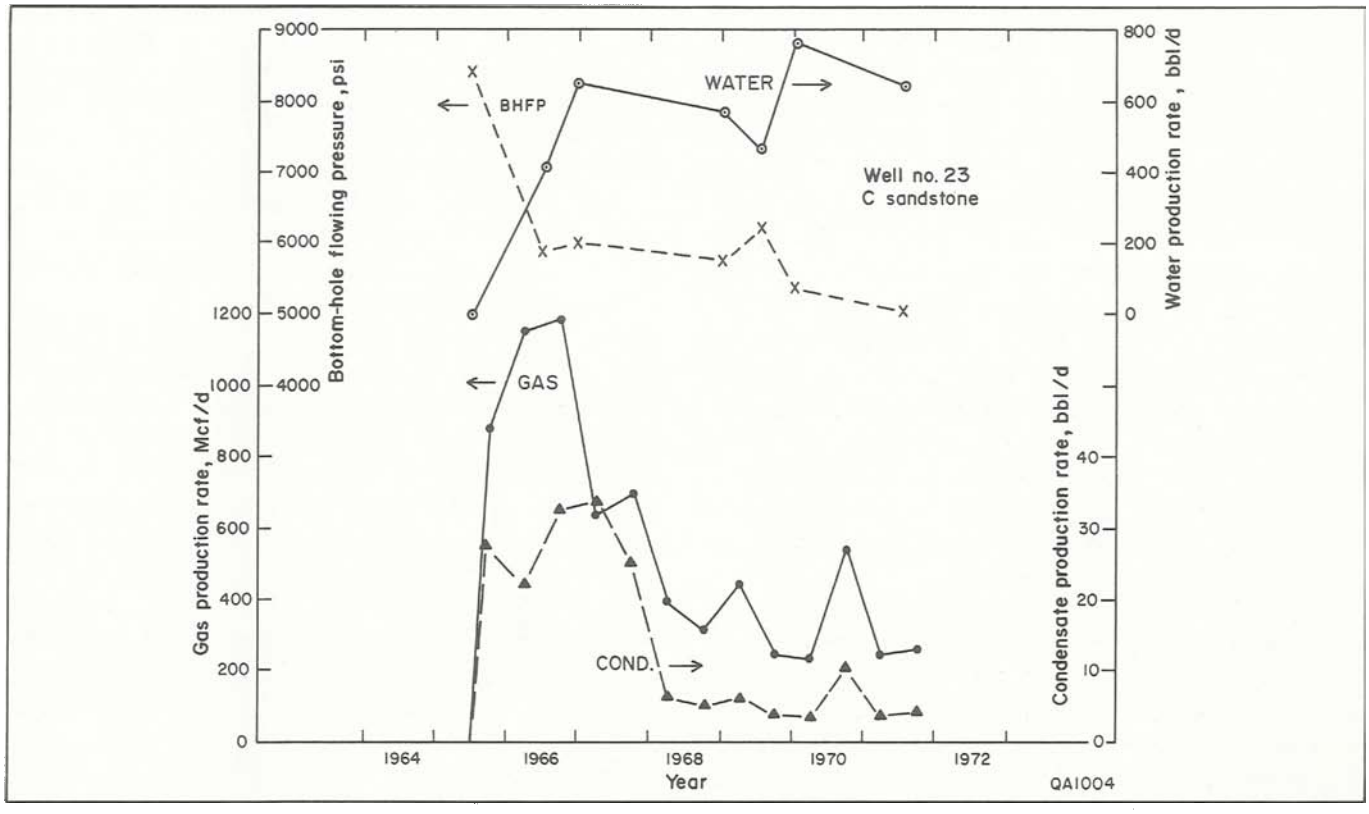

FIGURE 36. Reservoir production rates and bottom-hole flowing pressure versus time, Hackberry C sandstone, well 23, Port Arthur field.

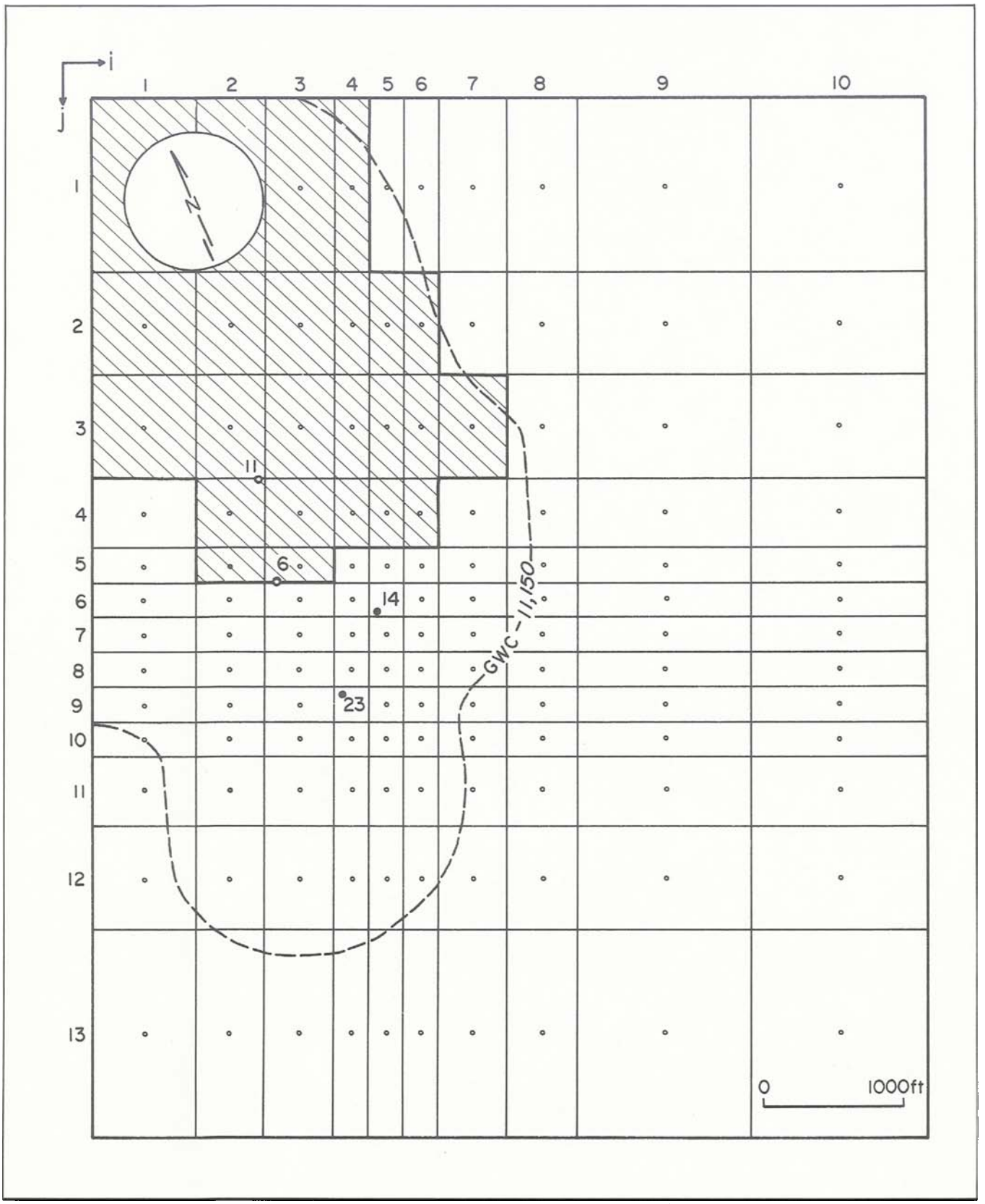

FIGURE 37. Simulator grid used for reservoir simulation of Hackberry C sandstone.

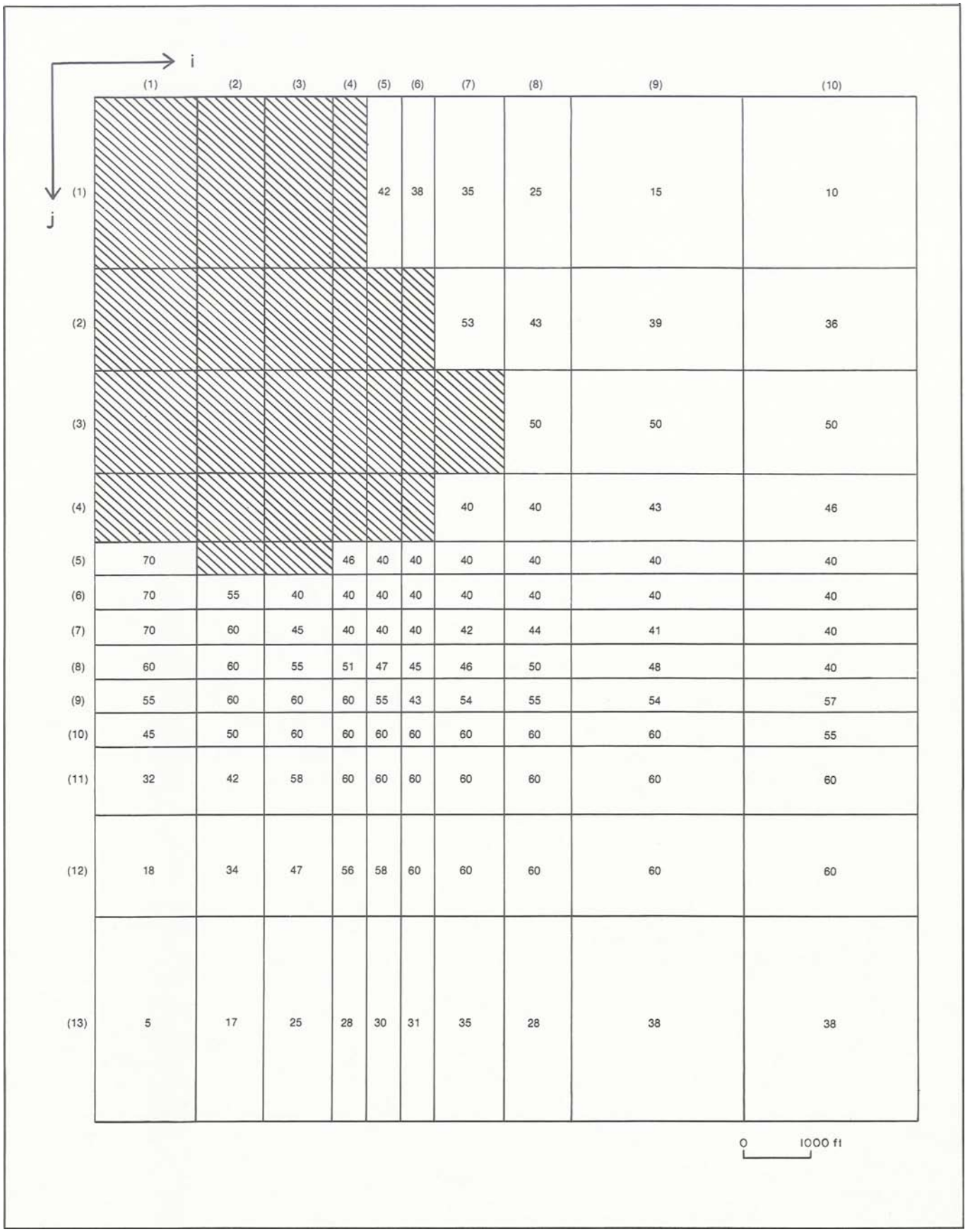

FIGURE 38. Distribution of sandstone thickness used for reservoir simulation of Hackberry C sandstone.

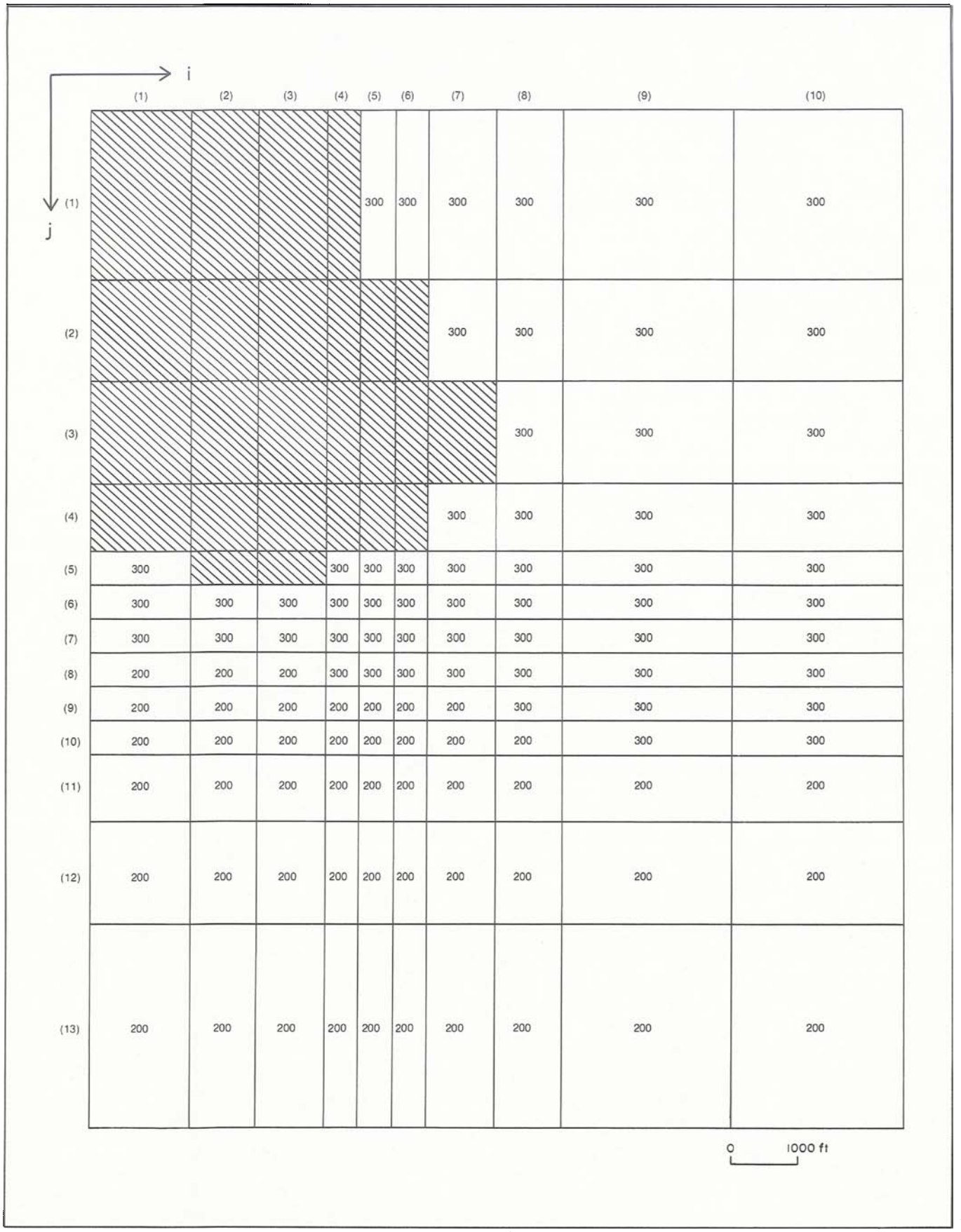

FIGURE 39. Permeability distribution used for reservoir simulation of Hackberry C sandstone.

Well 6 was not modeled because it produced a negligible amount of gas, whereas well 11 was deleted because it had a limited drainage, just over a 200-ft radius from the wellbore; it was depleted later to a pressure gradient of 0.6 psi/ft.

There also appears to be some geological support for thinking that the C sandstone in well 11 is not in communication with the C sandstone in wells 14 and 23. The SP log character of the C sandstone (fig. 14) shows that well 11 intersects a proximal suprafan facies, whereas wells 14 and 23 intersect a broad fan-channel-fill facies. The C sandstone is a composite of smaller sand bodies, each deposited in different sedimentary environments; the individual sand bodies may or may not be in communication.

Model Data and History Matches

The model data used in the simulation studies are shown in table 5. The history match is a trial-and-error procedure for adjusting certain sensitive parameters of input data to achieve a satisfactory match between the model and the history of pressure behavior and gas/water production rates in the C sandstone. On the first trial run (table 5), the numerical values used for input data were based on results of well log analysis, sidewall core analysis, well tests, and geological and engineering interpretations. The sensitivity of most parameters was investigated independently. The most sensitive parameters are gas-water contact, gas specific gravity, and relative permeability.

In preliminary history-match studies, the simulated results showed a discontinuity in the calculated BHFP at pressures from 7,000 to 7,500 psi when gas condensate was ignored in the studies. The discontinuity occurs at the dew point, which can be identified for the year 1966 from the plot of gas/condensate ratio versus time (fig. 40). The bottom-hole flowing pressure from calculated field data was about 7,300 psi in 1966. From this information, it was concluded that retrograde condensation existed in the C reservoir and that the dew point was about 7,300 psi. Liquid condensation will occur in the reservoir if the reservoir pressure falls below 7,300 psi. Some of the condensed liquid will adhere to the walls of the pore spaces in the rocks and become immobile. The resulting liquid loss will cause the gas produced at the surface to have a lower liquid content and the gas/condensate ratio to increase (fig. 40).

TABLE 5. Model data used in simulation studies.

Original water in place, MMbbl	314.9
Original free gas in place, Bcf	56.2
Reservoir temperature, °F	230
Initial pressure, psi	9115
Reservoir gas gravity, dimensionless ratio	0.7
Initial gas formation-volume factor, reservoir cf/scf	0.00289
Initial gas viscosity, cp	0.0365
Water viscosity, cp	0.3
Permeability, md	figure 39
Relative permeability curves	figure 41
Porosity, %	30
Net-sandstone thickness, ft	figure 38
Water compressibility, psi^{-1}	7×10^{-6}

The two-phase (gas and water) simulator ignores the third phase (gas condensate) because it was not designed to model a retrograde condensate reservoir. Test runs with the simulator and data collected from field production showed that compensation can be made for the retrograde reservoir behavior by adjusting the gas viscosity and relative permeability curves to smooth the pressure discontinuity and obtain a good history match.

Rates of gas and water production used in the reservoir simulation studies were obtained respectively from reported monthly production and water/gas ratios; gas rates were averaged for 6-month periods. Relative permeabilities of gas and water (fig. 41) were calculated using equations developed by Corey (1954). Exponent values in the Corey equation were adjusted to give a good match with performance.

History matches for bottom-hole flowing pressures and water rates for the C sandstone in well 14 are shown for the field production period from 1961 to 1972 (fig. 42). History matches for well 23 (not shown) were satisfactory but not as good as those obtained for well 14.

Predictions

A reservoir simulation prediction was made for a single test well located near well 14. A 10-year shut-in period (1973 to 1982) was modeled, followed by an 8-year production period (1983 to 1990). The maximum gas flow

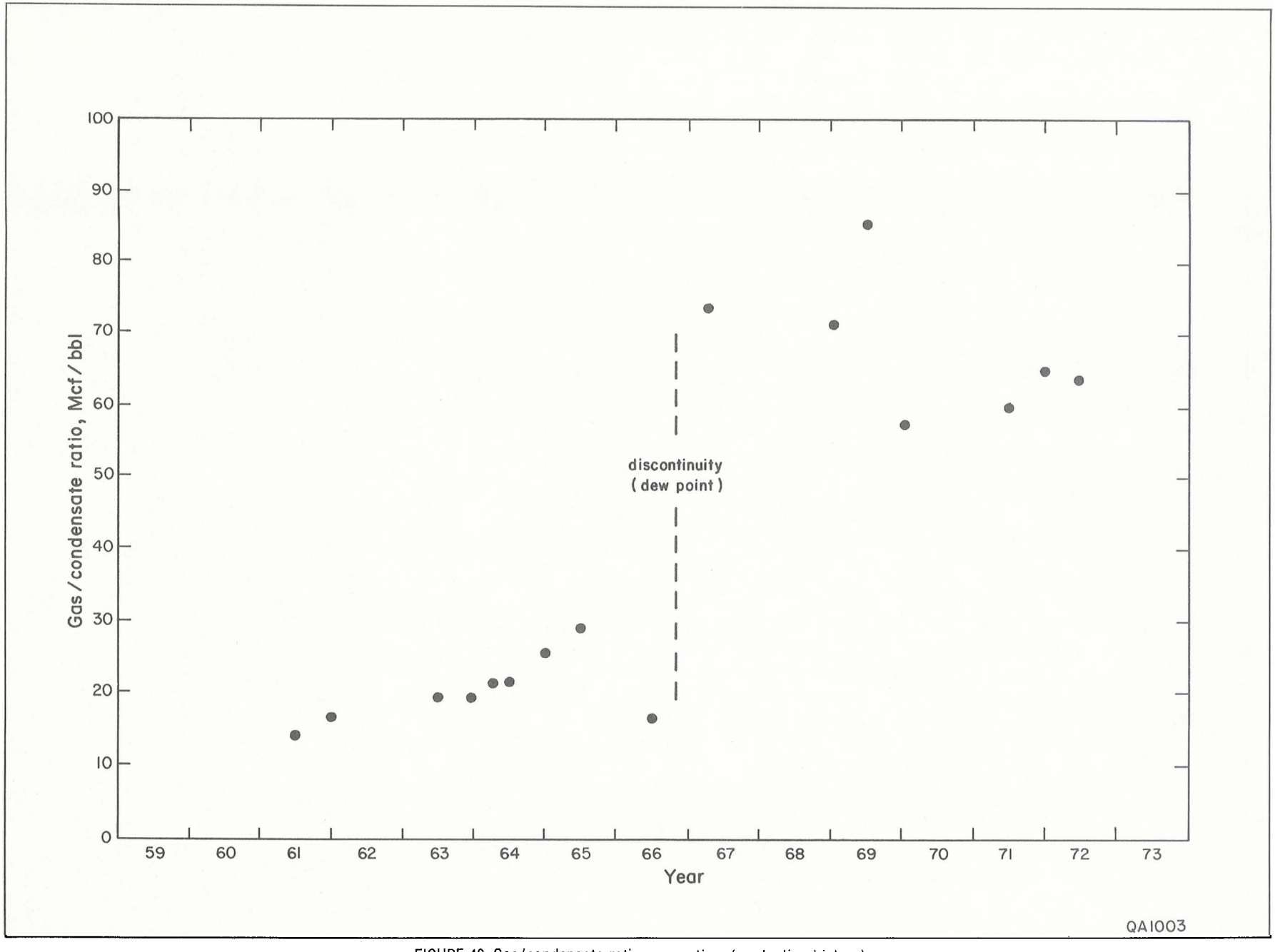

FIGURE 40. Gas/condensate ratio versus time (production history).

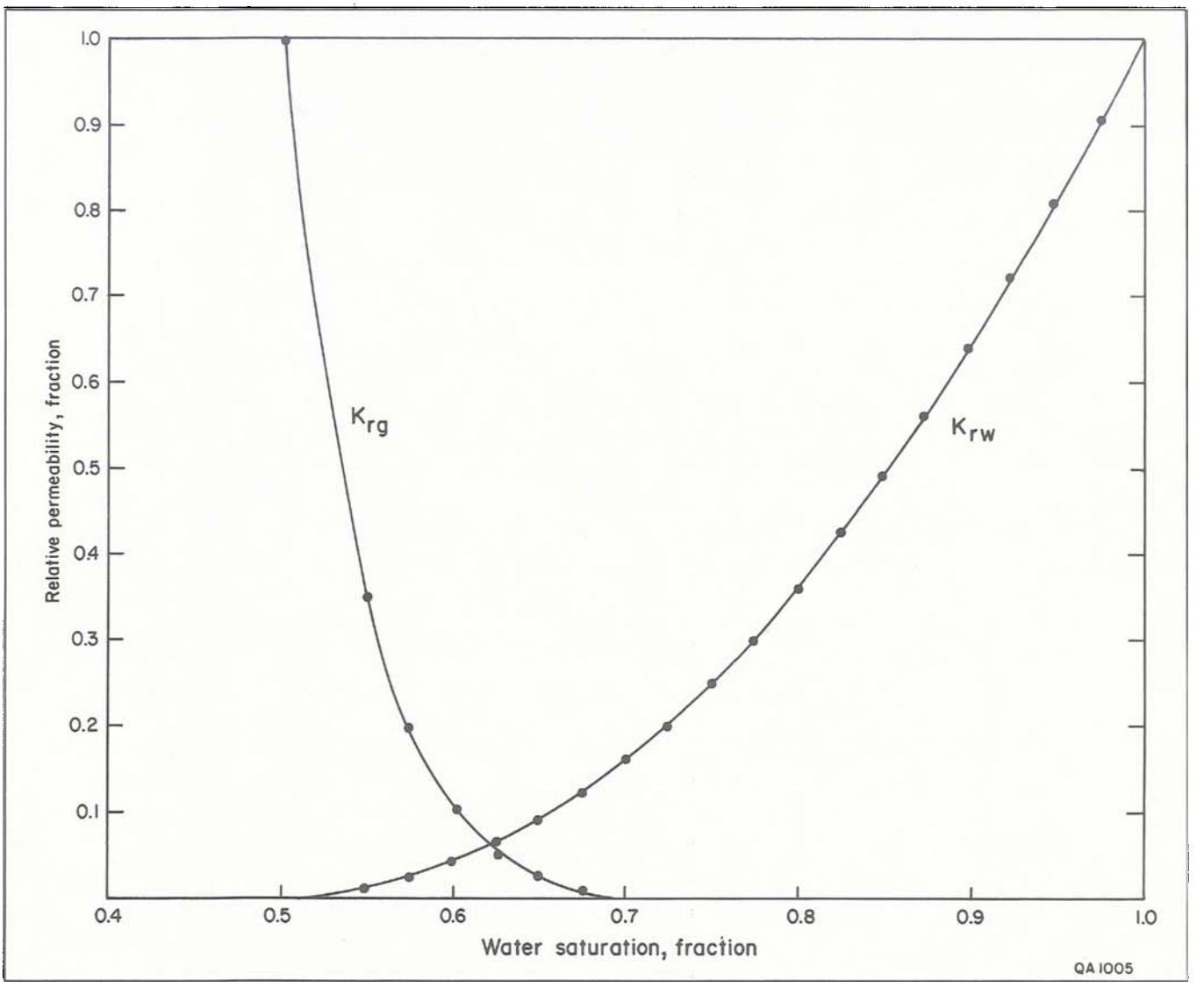

FIGURE 41. Relative permeability curves (Corey-type equation) used in reservoir simulation.

rate and minimum bottom-hole flowing pressure were set at 3,000 Mcf/d and 4,200 psi, respectively. The minimum bottom-hole flowing pressure* was calculated from the flow of a three-phase fluid (gas, condensate, and water) in a vertical pipe by the method of Orkiszewski (1967). Theoretically, the well will not flow at pressures below 4,200 psi without use of artificial lift methods. Within these constraints, gas flow rates from the Hackberry C sandstone would remain at 3,000 Mcf/d for the first 3 years, then decline to a minimum of 100 Mcf/d in the eighth year (fig. 43). Predictions of gas condensate production from the test well were made on the basis of the gas/condensate ratio (fig. 40) and the predicted gas flow rate (fig. 43). According to the model, water production would peak at 6,850 bbl/d in the second year and fall to 350 bbl/d in the eighth year, whereas the bottom-hole flowing pressure would decline from 6,632 to 4,200 psi during the production period. Cumulative production predicted for natural flow conditions would be 5.1 Bcf of gas, 51 Mbbl of condensate, and 8.94 MMbbl of water. If the original gas in place were 56.2 Bcf, as estimated by the model, then gas recovery would increase from 35 percent (primary) to 44 percent of OGIP if the co-production method were used (table 6).

*The minimum bottom-hole flowing pressure of a three-phase fluid is not to be confused with hydrostatic pressure, which is associated with a borehole containing a single-phase fluid (water or brine).

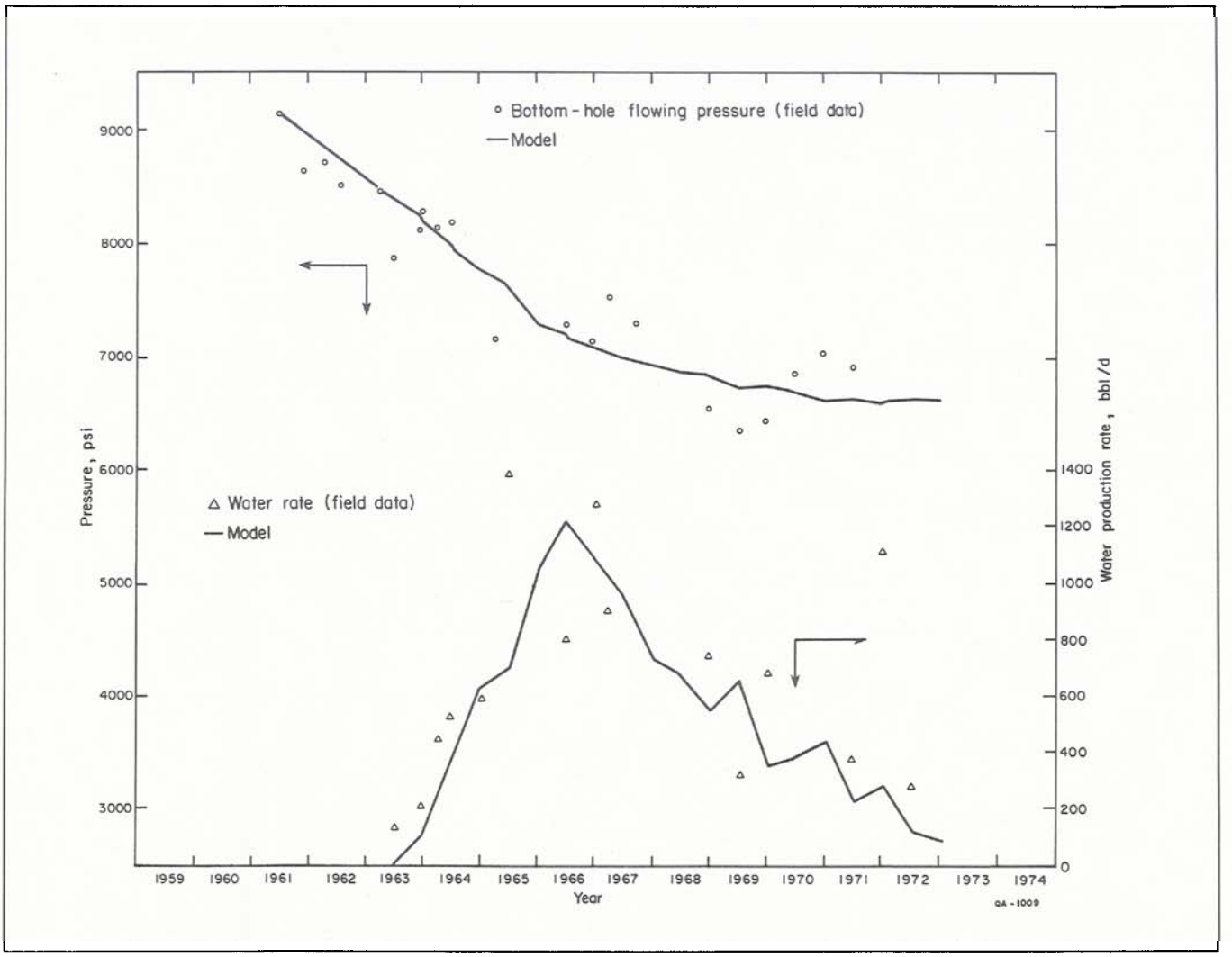

FIGURE 42. History matches for pressure and water production rates, Hackberry C sandstone, well 14, Port Arthur field.

Economic Analysis

Estimated total drilling costs for a test well to a depth of 11,650 ft and a salt-water disposal well to 4,500 ft are $3,837,280 (table 7); operating costs during the testing and production period average an additional $33,000/month. The property owner has an overriding royalty interest of 25 percent. The operator has 100 percent of the working interest and 75 percent of the revenue interest. Federal income taxes and other taxes are listed in table 7.

The cash-flow calculations made using the cost data (table 7) and the predicted flow rates (fig. 43) show a break-even gas price of $2.40/Mcf for a 15-percent rate of return after Federal income tax is paid (fig. 44). Break-even gas price is the price at which the project breaks even on a zero net-present-worth basis. Net present worth of the investment is about $986,000 for a gas price of $3.00/Mcf and increases rapidly for higher gas prices (fig. 45). Thus, the original investment would be paid off in 3 years. The economic outlook for the prospect might be even better if production from the Hackberry C sandstone and from other watered-out reservoirs in the field were commingled.

TABLE 6. Past and predicted production from Hackberry C sandstone (natural flow conditions).

	Gas (Bcf)	Condensate oil (Mbbl)	Water (Mbbl)	Final BHFP (psi)	Production life (years)
Primary production (wells 14 and 23)	11.79	494	4,700	6,632	11
Predicted production	5.10	51	8,940	4,200	8
Past recovery			35 percent OGIP		
Predicted recovery			44 percent OGIP		

TABLE 7. Cost data used in economic analysis.

Investment	Dollars
Production test well	
Tangible	1,783,040
Intangible	1,322,720
Disposal well	
Tangible	103,040
Intangible	224,560
Other capital costs	
Tangible	-0-
Intangible	403,920
TOTAL	3,837,280
Interest	**Percent**
Overriding royalty	25
Working interest	100
Net revenue	75
Taxes	**Percent**
Severance tax, gas	7.5
Severance tax, oil	4.6
Ad valorem tax	4.0
Federal income tax	46.0
Oil price	$30/bbl

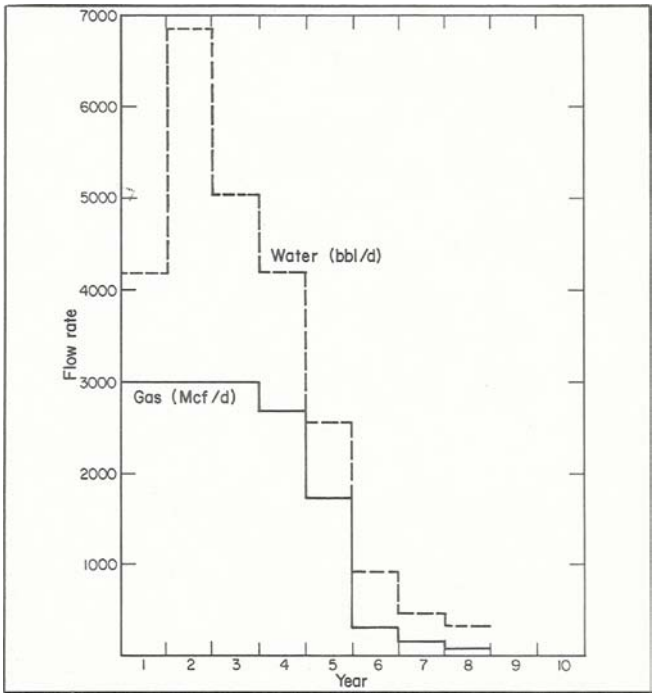

FIGURE 43. Predicted gas and water flow rates in Hackberry C sandstone.

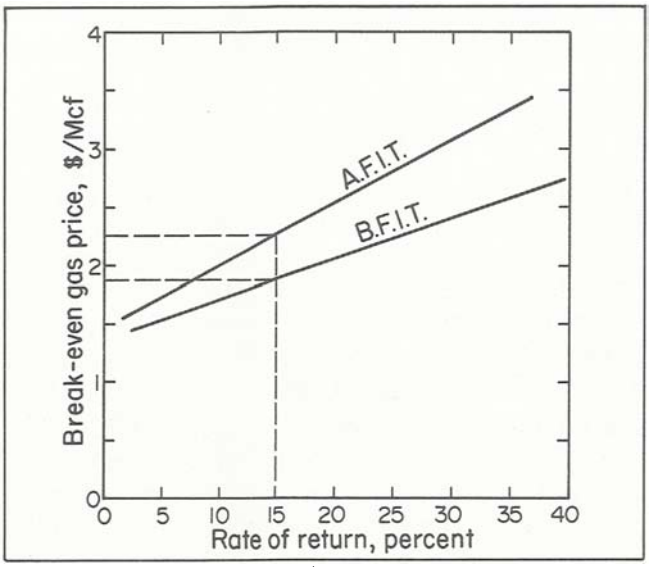

FIGURE 44. Break-even gas price versus rate of return before payment of Federal income tax (B.F.I.T.) and after payment of Federal income tax (A.F.I.T.).

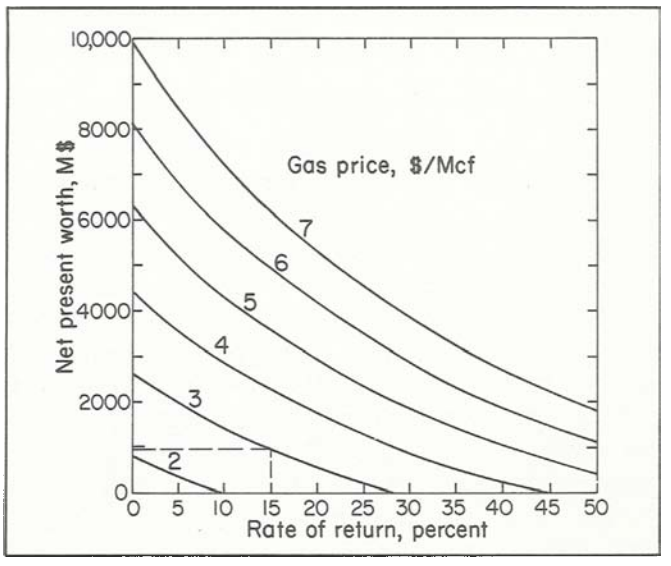

FIGURE 45. Net present worth versus rate of return after Federal income tax for different gas prices.

CONCLUSIONS AND RECOMMENDATIONS

1. Co-production of gas and water is an EGR method that has considerable potential for increasing the ultimate hydrocarbon recovery from abandoned reservoirs.
2. Reservoir simulation studies predict, for the Port Arthur test case, that the gas remaining in the abandoned C reservoir exceeds 60 percent of the OGIP; an additional 9 percent can be recovered by the co-production method during the natural flowing life of a test well.
3. Results obtained from reservoir modeling suggest that a successful field test conducted for research and development would pay off the original investment in 3 years. The break-even gas price is $2.40/Mcf for a 15-percent return on the investment after payment of Federal income taxes.
4. Only the C reservoir has been considered in this analysis. The co-production of several additional abandoned reservoirs in the Port Arthur field could substantially improve the economic outlook.
5. This analysis of the Port Arthur field is an example of how new technology and increased prices can make it worthwhile to reconsider when to abandon watered-out reservoirs.

It is recommended that a designed test well be drilled on a site about 200 ft southwest of well 14. The exact location may be determined by the location of suitable elevated roads and by the condition of the old surface site of well 14, which is located in a swampy area. Projected depths of the well are 11,650 ft to penetrate all the lower Hackberry sandstones, 11,850 ft to penetrate the *Nodosaria* sandstone, and about 13,500 ft to penetrate the Vicksburg interval. An alternate drill site located about 200 ft from well 31 along a line connecting wells 31 and 14 would give a better exposure of the B-2 sandstone.

ACKNOWLEDGMENTS

Funds for this project were provided by the Gas Research Institute under GRI contract no. 5080-321-0398. Special thanks go to B. R. Weise, L. A. Jirik, H. S. Hamlin, S. L. Hallam, M. B. Edwards, R. A. Schatzinger, N. Tyler, and D. W. Downey for screening many gas fields during geological work, which eventually resulted in the selection of the Port Arthur field as a prime prospect for this investigation. Victor Lombeida, Evans Jegbefume, Jackson Yoong, Wahiduzzaman Mirza, Yueming Chen, Sam Cho, and Srikanta Mishra were responsible for calculating numerous reservoir parameters.

Certain types of work required in support of this project were subcontracted by the Gas Research Institute and the Bureau of Economic Geology to J. R. Butler and Company, Wattenbarger and Associates, GeoQuest International, and Lewis Technical Services. The well log analytical work was supervised by Brian E. Ausburn, J. R. Butler and Company. Seismic data processing and modeling was done by E. W. Meanley (reviewed by D. L. Kelm and J. R. Patch), GeoQuest International. Ernest C. Geer, Transco Development Company, provided constant help and guidance throughout this program.

Companies that provided valuable information include Michel T. Halbouty Energy Company, Prudential Drilling Company, Texaco,

Amoco Production Company, J. C. Barnes Company, United Energy Company, Transco Development Company, and Eaton Operating Company.

The manuscript was word processed by Dorothy C. Johnson and typeset by Fannie M. Sellingsloh, under the supervision of Lucille C. Harrell. Illustrations were prepared by J. T. Ames, R. S. Baum, T. M. Byrd, M. R. Day, M. L. Evans, and J. A. McClelland, under the direction of Richard L. Dillon, chief cartographer. Text illustration printing was by James A. Morgan. Jamie S. Haynes designed this publication; editing was by R. Marie Jones-Littleton.

REFERENCES

Ausburn, B. E., Skirvin, R. T., and Hyun, I. S., 1982, Volumetric analysis of Frio sands, Port Arthur field: Report from J. R. Butler Company to The University of Texas at Austin, Bureau of Economic Geology, 85 p.

Berg, R. R., and Powers, B. K., 1980, Morphology of turbidite-channel reservoirs, lower Hackberry (Oligocene), southeast Texas: Gulf Coast Association of Geological Societies Transactions, v. 30, p. 41-48.

Bornhauser, Max, 1960, Depositional and structural history of northeast Hartburg field, Newton County, Texas: American Association of Petroleum Geologists Bulletin, v. 44, no. 4, p. 458-470.

Boyd, W. E., Jr., Christian, L. D., and Danielsen, C. L., 1982, Secondary gas recovery from a watered-out reservoir: Presented at the 57th Annual Fall Technical Conference and Exhibition of the Society of Petroleum Engineers of AIME, New Orleans, paper 11158, 10 p.

Brinkman, F. P., 1981, Increased gas recovery from a moderate water drive reservoir: Journal of Petroleum Technology, v. 33, no. 12, p. 2375-2480.

Chesney, T. P., Lewis, R. C., and Trice, M. L., 1982, Secondary gas recovery from a moderately strong water drive reservoir, a case history: Journal of Petroleum Technology, v. 34, no. 9, p. 2149-2157.

Corey, A. T., 1954, The interrelation between gas and oil relative permeabilities: Producers Monthly, November issue, p. 38-41.

Denham, L. R., 1981, Extending the resolution of seismic reflection exploration: Journal of Canadian Society of Exploration Geophysicists, v. 17, no. 1, p. 43-54.

Domenico, S. N., 1976, Effects of brine-gas mixture velocity in an unconsolidated sand reservoir: Geophysics, v. 41, p. 882-894.

Dunlap, H. F., and Dorfman, M. H., 1981, Problems and partial solutions in using the SP log to predict water salinity in deep hot wells: Proceedings, Fifth United States Geopressured-Geothermal Energy Conference, Louisiana State University, p. 189-192.

Ewing, T. E., and Reed, R. S, in press, Depositional and structural controls of lower Hackberry sandstone reservoirs in southeast Texas: The University of Texas at Austin, Bureau of Economic Geology, Geological Circular.

Galloway, W. E., Hobday, D. K., and Magara, K., 1982, Frio Formation of the Texas Gulf Coastal Basin—depositional systems, structural framework, and hydrocarbon origin, migration, distribution, and exploration potential: The University of Texas at Austin, Bureau of Economic Geology Report of Investigations No. 122, 78 p.

Gardner, G. H. F., Gardner, L. W., and Gregory, A. R., 1974, Formation velocity and density—the diagnostic basics of stratigraphic traps: Geophysics, v. 39, p. 770-780.

Garrett, J. H., 1938, The Hackberry assemblage—an interesting foraminiferal fauna of post-Vicksburg age from deep wells in the Gulf Coast: Journal of Paleontology, v. 12, p. 309-317.

Geer, E. C., and Cook, H. L., 1978, Enhanced gas recovery from geopressured aquifers: Presented at the 53rd Annual Fall Meeting of the Society of Petroleum Engineers of AIME, Houston, paper 7541, 8 p.

Geertsma, J., 1961, Velocity log interpretation: the effect of rock bulk compressibility: Society of

Petroleum Engineers of AIME Transactions, v. 222, p. 235-253.

Gregory, A. R., Dodge, M. M., Posey, J. S., and Morton, R. A., 1980, Volume and accessibility of entrained (solution) methane in deep geopressured reservoirs—Tertiary formations of the Texas Gulf Coast: The University of Texas at Austin, Bureau of Economic Geology, Report to the U.S. Department of Energy, Division of Geothermal Energy, Contract No. DE-AC08-78ET01580, 390 p.

Gregory, A. R., Jirik, L. A., Reed, R. S., Weise, B. R., and Morton, R. A., 1981, Location and evaluation of reservoirs containing solution gas and free gas—Texas Gulf Coast: Proceedings, Fifth United States Geopressured-Geothermal Energy Conference, Louisiana State University, p. 255-257.

Gregory, A. R., Lin, Z. S., Reed, R. S., Morton, R. A., and Ewing, T. E., 1983a, Exploration and production program for locating and producing prospective aquifers containing solution gas and free gas—Texas Gulf Coast: The University of Texas at Austin, Bureau of Economic Geology, Final report to the Gas Research Institute, Contract No. 5080-321-0398, 197 p.

Gregory, A. R., Lin, Z. S., Reed, R. S., Morton, R. A., and Rogers, L. A., 1983b, Watered-out gas reservoirs profitable via enhanced recovery: Oil and Gas Journal, v. 81, no. 11, p. 55-60.

Halbouty, M. T., and Barber, T. D., 1961, Port Acres and Port Arthur fields, Jefferson County, Texas: Gulf Coast Association of Geological Societies Transactions, v. 11, p. 225-234.

Hottmann, C. E., and Johnson, R. K., 1965, Estimation of formation pressures from log-derived shale properties: Journal of Petroleum Technology, v. 17, p. 717-723.

Kehle, R. O., 1971, Geothermal survey of North America, 1971 annual progress report: American Association of Petroleum Geologists, Research Committee, unpublished report, 31 p.

Lutes, J. L., Chiang, C. P., Rossen, R. H., and Brady, M. M., 1977, Accelerated blowdown of a strong water-drive gas reservoir: Journal of Petroleum Technology, v. 29, no. 12, p. 1533-1538.

Meanley, E. S., 1982, Seismic processing and modeling, Port Arthur field: Report from GeoQuest International, Inc., to The University of Texas at Austin, Bureau of Economic Geology, 84 p.

Orkiszewski, J., 1967, Predicting two-phase pressure drops in vertical pipe: Society of Petroleum Engineers of AIME Transactions, v. 240, p. 829-838.

Paine, W. R., 1968, Stratigraphy and sedimentation of subsurface Hackberry wedge and associated beds of southwestern Louisiana: American Association of Petroleum Geologists Bulletin, v. 52, no. 2, p. 322-342.

Price, L. C., Blount, C. W., MacGowen, D., and Wenger, L., 1981, Methane solubility in brines with application to the geopressured resource: Proceedings, Fifth United States Geopressured-Geothermal Energy Conference, Louisiana State University, p. 205-214.

Reedy, F., Jr., 1949, Stratigraphy of Frio Formation, Orange and Jefferson Counties, Texas: American Association of Petroleum Geologists Bulletin, v. 33, no. 11, p. 1830-1858.

Schlumberger Limited, 1978, Log interpretation charts, Gen 7: p. 3.

Walker, R. G., 1979, Facies models 8, turbidites and associated coarse clastic deposits, *in* R. G. Walker, ed., Facies models: Geological Association of Canada, *in* Geoscience Canada, reprint series 1, p. 91-103.

Weise, B. R., Jirik, L. A., Hamlin, H. S., Hallam, S. L., Edwards, M. B., Schatzinger, R. A., Tyler, N., and Morton, R. A., 1981, Geologic studies of geopressured and hydropressured zones in Texas: supplementary tasks: The University of Texas at Austin, Bureau of Economic Geology, final report to the Gas Research Institute, Contract No. 5011-321-0125, 120 p.

APPENDIX A: Metric conversion factors.

Customary unit		Conversion factor		Preferred metric unit
acre	×	0.4046856	=	ha (hectares)*
acre-ft	×	1,233.482	=	m^3
acre-ft	×	0.1233482	=	ha-m
bbl (42 gals)	×	0.158983	=	m^3
bbl/acre-ft	×	0.0001288931	=	m^3/m^3
bbl/d	×	0.1589873	=	m^3/d
°C	+	273.1500	=	°K
°F		(°F −32)/1.8	=	°C
ft	×	0.3048	=	m
gal	×	0.003785412	=	m^3

Customary unit		Conversion factor		Preferred metric unit
lb/gal	×	119.8264	=	kg/m^3
md	×	0.0009869233	=	μm^2
mi	×	1.609344	=	km
mi^2	×	2.589988	=	km^2
psi	×	6.894757	=	kPa
psi/ft	×	22.62059	=	kPa/m
scf (std ft^3)	×	0.02831685	=	m^3
scf/bbl	×	0.1801175	=	std m^3/m^3

*1 ha (hectare) = 10,000 m^2 (2.47 acres)

APPENDIX B: Nomenclature.

A.F.I.T.	=	after Federal income tax
bbl	=	barrel, 42-gallon capacity
B.F.I.T.	=	before Federal income tax
BHFP	=	bottom-hole flowing pressure, psi
BHP	=	bottom-hole pressure, psi
BHSIP	=	bottom-hole shut-in pressure, psi
BHT	=	bottom-hole temperature, °F
Bscf, or Bcf	=	billion standard cubic feet
B_w	=	water formation volume factor, dimensionless
°C	=	degrees Celsius (centigrade)
CH_4	=	methane
C_p	=	compaction correction factor
D	=	depth, feet
d	=	day
dB	=	decibels
DST	=	drill-stem test
F	=	formation factor
°F	=	degrees Fahrenheit
FPG	=	formation pressure gradient, psi/ft
g/L	=	grams per liter
GOR	=	gas-to-oil ratio
GP	=	geopressure
GWC	=	gas-water contact

Krg	=	relative permeability to gas
Krw	=	relative permeability to water
m	=	cementation factor
md	=	millidarcy
mi	=	mile or miles
MMscf, or MMcf	=	million standard cubic feet
Mscf, or Mcf	=	thousand standard cubic feet
P/Z	=	pressure/gas compressibility factor, ratio
R_m	=	mud resistivity, ohm-meters
R_{mf}	=	mud filtrate resistivity, ohm-meters
RMS	=	root mean square
R_{sh}	=	shale resistivity, ohm-meters
scf	=	standard cubic feet
T_L	=	temperature measured in borehole and recorded on well log header, °F
ΔT_f	=	transit time of fluid contained in pore spaces of rock, μ sec/ft
ΔT_{log}	=	transit time from acoustic log, μ sec/ft
ΔT_m	=	transit time of solid matrix material of rock, μ sec/ft
WHSIP	=	wellhead shut-in pressure, psi
Z	=	gas compressibility factor, dimensionless